Nagra
Nationale
Genossenschaft
für die Lagerung
radioaktiver Abfälle

Cédra
Société coopérative
nationale
pour l'entreposage
de déchets radioactifs

Cisra
Società cooperativa
nazionale
per l'immagazzinamento
di scorie radioattive

TECHNICAL REPORT 85-17

Gas Formation in a L/ILW Repository and Gas Transport in the Host Rock

Marie Wiborgh
Lars O. Höglund
Karin Pers

December 1986

KEMAKTA Konsult AB, Stockholm, Sweden

Parkstrasse 23 5401 Baden/Schweiz Telephon 056/20 55 11

Nagra
Nationale
Genossenschaft
für die Lagerung
radioaktiver Abfälle

Cédra
Société coopérative
nationale
pour l'entreposage
de déchets radioactifs

Cisra
Società cooperativa
nazionale
per l'immagazzinamento
di scorie radioattive

TECHNICAL REPORT 85-17

Gas Formation in a L/ILW Repository and Gas Transport in the Host Rock

Marie Wiborgh
Lars O. Höglund
Karin Pers

December 1986

KEMAKTA Konsult AB, Stockholm, Sweden

Parkstrasse 23 5401 Baden/Schweiz Telephon 056/20 55 11

Der vorliegende Bericht wurde im Auftrag der Nagra erstellt. Die Autoren haben ihre eigenen Ansichten und Schlussfolgerungen dargestellt. Diese müssen nicht unbedingt mit denjenigen der Nagra übereinstimmen.

Le présent rapport a été préparé sur demande de la Cédra. Les opinions et conclusions présentées sont celles des auteurs et ne correspondent pas nécessairement à celles de la Cédra.

This report was prepared as an account of work sponsored by Nagra. The viewpoints presented and conclusions reached are those of the author(s) and do not necessarily represent those of Nagra.

SUMMARY

In a repository for low- and intermediate-level radioactive waste, gases will be formed due to corrosion, microbial degradation and radiolytic decomposition.

The predominant gas formation process is anaerobic corrosion of metals which yields over 90% of all gases formed, based on a corrosion rate of 10^{-4} -10^{-3} mm/year.

In this report, gas transport in the system of engineered barriers and gas transport in the host rock are treated separately.

The pressure build-up required to form cracks in the repository liner has been estimated and compared with the pressure required for gas transport in an unfractured barrier. The assumed range of permeabilities for the concrete barrier is $1 \cdot 10^{-20}$ $-1 \cdot 10^{-17}$ m^2. The gas transport in the host rock is calculated for permeabilities of $1 \cdot 10^{-19}$ - $1 \cdot 10^{-15}$ m^2.

The transport routes for the gases are the undisturbed host rock and the lineaments. The gas transport capacity in the host rock is sufficiently high to balance the rate of gas formation and has been found to be independent of the capacity in the lineaments when the permeability in the host rock is higher than 10^{-17} m^2.

The gas transport capacities are calculated for a rock material with distributed fissure sizes. The relative permeability for the gas has been calculated using capillary pressure curves for three different rock materials - dolomite, sandstone and limestone. Additional calculations have been made for uniformly sized fissures.

ZUSAMMENFASSUNG

In einem Endlager für schwach- und mittelaktive radioaktive Abfälle können durch Korrosion, mikrobiellen Abbau und radiolytischen Zerfall Gase entstehen.

Die anaerobe Korrosion von Metallen ist der wichtigste Prozess mit einem Anteil von 90 Prozent der entwickelten Gase, basierend auf einer Korrosionsrate von 10^{-4}-10^{-3} mm/Jahr.

In diesem Bericht wird der Gastransport im System der technischen Barrieren und im Wirtgestein separat behandelt.

Der Druckaufbau, der zur Rissbildung in der Endlagerauskleidung führt, wurde abgeschätzt und mit dem für den Gastransport in einer intakten Barriere benötigten Druck verglichen. Der angenommene Permeabilitätsbereich für die Betonbarriere beträgt $1 \cdot 10^{-20}$ bis $1 \cdot 10^{-17}$ m^2. Der Gastransport im Wirtgestein wird für Permeabilitäten von $1 \cdot 10^{-19}$ bis $1 \cdot 10^{-15}$ m^2 berechnet.

Die Transportwege für die Gase sind das ungestörte Wirtgestein und Klüfte. Die Transportkapazität im Wirtgestein ist genügend hoch, um das produzierte Gas entweichen zu lassen und ist unabhängig von der Kapazität in den Klüften, wenn die Permeabilität im Wirtgestein grösser als 10^{-17} m^2 ist.

Die Gastransportkapazitäten werden für ein Gesteinsmaterial mit verschiedenen Kluftöffnungen berechnet. Die relative Permeabilität für das Gas wurde mit Kapillardruck-Kurven für drei verschiedene Gesteinsmaterialien - Dolomit, Sandstein, Kalk - berechnet. Zusätzliche Berechnungen wurden für Klüfte mit konstanter Grösse durchgeführt.

RESUME

Dans un dépôt final pour déchets de faible et moyenne radioactivité, des gaz peuvent se former suite à la corrosion, à la dégradation microbienne et à la décomposition radiolytique.

Le processus prédominant de formation de gaz est la corrosion anaérobie de métaux, qui donne lieu à plus de 90 pour cent de tous les gaz produits, sur la base d'un taux de corrosion de 10^{-4}-10^{-3} mm/an.

Ce rapport aborde séparément le transport de gaz dans le système des barrières ouvragées et dans la roche d'accueil.

La montée en pression, qui conduit à la formation de fissures dans le revêtement du dépôt final, a été estimée et comparée à la pression nécessaire au transport de gaz dans une barrière intacte. La perméabilité pour les barrières de béton, s'étend de $1 \cdot 10^{-20}$ à $1 \cdot 10^{-17}$ m^2. Le transport de gaz dans la roche d'accueil est calculé pour des perméabilités de $1 \cdot 10^{-19}$ à $1 \cdot 10^{-15}$ m^2.

La roche d'accueil non perturbée et les diaclases constituent les voies de transport des gaz. La capacité de transport dans la roche d'accueil est suffisamment élevée pour équilibrer le taux de formation de gaz et s'est avérée indépendante de celle constatée dans les diaclases, pour une perméabilité dans la roche d'accueil supérieure à 10^{-17} m^2.

Les capacités de transport de gaz sont calculées pour un matériel rocheux présentant différentes ouvertures de diaclase. La perméabilité relative pour les gaz a été calculée à l'aide de courbes de pression capillaire pour trois roches différentes: dolomie, grès, calcaire. Des calculs additionnels ont été effectués pour des diaclases de dimension uniforme.

CONTENTS

LIST OF TABLES

LIST OF FIGURES

1. INTRODUCTION

Low-and intermediate-level radioactive waste in Switzerland will be disposed of in an underground facility, a so-called type B repository.

The actual site for this repository has not yet been decided. For the purposes of Project Gewähr, Oberbauen Stock has been chosen as a site. The design and location of the repository and the characteristics of the host rock are given in NGB 85-06 and NGB 85-07.

When low-and intermediate-level radioactive waste is disposed of in an underground repository, many chemical reactions may occur between the materials present. Among these reactions, some may result in the production of gases, e.g. radiolytic decomposition, microbial degradation and corrosion.

The aim of the first part of this report is to indicate the amounts of gases produced in a type B repository and their possible consequences.

The report shows the sensitivity of gas formation to different conditions and assumptions, such as the material content, the water chemistry and the rates of the reactions involved.

The transport of the gases through the technical barriers of the near-field and through the surrounding host rock is estimated in the second part of the report. To improve understanding, these two calculations are done independently, one for the near-field and one for the host rock, assuming no resistance in the near-field.

These calculations indicate the extent of the gas transport capacity in the host rock at the model site. They also indicate the sensitivity of the gas transport capacity to the hydrostatic pressure at the repository location, and to characteristics of the host rock such as permeability and pore size distribution.

Under some conditions, gas may accumulate within the repository or in the zone decompressed during excavation and cause a pressure build-up. These conditions are identified and discussed. The implications for the rate of release of radionuclides is not dealt with in this report.

2. GENERAL INFORMATION ON THE REPOSITORY

In order to estimate the gas formation in a type B repository and the possibilities for gas transport from the repository, the physical and chemical conditions must be clearly defined. This is achieved by:

- The waste inventory /NGB 85-02/ which specifies the nuclide and chemical composition of all types of waste concerned. It also gives the necessary information about matrix and containers used.
- The repository design /NGB 85-07 and NGB 85-08/ which specifies design, dimensions, materials and their properties.
- Site-specific data /NTB 84-20/ on the host rock properties, water chemistry etc. for the selected Oberbauen Stock model site, see reference /1/.

In this chapter the data necessary for the calculations in this report are summarized.

2.1. Waste and storage containers

The low-and intermediate-level waste foreseen for the type B repository can be divided into four main groups with reference to origin:

- OPERATIONAL WASTE
- REPROCESSING WASTE
- DECOMMISSIONING WASTE
- MIF-WASTE (RESEARCH, MEDICINE AND INDUSTRY)

A condensed description of the waste from a chemical and physical point of view is given in Table 1. The characteristics are given for the waste container, the conditioning material and the waste separately. Within the four groups mentioned above, the waste is divided into sub-categories. The figures in Table 1 are average values derived from about 200 different types of waste, for a nuclear power program of 240 GWa.

This information was used as input data for the calculations presented in NGB 85-08. Later, improved information was obtained regarding some of the waste. In some cases this new information is of such interest for the near-field analysis that it is introduced in this report. The deviations from the results presented in NGB 85-08 are discussed in each case.

The OPERATIONAL WASTE is divided into four sub-categories:

- Ion exchange resins
- Concentrates and sludges
- Solids
- Ashes

The type of waste container used is a steel drum with an internal volume of approximately 200 l. The predominant conditioning material is concrete. Bitumen and plastic are used for only 10% of the waste.

The REPROCESSING WASTE is divided into:

- Ion exchange resins
- Concentrates and sludges
- Solids

The main type of container is made of concrete and has an internal volume of 200 to 400 l, with concrete also serving as conditioning material. For the sub-category containing ion exchange resins, steel drums with an internal volume of 200 l are used with bitumen as conditioning material.

The DECOMMISSIONING WASTE is divided into:

- Activated steel
- Activated concrete
- Solids
- Concentrates

Activated steel is the predominant sub-category. For all sub-categories, concrete containers with an internal volume of 14.6 m^3 are used with concrete as conditioning material.

The MIF-WASTE is not divided into sub-categories owing to the small amounts of waste involved. All the waste is contained in steel drums with an internal volume of 200 l and conditioned with concrete.

Table 1. General physical and chemical description of the waste

Waste category	Waste container			Quantity	Conditioning material kg/cont.	Specification of waste (kg/waste container)								
	Type	Void m^3	Inner volume m^3			Steel	Zn/Al	Salt conc.	Ion exch. resins	Ashes	Cellulose	Concrete	Plastic	Other solids
OPERATIONAL														
Ion exch. resins	steel drum	0-0.01	0.16-0.20	161 931	concrete 210-280				60-80					
	"-	0	0.05	4 217	plastic 20				40					
	"-	0-0.01	0.20	22	bitumen 70-100				20-30					
Concentrates and sludges	steel drum	0	0.20	2 610	concrete 380			20						
	"-	0	0.20	2 748	bitumen 120			90-100						
Solids	steel drum	0-0.01	0.20	36 725	concrete 150-320	10-200							0-20	0-100
Ashes	steel drum	0.005	0.15	2 640	concrete 200					70				
REPROCESSING														
Ion exch. resins	concrete container	0.02	0.4	786	concrete 550				90					
Concentrates and sludges	steel drum	0.03	0.2	19 650	bitumen 160			100						
Solids	concrete container	0	0.2-0.4	52 662	concrete 0-700	400-600	10-15				100		10-15	
DECOMMISIONING														
Activated steel	concrete container	0	14.6	2 921	concrete 26 000-35 000	1000-20000	0-500							
Activated concrete	concrete container	0	14.6	527	concrete 17 000-19 000	0-1700						4 000-23 000		
Concentrates	concrete container	0	14.6	583	concrete 15 000			15 000						
Solids	concrete container	0	14.6	442	concrete 13 000-23 000	0-4500				0-1800			4 000-10 000	3 800-7 000
MIF-WASTE	steel drum	0.005	0.20	35 000	concrete 200									100

Table 2 shows the contributions to the total amounts of different materials in the repository of the different waste categories itself, as well as the conditioning material used for immobilisation of the waste.

Table 2. Summary of total amounts of materials originating from waste and conditioning material (tonnes) (Inventory version of July 1984 /NGB 85-02/)

Conditioning material	Operational waste	Reprocessing waste	Decommissioning waste	MIF waste	Whole repository
Concrete	54,730	9,120	118,280	8,410	190,600
Bitumen	300	3,100	-	-	3,400
Plastics	100	-	-	-	100
Waste					
Steel	2,800	23,600 (8,300)*	39,700	-	66,100 (50,800)*
Al/Zn	-	600	6	-	600
Salt/concentrates	300	1,800	8,500	-	10,600
Ashes	200	-	100	-	300
Glass	400	-	-	-	400
Ion exchange resins	12,200	100	-	-	12,300
Concrete	20		4,300	-	4,300
Cellulose	-	- (5,300)*	-	-	- (5,300)*
Plastic	5	600	3,000	-	3,600
Other organics	0	1	-	-	1
Other solids	3,000		2,400	3,300	8,700

* The December 1984 inventory /NTB 84-47/.

The total amount of conditioning material used for the waste is roughly 200,000 tonnes. Concrete is the predominant material, representing over 95% of the total amount. The other conditioning materials - bitumen and plastic - are only used for some of the operational and reprocessing waste.

In the waste, steel is the principal material with respect to weight: about 60% from the decommissioning waste, less than 40% from the reprocessing waste and the rest from the operational waste.

The main materials besides steel are ion exchange resins and salt concentrates. Operational waste contributes nearly all ion exchange resins and decommissioning waste is the predominant source for salt concentrates.

Table 3 gives an overview of the most important materials introduced into the repository. In this Table not only the waste itself and its conditioning materials are considered, but also the 20 m^3 storage containers which are used as an overpack for all the waste drums.

Table 3. Summary of materials introduced into the repository including storage containers (tonnes)

	Concrete	Steel	Aluminium and Zinc	Organic material*
Waste and waste matrix	194,900	66,100	600	19,400
Waste container	59,300	15,300	-	-
Backfill in storage containers	164,000	-	-	-
Storage containers	174,900	22,100	-	-

* Bitumen, plastic, ion exchange resins and other organic materials.

The data given in this section serve as a general basis for all estimates regarding gas formation presented in this report. Additional data required for the quantitative evaluation of the various gas formation processes which occur within the repository are given in connection with the description of the different processes, see Sections 3.2, 3.3, 3.4.

2.2 Repository design

The assumptions made regarding repository design for estimation of gas formation and gas transport are based on design data for Project Gewähr presented in NGB 85-06 and NGB 85-07.

Figure 1 shows a schematic presentation of the type B repository tunnel system in the host rock.

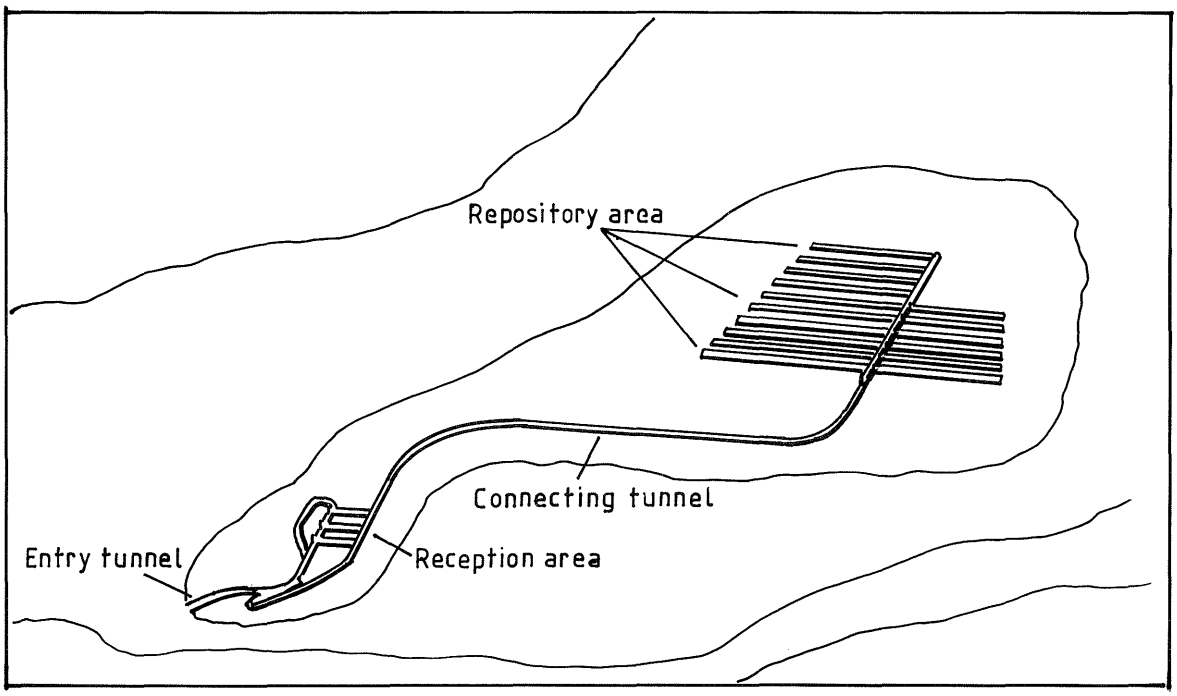

Figure 1. Perspective view of the type B repository in the host rock

Figure 2 shows a cross-section of a cavern indicating the storage pattern for the containers, thickness of repository liner and some overall dimensions.

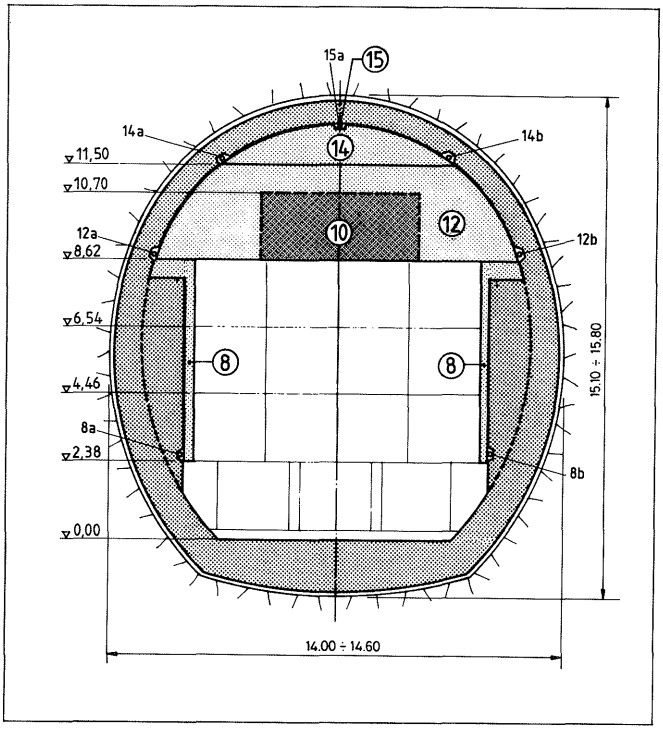

Figure 2. Cross-section of a cavern

An overview of additional design data on the type B repository is presented below in Table 4.

Table 4. Repository design data /NGB 85-07/

Total volume of storage containers	320,000 m^3
Total volume of repository backfill	300,000 m^3
Total volume of repository lining	200,000 m^3
Total volume of the whole repository	820,000 m^3
Cross-sectional area of cavern	176 m^2
Total repository length	4,660 m

The previous section provides details of the waste materials in the storage containers. In order to obtain an idea of the total amount of the main materials in the entire repository, the material originating from repository backfill and the repository lining is presented in Table 5.

Table 5. Total content of concrete and steel in the repository backfill and lining (tonnes)

	Concrete	Steel
Repository backfill	277,000	-
Repository lining	410,800	40,100

The repository lining is assumed to be reinforced with 200 kg steel per m^3 concrete.

In addition to the general design information presented here, the specific data used in the repository design for gas formation and gas transport estimates are presented under the heading 'Data used' for each section.

2.3 Site-specific data

This section contains general characteristic data relevant to the Oberbauen Stock reference site. The host rock of Oberbauen Stock consists of Valanginian marls. The composition of Valanginian marl is given in Table 6.

Table 6. Mineral constituents of Valanginian marl

Calcium carbonate	35-65 %
Swelling clay minerals	5-15 %
Non-swelling clay minerals, quartz and other minerals	20-60 %

The water analyses from Oberbauen Stock are presented in Table 7 /NTB 84-20/. A major observation which can be made from the Table is that reducing (or anaerobic) conditions prevail. This is demonstrated by the presence of sulphide, $KMnO_4$-consumption, absence of O_2 etc. This subject is dealt with in Section 3.2.

The repository is assumed to be located 450 m above sea-level. Hydraulic calculations presented in NGB 85-08 for this location give a hydraulic pressure in the repository of 1-2 MPa.

The host rock shows two systems of discontinuities (lineaments) with the same strike direction (east-west) but with different angles: 45^{o} towards the south and 45^{o} towards the north. The frequency of lineaments is estimated to be 0.2 m^{-1}, with a thickness of 0.02-0.05 m. Another disturbed zone is the 12-17 m thick decompressed zone which can be formed around the repository during excavation of the tunnels /NTB 85-30/.

Table 7. Groundwater analysis from Oberbauen Stock /NTB 84-20/

	Los Huttegg access tunnel 70	Los Huttegg access tunnel 70 Tm 190 average value	Los Huttegg parallel tunnel 73 Tm 275	Los Huttegg ventilation tunnel 72 Tm 370	Seeröhre 125.873.80 Central Huttegg 16 G 29 Seezentrale Süd, drilling	Seeröhre km 126.262 tunnel 77 Tm 388.5 pilot drilling	Seeröhre km 126.262 tunnel 77 Tm 388.5 excavation front
Date	8.10.71	14.12.71			10.12.73	23.10.73	19.10.73
Temperature(°C)							
pH-value	8.93	9.3	8.7	9.1	7.6	8.25	8.5
electricalconductivity at 20°C (Scm^{-1})	1120	3350		6100	46000	3580	3100
Degree of hardness(French H°):							
Carbonate			3.2	7.4	24.3	2.8	
No carbonate			0	0	359.1	0	
Total	0.75	0.7	3.2	7.4	383.4	2.8	2.2
Concentration(mg/l):							
Sulphate SO_4	trace	5	382	225	101	47	1.8
Chloride Cl	7.6	36	145	1660	20100	174	203
Nitrate NO_3		0					
Nitrite NO_2	0.02	0.02					
Ammonium NH_4	1.0	5.0			15		
Sulphide S		21	92	0		84	85
H_2S		pos.					
$KMnO_4$-consumption (mg/l):	72.5	112					
Alkalinity (mval/l)							
Phenolphthalein p		2.0	1.1	6.8			1.2
Methylorange m		13.2	28.0	36.8		38.0	33.1
Control of:							
Iron tot. Fe^{2+}							
Sodium Na		pos.				strong pos.	strong pos.
Potassium		trace				trace	trace
Oxygen							
Calculated (mg/l):							
Sodium bicarbonate $NaHCO_3$		743	2110	1820		3145	2542
Sodium carbonate Na_2CO_3		212	117	720			127
Calcium carbonate Ca_2CO_3		7					22
Sodium sulphate Na_2SO_4			563	333		69	27

An overview of hydraulic conductivity ranges and porosities for the host rock and the discontinuities are presented in Table 8 /NGB 85-07/. The additional data used for the gas transport calculations in the host rock are given in Chapter 5.

Table 8. Hydraulic conductivities and porosities for Oberbauen Stock

	Hydraulic conductivity (m/s)	Porosity (%)
Host rock, large scale	10^{-10}-10^{-8}	3
Lineaments	10^{-9}-10^{-7}	3
Decompressed zone	10^{-10}-10^{-7}	4

3. GAS FORMATION

3.1 Gas formation processes in general

Gas in a type B repository is mainly formed by three different processes:

- Corrosion of metals present in the waste, the waste containers, storage containers and repository structures.
- Microbial degradation of organic constituents of the waste and the conditioning materials.
- Radiolytic decomposition of water and organic materials.

The three processes are first treated independently under separate headings. For each of these the mechanisms are identified, the data used are discussed and the resulting gas formation is presented.

Finally, in a separate section, the results are combined into a total gas formation comprising all processes and the whole repository. This total is used as an input for the gas transport calculations.

3.2 Corrosion

3.2.1 General

Corrosion of metals is the most important mechanism for gas formation in a type B repository.

Large amounts of metals will be present:

- The waste itself will contain steel, aluminium and zinc.
- Steel drums are used as containers for nearly all the waste.
- The concrete containers used as overpack for all the waste drums are reinforced with steel.
- Steel bars are also used as reinforcement in the lining and other structures of the repository.

The contribution of steel from the above sources to the total steel content in the repository is illustrated in Figure 3.

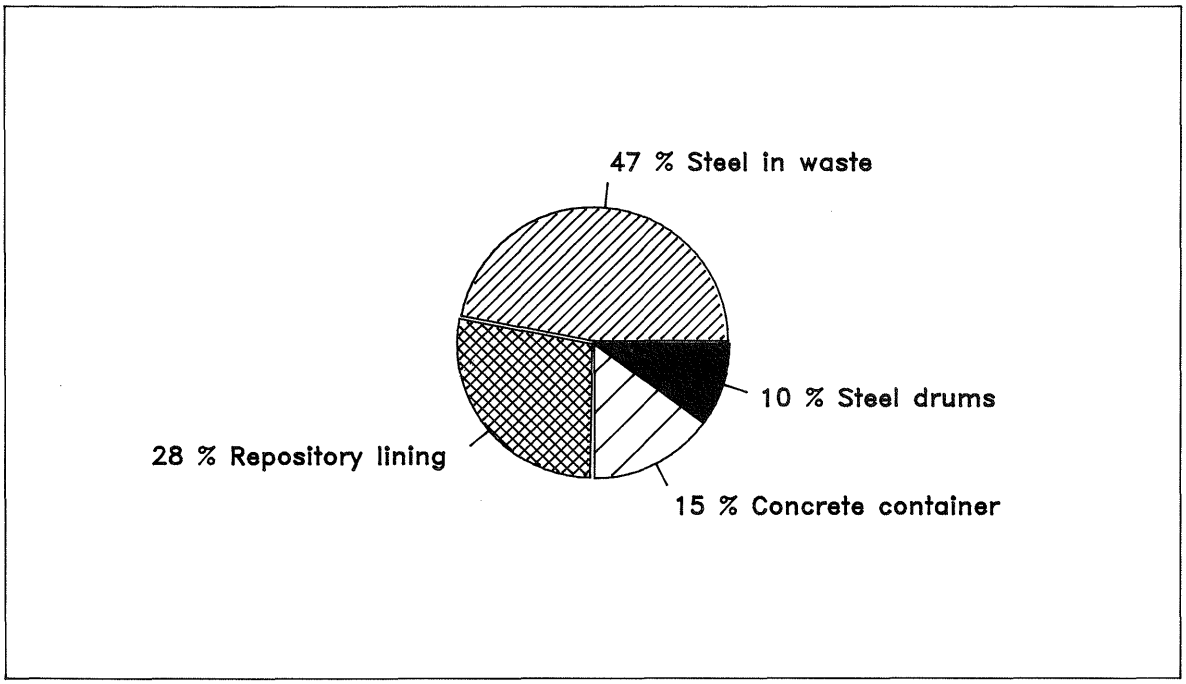

Figure 3. Distribution of the steel content in the repository /NGB 85-02/

Two different corrosion processes exist. Which one will take place depends on the environmental conditions.

During the initial period after closure of the repository, the environment will be aerobic as large volumes of air will be present in pores and voids in the repository. During this period, the corrosion of metals will not yield any gas as a reaction product. The corrosion mechanisms and corrosion rates are presented in Section 3.2.2.

The oxygen will be consumed both by corrosion and by microbial activities (Appendix A). As the groundwater in the surrounding rock is free from oxygen (see Section 2.1.3, Table 7), no oxygen supply will exist and the environmental conditions in the repository will change and become anaerobic and formation of hydrogen will begin. Corrosion mechanisms and reported corrosion rates for anaerobic conditions are presented in Section 3.2.3.

The total content of metals in the repository defines the maximum amount of hydrogen that can theoretically be formed.

The rate at which the gas is formed is a product of the metal surface available for corrosion and the corrosion rate per unit surface area.

The corrosion rates used are presented and discussed in Section 3.2.4.

The quantitative estimation of gas formation due to corrosion is presented in Section 3.2.5 and accompanied by a discussion of sensitivity to chosen assumptions.

3.2.2 Aerobic corrosion mechanisms and rates

Initially, oxygen is present in the repository. Iron corrodes under aerobic conditions according to the following reaction /2/.

$$Fe(s) + H_2O + 1/2\ O_2 \Rightarrow Fe(OH)_2(s) \quad (R3-1)$$

This process is relatively fast in the case of carbon steel, whereas stainless steels are passivated by an oxide film. The corrosion of carbon steel, aluminium and microbial degradation of organic materials (predominantly cellulose) will consume the initial amount of oxygen rapidly. In Appendix A the duration of the aerobic phase is estimated at less than 10 years and partly even less than one year. The time depends very much on the type of waste and containers and may therefore be different in different areas of the repository. The groundwater flowing into the repository is reported to contain ferrous iron as well as sulphides, which is a strong indication that the water is reducing. This means that when the initial amount of oxygen has been consumed, no more oxygen will be transported to the repository.

Significant amounts of aluminium and also some zinc are present in the waste. Both metals corrode at a high rate in a strongly alkaline environment. As zinc is present as a thin surface protective layer, it will be completely consumed shortly after being exposed to concrete-controlled pore-water.

This may also apply to thin aluminium objects, since corrosion in an aerobic, alkaline environment is fast /3/. As the corrosion rate of objects embedded in concrete might be slower, it has, for the sake of conservatism, been assumed in the gas transport calculations that 50% of the corrosion of aluminium takes place after the closure of the repository, during the anaerobic period, see Section 3.2.3.3.

Table 9. Reported corrosion rates under aerobic conditions

Material environment	Rate mm/year	Ref.
Carbon steel in chloride-free concrete	$4 \cdot 10^{-5}$	/4/
Carbon steel in chloride-containing concrete	$2 \cdot 10^{-3}$	/4/
Carbon steel pitting corrosion	10^{-2} - 10^{-1}	/5/
Aluminium 0.2N Na_2CO_3 T 17-20°C	1.6	/3,6/
Aluminium 0.2N NaOH T 17-20°C	$3.9 \cdot 10^{1}$	/3,6/
Zinc 0.2N Na_2CO_3 17-20°C	$1.0 \cdot 10^{-2}$	/3,6/
Zinc 0.2N NaOH 17-20°C	$2.5 \cdot 10^{-1}$	/3,6/

3.2.3 Anaerobic corrosion mechanisms and rates

3.2.3.1 Mechanism for iron corrosion

In the repository, the expected temperature is around 25°C and the pH will initially be about 13, but will decrease in time to about 10.5.

From a thermodynamic point of view, the ultimate corrosion product should, in the alkaline region, be magnetite formed in the overall anodic reaction:

$$3\ Fe + 4\ H_2O \leftrightharpoons Fe_3O_4 + 8\ H^+ + 8\ e^- \qquad (R3\text{-}2)$$

For the iron-water system, two equilibrium diagrams are given by Pourbaix /7/ (Figures 4 and 5, based on $Fe(OH)_2$ and Fe_3O_4 as reaction products respectively).

The dashed lines express the reduction equilibrium of water according to the reaction $H_2 = 2H^+ + 2e^-$ at a hydrogen pressure of 1 atm.

The continuous lines marked with 10^0, 10^{-2}, 10^{-4} and 10^{-6} represent the value of the concentration (activity) in moles/l of the dissolved iron compound, in equilibrium with the solid substance.

The lines between two solid substances express the equilibrium condition between the solid substances in question.

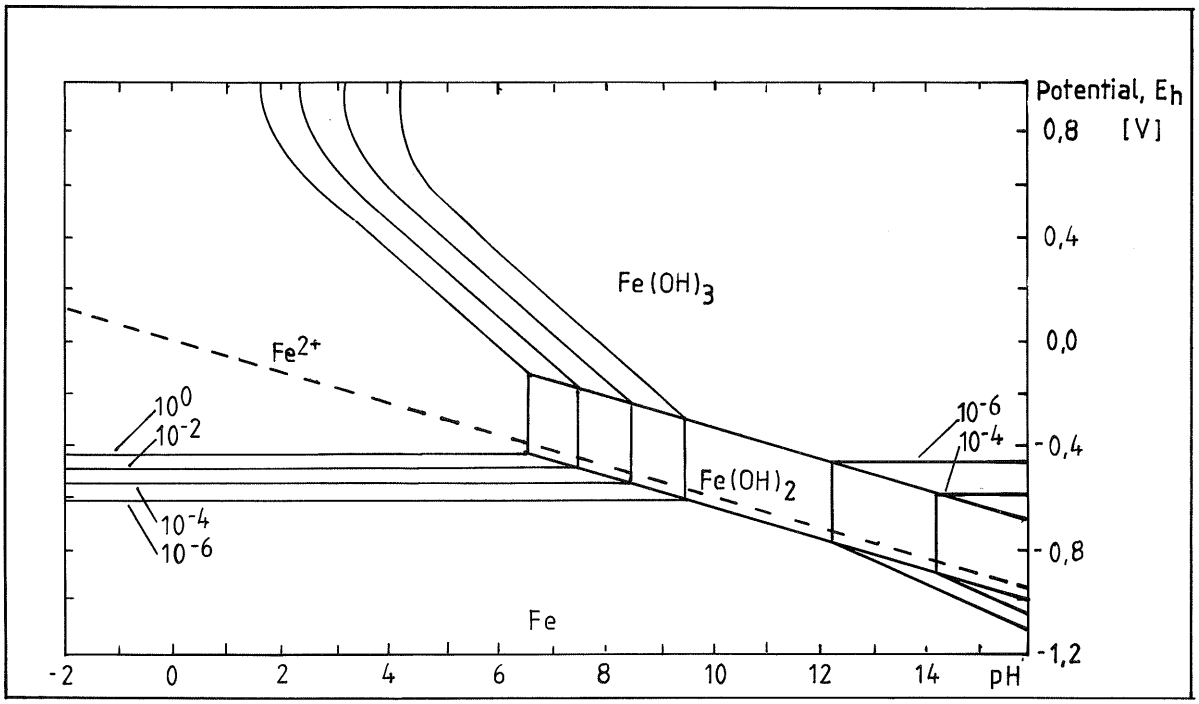

Figure 4. Potential/pH equilibrium diagram for the system iron-water at 25°C (considering Fe, $Fe(OH)_2$ and $Fe(OH)_3$ as solid substances). From reference /7/.

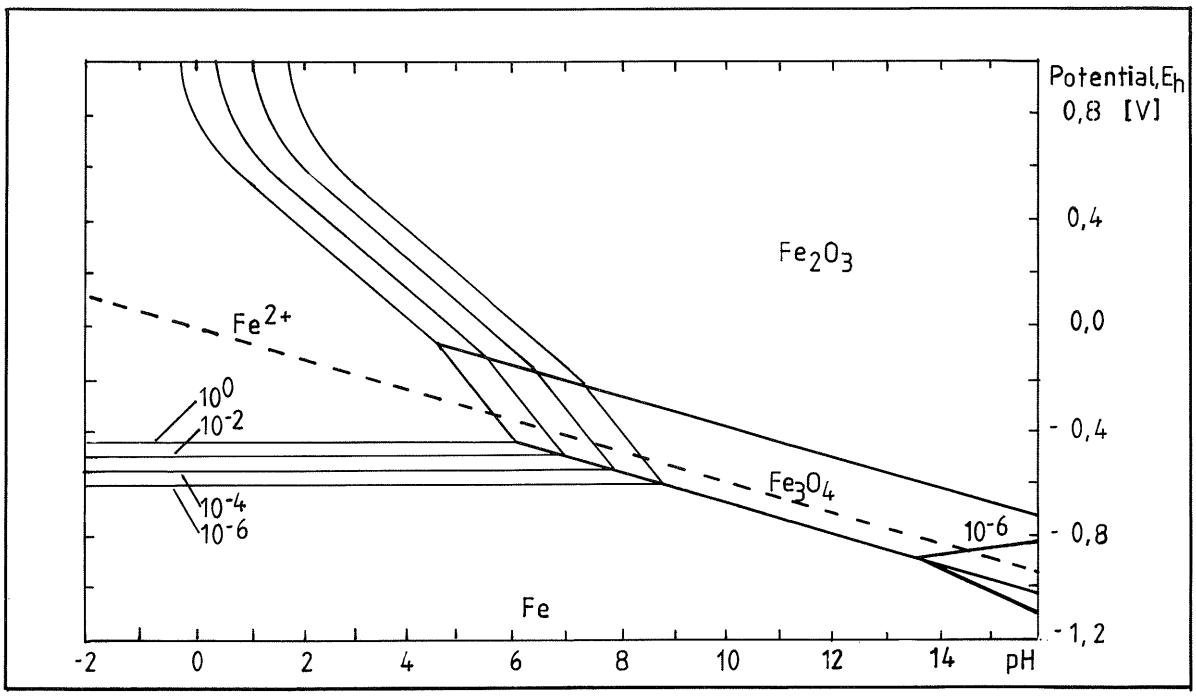

Figure 5. Potential/pH equilibrium diagram for the system iron-water at 25°C (considering Fe, Fe_3O_4 and Fe_2O_3 as solid substances). From reference /7/

If these two diagrams are combined, it seems that Fe_3O_4 is found at a lower electrode potential than $Fe(OH)_2$. According to the equilibrium formulae for iron and its oxides and hydroxides, it is however /7/ not clear whether $Fe(OH)_2$ or Fe_3O_4 is the primarily formed substance on corrosion of iron.

Recent publications suggest revision of the potential-pH-diagram for iron given by Pourbaix /7/. Silverman /8/ has re-derived these diagrams from data presented by Baes and Mesmer /9/. The modification consists of a new region of solid $Fe(OH)_2$ between the regions of stability for Fe and Fe_3O_4 (Figure 6).

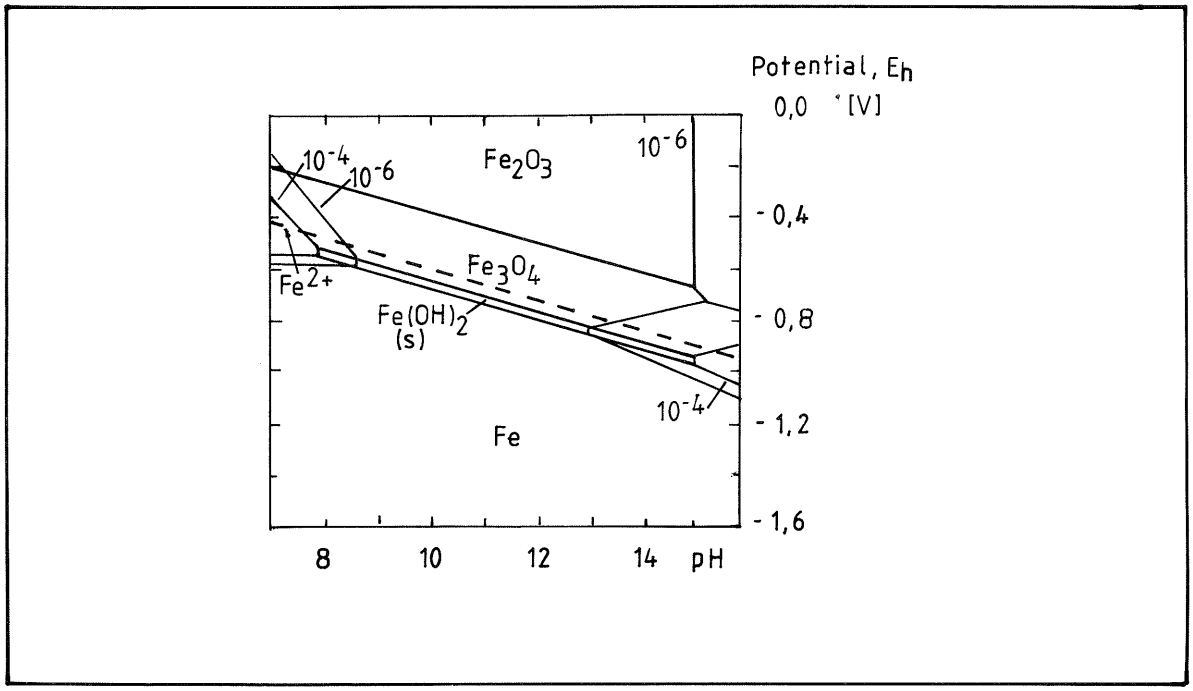

Figure 6. Potential/pH equilibrium diagram for the system iron-water at 25°C (considering Fe, Fe_3O_4 and Fe_2O_3 as solid substances). From reference /8/

Other experimental studies of corrosion of iron have confirmed that the primary corrosion product in the anodic reaction at temperatures below 60°C in oxygen-free solutions /10/ is $Fe(OH)_2$;

$$Fe + 2\ H_2O \langle = \rangle Fe(OH)_2 + 2\ H^+ + 2\ e^- \qquad (R3\text{-}3)$$

The $Fe(OH)_2$ can, in a second step, be transformed into Fe_3O_4 by the reaction:

$$3\ Fe(OH)_2 \ <=>\ Fe_3O_4 + 2\ H_2O + 2\ H^+ + 2\ e^- \qquad (R3\text{-}4)$$

The last reaction is probably kinetically hindered at temperatures below 60°C /10/.

The formation of a layer of $Fe(OH)_2$ affects the corrosion rate. Stepina and Iofa have shown(/11/, /9/) with electrochemical experiments that the anodic current decreases with time proportionally to $t^{-1/2}$. The $Fe(OH)_2$-layer is rather porous and will most probably not lead to passivity but rather reduce the corrosion rate.

The simultaneous cathodic reaction is;

$$2\ H_2O + 2\ e^- \ <=>\ H_2(g) + 2\ OH^- \qquad (R3\text{-}5)$$

which generally occurs in two steps /12/

$$H_2O + e^- \ <=>\ H + OH^- \qquad (R3\text{-}5a)$$

$$H_2O + H + e^- \ <=>\ H_2(g) + OH^- \qquad (R3\text{-}5b)$$

The hydrogen pressure has an effect upon the kinetics of the dissociation reaction:

$$H_2 \ <=>\ 2\ H_{ads} \qquad (R3\text{-}6)$$

In an underground repository with hydrostatic pressure from the groundwater, the hydrogen pressure is substantially higher than 0,1 MPa, which gives a lower electrode potential for the hydrogen electrode. An increased hydrogen pressure leads to a reduced driving force for the corrosion reaction. At a pressure above 4MPa and room temperature, the formation of $Fe(OH)_2$ would be inhibited. However, in the repository at Oberbauen Stock, the maximum hydrogen pressure that can be expected is in the range of 1-3 MPa, meaning that the rate of corrosion could decrease, but will not stop completely.

3.2.3.2 Concluding remarks regarding corrosion mechanisms and rates

The first step in the anodic dissolution of iron is most probably the formation of $Fe(OH)_2$. The corrosion rate of iron at temperatures less than 50°C and atmospheric pressure in concrete is probably in the range of 10^{-4}-10^{-3} mm Fe per year. This corresponds to a hydrogen evolution of $3.7 \cdot 10^{-4}$ - $3.7 \cdot 10^{-3}$ m^3 (STP) H_2/m^2,year /12/. An increased hydrogen pressure and growing layers of $Fe(OH)_2$ is expected to lead to a reduced driving force for the corrosion reaction and thereby reduce the corrosion rate, but by how much is not known.

Reported corrosion rates for steel in concrete are summarized in Table 10.

Table 10. Reported corrosion rates for steel under anaerobic conditions

Corrosion rates measured in an alkaline environment	Corrosion rate mm/year	Method of analysis	Ref.
Steel embedded in Portland cement or massive cement at 45°C	10^{-4} - 10^{-3}	Potentio-metric	/13/
Steel in water, CO_2-pressure: 0.1 MPa at 25° C	$7 \cdot 10^{-2}$	H_2-measurement	/NTB 83-16/
Unalloyed steel and cast iron in aerated sea water at 90° C	$8 \cdot 10^{-3}$	Gravimetric	/3/
Steel in concrete	10^{-3} - 10^{-2}	Estimation	/5/
Stainless steel in concrete	10^{-3}	Estimation	/5/

3.2.3.3 Corrosion mechanism of other metals

Aluminium is, under normal conditions, protected against corrosion by a layer of oxide. At high pH, the aluminium oxide is soluble and the protection is lost as indicated in reaction (R3-7). This explains the high corrosion rates presented in Table 9 in Section 3.2.2 and in Table 11.

$$2\ Al + 2\ OH^- + 2\ H_2O \leftrightarrows 2\ AlO_2^- + 3\ H_2 \quad (R3\text{-}7)$$

Table 11. Reported corrosion rates for zinc and aluminium under anaerobic conditions

Material, environment	Temperature	Rate (mm/year)	Ref.
Aluminium 1% Na_2CO_3 (nitrogen gas)	room temperature	4.5	/14/
Aluminium 0.1% NaOH (nitrogen gas)	room temperature	$1.6 \cdot 10^{1}$	/14/
Zinc water	room temperature	$3.0 \cdot 10^{-2}$	/14/

3.2.4 Data used

The calculation of the amount of hydrogen generated in the repository under anaerobic conditions requires the following information:

- The surface area of corroding metals. This is obtained by multiplying the weight of the different groups of metal items with a surface area to mass ratio for the items.

- The corrosion rate expressed in mass per unit surface area and year.

- A constant showing the amount of hydrogen generated per unit mass of corroded metal, obtained by combining the stoichiometry of the reaction with the density of the metal.

The weight of typical metal items is obtained from the inventory /NGB 85-02/ and presented in Table 12. No range of uncertainty was assumed for these figures except for the decrease in the amount of "steel in waste" introduced in the revised December 1984 inventory /NTB 84-47/.

The surface area to mass ratios are presented in Table 13. An estimated degree of uncertainty is also indicated in the Table.

The total surface area of the steel drums is large but well-known. Some uncertainty exists regarding the quantity and dimensions of reinforcement bars. For the last two items in Table 13, the figures represent estimates based on the types of waste present, e.g. pumps, tools.

The corrosion rates used in the calculations as presented in Table 14 are extracted from Tables 10 and 11. The minimum values are based on the observation that corrosion decreases with time. The expected influence of the hydrogen pressure within the repository and the formation of corrosion products at the metal surface are also taken into account.

To calculate the theoretical volume of hydrogen generated per unit of weight of iron, the following reaction is used (R3-8):

$$3\ Fe + 4\ H_2O \Rightarrow Fe_3O_4 + 4\ H_2 \qquad (R3\text{-}8)$$

which is the sum of the reactions (R3-3) and (R3-4) above.

Table 12. Total weight of the different groups of metal items in the repository

Metal items	Total weight (tonnes)
Steel drums in concrete	13,600
Steel drums in bitumen	800
Steel drums in plastic	100
Reinforcement in drums	730
Steel in waste	66,100 (50,800)*
Aluminium and zinc	600
Reinforcement in concrete containers	22,100
Reinforcement in repository liner	40,100

* The December 1984 inventory /NTB 84-47/.

Table 13. The surface area to mass ratios (m^2/kg)

	Surface/mass		
	Minimum	Base case	Maximum
Aluminium	$1 \cdot 10^{-2}$	$1 \cdot 10^{-2}$	$1 \cdot 10^{-2}$
Steel drums	$1.7 \cdot 10^{-1}$	$1.7 \cdot 10^{-1}$	$1.7 \cdot 10^{-1}$
Reinforcement	$3.2 \cdot 10^{-2}$	$4.3 \cdot 10^{-2}$	$4.3 \cdot 10^{-2}$
Decommissioning waste	$5 \cdot 10^{-3}$	$5 \cdot 10^{-3}$	$7 \cdot 10^{-3}$
Operational, reprocessing and MIF waste	$1 \cdot 10^{-2}$	$1 \cdot 10^{-2}$	$5 \cdot 10^{-2}$

Table 14. Selected corrosion rates (mm/year)

	Minimum	Base case	Maximum
Steel drums in concrete	10^{-5}	10^{-4}	10^{-3}
Steel drums in bitumen	10^{-4}	10^{-3}	10^{-3}
Steel drums in plastic	10^{-4}	10^{-3}	10^{-3}
Reinforcement in drums	10^{-5}	10^{-4}	10^{-3}
Steel in waste	10^{-5}	10^{-4}	10^{-3}
Aluminium	1	1	1
Reinforcement-concrete containers	10^{-5}	10^{-4}	10^{-3}
Reinforcement-repository lining	10^{-5}	10^{-4}	10^{-3}

3.2.5 Quantitative estimation of gas formation

The calculated amounts of gases formed are presented in Table 15 and Figures 7 and 8.

- Table 15 gives the theoretical volumes of hydrogen which can be generated by total corrosion of each of the different groups of metal items in the repository.

- Figure 7 illustrates the rate of hydrogen generation from each of these groups of metal items and the time for complete corrosion.

- Figure 8 shows the total accumulated volume of gas formed. The expected range of uncertainty is also indicated.

From Table 15 it can be seen that the steel waste and the reinforcement bars are the most important potential sources of hydrogen.

Table 15. Theoretical amounts of gas formed by complete corrosion of different groups of metal items in the repository

Origin of metal	Total theoretical volume m^3 (STP) of gas
Steel drums in concrete	$7.2 \cdot 10^6$
Steel drums in bitumen	$0.4 \cdot 10^6$
Steel drums in plastic	$0.05 \cdot 10^6$
Reinforcement in drums	$0.39 \cdot 10^6$
Steel waste	$35 \cdot 10^6$ $(27 \cdot 10^6)$*
Aluminium and Zinc	$0.74 \cdot 10^6$**
Reinforcement-concrete containers	$12 \cdot 10^6$
Reinforcement-repository lining	$21 \cdot 10^6$
Whole repository	$77 \cdot 10^6$ $(69 \cdot 10^6)$*

* The December 1984 inventory /NTB 84-47/
** 50% of this volume is produced before storage

Figure 7 illustrates that the steel waste contributes very little to the rate of gas production during the most important period of time. This is due to the low rate of corrosion and a small specific surface area.

During the first 20 years, the content of aluminium may be of predominant importance but there is considerable uncertainty on this point.
If the corrosion rates obtained with tests in solutions of the same pH as in concrete are applied, the aluminium will be consumed shortly after being brought in contact with the concrete and almost all the hydrogen will be released before closure of the repository. In the calculations, it has therefore been assumed that the aluminium content has corroded to 50% before closure of the repository. It is, however, possible that corrosion is much slower when

aluminium is embedded in concrete.

After the first 20 years, the predominant source of gas production is the corrosion of steel drums and reinforcement bars. Some of the drums (those with an organic materials matrix) are assumed to corrode faster than those protected by a concrete layer on both sides of the steel sheet.

The change in the inventory regarding the steel waste as indicated in Table 12 has a very marginal effect. The uncertainty in the amount of reinforcement bars is more important.

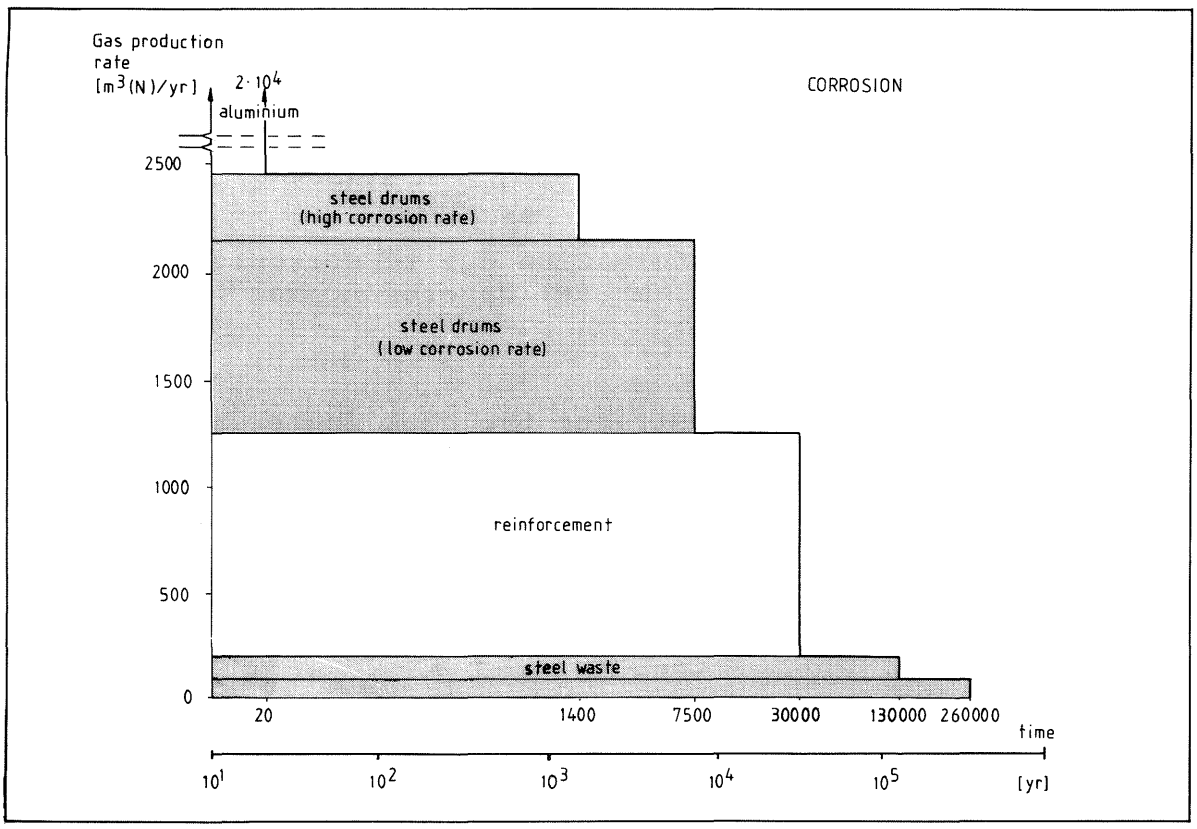

Figure 7. Annual rate of gas formation for different metals in the waste, base case; m^3 (N) denotes normal cubic metres at STP

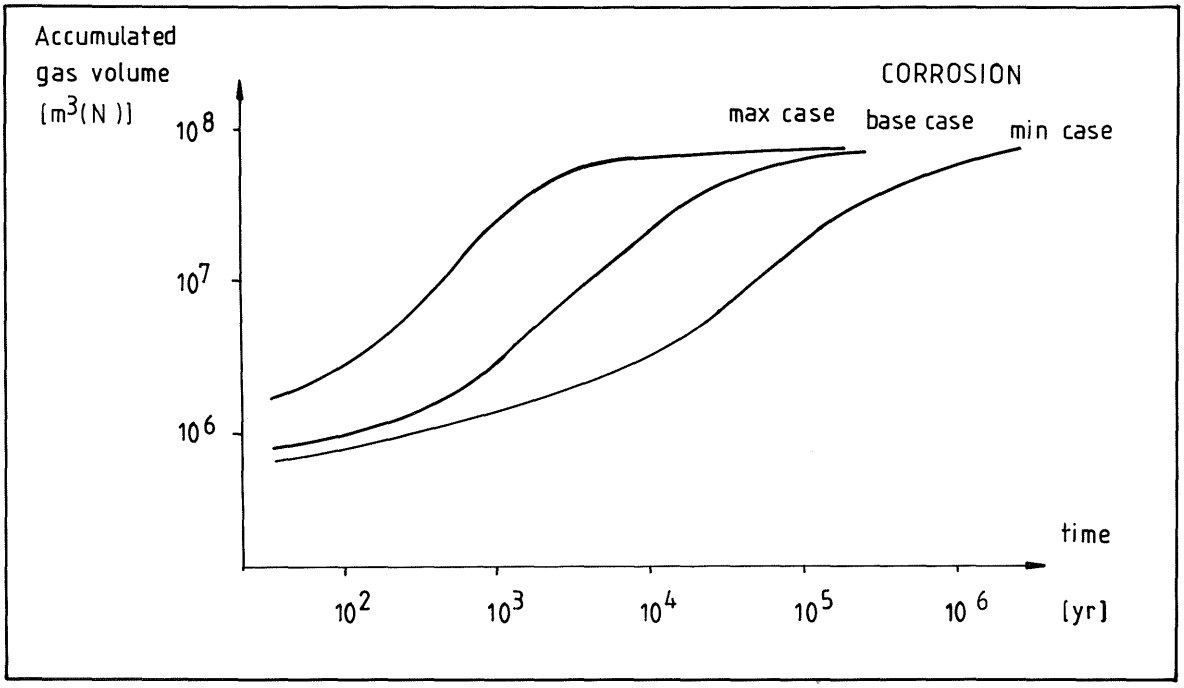

Figure 8. Accumulated gas formation due to corrosion for the whole repository. m^3 (N) denotes normal cubic metres at STP

Figure 8 also illustrates the high degree of uncertainty in the gas production figures. The difference between the lowest and highest estimates of accumulated volumes varies from a factor of 3 in the beginning to a factor of 50 after 5,000 years.

3.3 Microbial degradation

3.3.1 General

In the following sections, the possibility of microbial activity and the influence of this on a repository are discussed.

Microorganisms are uni- or multicellular organisms comprising bacteria, viruses, actinomycetes, fungi, algae and protozoa. Degradation of materials is caused by microorganisms oxidizing organic or inorganic material in order to utilize the energy released. In addition, an oxygen source, water and some nutrients are required for microbial activity.

As long as free oxygen is present, this will be the prime oxygen source in the local environment. When the free oxygen is consumed, other microorganisms which use chemically bound oxygen, e.g. oxygen bound in nitrate, sulphate or carbon dioxide, take over. In each individual reaction in the sequence of degradation of organic material, specialized species of microbes utilize the energy released.

Microorganisms will almost always be present in the environment. Species have been observed growing in extremely hot ($>+100^{o}C$) or cold ($<-2^{o}C$) environments, at high pressure (180 MPa) or high salinity (>50 wt% salt) /15/.

Although the pH interval 6-8 is most favourable for microbial activity, species exist which are active both at pH 13 and pH 0. Several microorganisms can also tolerate radioactive doses up to high levels.

There are three aspects which can have a bearing upon the long-term behaviour of the repository:

- Gases produced by microbial degradation, such as hydrogen and methane, and gases produced by other processes can contribute to the displacement of contaminated pore-water from the repository.

- Production of organic compounds, such as organic acids and alcohols, which can act as complexing agents or otherwise increase the mobility of radionuclides in the repository. This subject is treated by Allard in reference /NTB 85-19/.

- Decrease in pH in the local environment, which is a result of the production of carbon dioxide from microbial degradation, will have an influence on the chemical and biological processes in the repository. The carbon dioxide formed will be absorbed by the concrete and the concrete pore-water. This may result, at least locally, in a lower pH, which may increase the rate of corrosion and, thereby, the production of hydrogen.

The highest rate of degradation with existing environmental conditions occurs when the organic material and water are being mixed. The microorganisms have a maximum availability of the compounds necessary for their metabolism. When no mixing occurs, micro-environments are formed where the rate of degradation will be determined by the local availability of nutrients and water. In an alkaline environment, on the other hand, a more favourable local environment for microorganisms will be formed since the carbon dioxide produced will reduce the pH. This can facilitate growth of other species of microorganisms.

The principal course of events is that large molecules, e.g. fats, proteins and hydrocarbons, degrade to smaller molecules. The decomposition reactions result in products such as organic acids and gases, as described in Section 3.3.2. The final products are carbon dioxide, hydrogen, methane and hydrogen sulphide. If the environment is alkaline and/or if iron is present in the solution, the sulphur forms FeS instead of H_2S, until most of the ferrous ions are used up.

Both the pH and the redox potential (pe) decrease continuously during degradation; see Figure 9. The pH decreases because of hydrolysis of the generated carbon dioxide. The redox potential decreases due to consumption of the oxidizing agents. The first oxidizing agent consumed is free oxygen, which is the easiest to reduce. When all free oxygen is consumed, nitrate is reduced to ammonia and other nitrogen compounds. In the final stages of degradation, other microorganisms will reduce sulphate to sulphide, as well as carbon dioxide and hydrogen to methane.

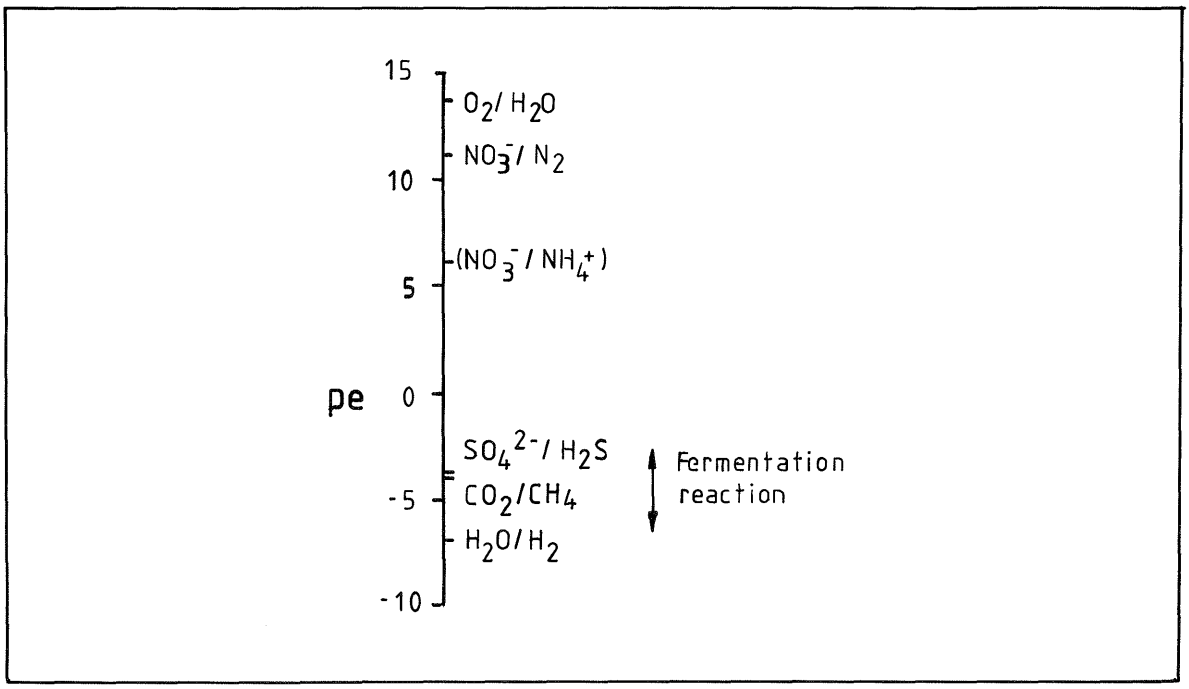

Figure 9. Approximate redox potential at which various redox reactions occur in water at pH 7 and 25°C /16/

3.3.2 Microbial degradation mechanisms

Different degradation mechanisms are possible, depending on the redox potential. These reactions are presented in Figure 9, showing the sequence which can be expected in a closed repository and the approximate redox potential at which the individual reactions will occur.

3.3.2.1 Aerobic conditions

The degradation of hydrocarbons in an aerobic environment consumes the free oxygen and converts hydrocarbons into compounds with lower molecular weight. An example of this is shown according to Rennerfelt /17/ for the degradation of asphalt:

$$n(C_{71}H_{104}ONS)+100O_2 \Rightarrow 71CO_2+NO_3^-+SO_4^{2-}$$
$$+52H_2O+\text{energy} \qquad \text{(R3-9)}$$

The redox potential is about 14 when free oxygen is present; see Figure 9. The aerobic degradation of hydrocarbons and the corrosion of metals will consume the oxygen present in the repository in a few years time (Appendix A). In repository sections with a large content of organic material and steel, the aerobic period may last for only a few months.

3.3.2.2 Anaerobic conditions

When oxygen is consumed, pe decreases and denitrification reactions will start; see Figure 9. In these reactions the microorganisms will use the nitrate ions to oxidize organic carbon to CO_2. In this way the nitrate ions are reduced in a complex series of reactions as indicated below.

$$NO_3^- \rightarrow NO_2^- \rightarrow NO \rightarrow N_2O \rightarrow N_2 \qquad \text{(R3-10)}$$
$$\searrow NH_4^+$$

The stoichiometry of the most important reaction is:

$$2.5\ C_{org} + 2\ NO_3^- + 2\ H^+ \Rightarrow N_2 + 2.5\ CO_2 + H_2O \qquad \text{(R3-11)}$$

Nitrite can also be reduced to ammonia according to the following reaction:

$$2\ H^+ + NO_2^- + H_2O \Rightarrow NH_4^+ + 1.5\ O_2 \qquad \text{(R3-12)}$$

At pe below zero (-3 to -4), the microorganisms start to reduce sulphate, oxidizing organic material to CO_2 and producing sulphide or sulphur complexes as by-products. The stoichiometry of the reaction is:

$$SO_4^{2-} + 2\ C_{org} + 2\ H_2O \Rightarrow H_2S + 2\ HCO_3^- \qquad \text{(R3-13)}$$

Since the reaction products are acidic compared to an alkaline concrete water, they react further and form HS^- and CO_3^{2-}. Organic material is also degraded during formation of CO_2 according to the following general reaction:

$$\text{organic compound A} \Rightarrow \text{organic compound B} + CO_2 + H_2 + CH_4 \qquad \text{(R3-14)}$$

The simplest (and one of the most important) is methane generation

$$^{2}C_{org} + 2\ H_2O \Rightarrow CO_2 + CH_4 \qquad (R3\text{-}15)$$

According to Wetzel /18/, 70 % of the methane gas originates from this reaction, and the remainder from the reaction between hydrogen and carbon dioxide:

$$CO_2 + 4H_2 \Rightarrow 2H_2O + CH_4 \qquad (R3\text{-}16)$$

This happens when pe is about -4.

3.3.2.3 Products

Figure 10 shows the intermediate products and the gases finally produced by microbial anaerobic digestion /19/. Phase 1, which is faster than Phase 2, results in the formation of alcohols, different acids, hydrogen and carbon oxides. These gases can then react to form a new gas, methane. The other intermediate products decompose to form methane and carbon dioxide.

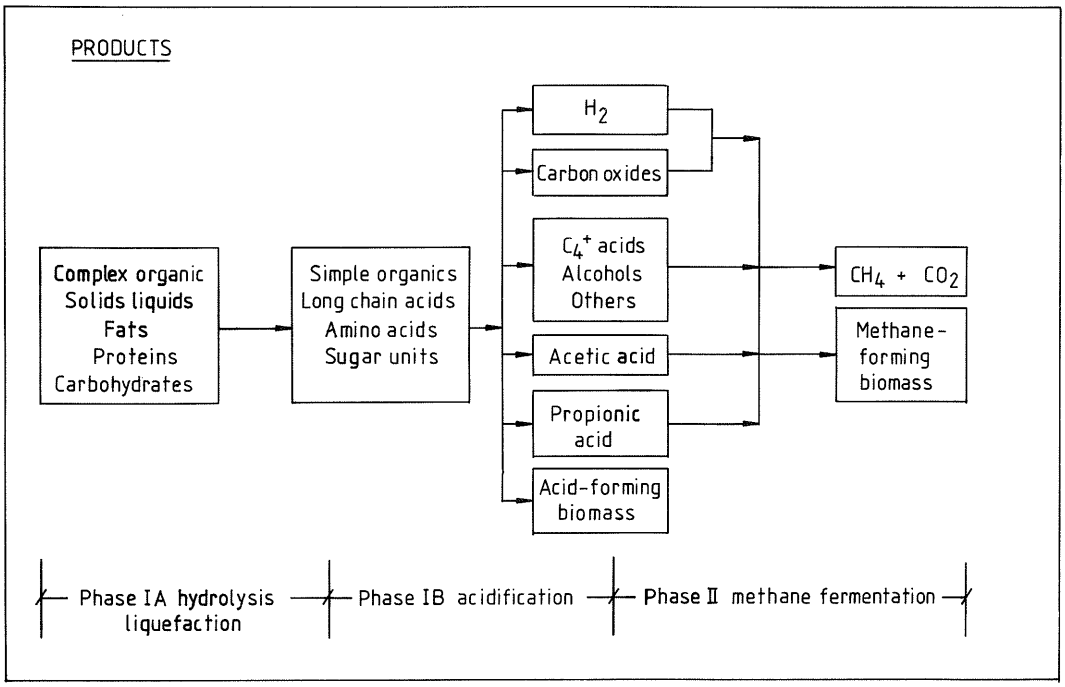

Figure 10. Microbial phases in anaerobic digestion /19/.

In the conversion of carbohydrates, carbon dioxide and methane are produced according to the consecutive reactions:

$$(C_6H_{10}O_5)_x + x\ H_2O \langle=\rangle x\ C_6H_{12}O_6 \langle=\rangle 3x\ CH_4 + 3x\ CO_2 \quad \text{(R3-17)}$$

The theoretical amount of gas formed by these reactions is 6 moles of dry gas for each 162 g of cellulose fermented /20/. This corresponds to 37 moles or 830 l(STP) of gas per kg cellulose. The experimental yield /21/ is usually around 40-50% of the theoretical yield and is reported to contain about 60% methane and 40% carbon dioxide /21/, /22/, /23/. This indicates that the degradation mechanisms are not fully understood and that reactions other than those shown in (R3-17) may exist.

3.3.3 Microbial degradation rates

The oxygen present will be consumed before or shortly after the closure of the repository. Therefore, only anaerobic degradation will be considered in the gas formation calculations.

The materials which can serve as organic nutrients and are present in substantial quantities are cellulose, bitumen, ion exchange resins and plastics of different compositions.

For all these materials, qualitative evidence seems to show that they can be attacked by microorganisms under anaerobic conditions. Information about the rate of degradation is, however, limited.

Cellulose is readily consumed due to the large surface available and to favourable chemical composition. Quantitative information about the rate is given in the Sandia reports /24, 25/ and in the report by Rennerfelt /17/. In the Sandia reports, gas generation rates are measured for different wastes containing cellulose. The production rates are in terms of moles of gas generated per drum and year.

From this existing data, degradation rates in terms of moles of gas per year and kg cellulose have been derived.
All investigations of microbial degradation of bitumen indicate that such an attack exists /17,26, NTB 83-18/. This is also supported by observations of other petrol components /15/. Gas formation rates are given in the Sandia reports /24,25/.

Among the plastics, some are readily /26/ attacked by, and some are rather inert to, microorganisms e.g. polythene /24,26/. In reference /NTB 84-07/ it is said that even though plastic material has been thought of as resistant to microbial degradation, it has been shown that additives, plasticisers and antioxidants are readily degraded. In a long term aspect plastics must therefore be thought of as non-resistant to microbial degradation.

As a mixture of plastics will be present in the waste and no reported data are available, the following assumption about degradation of plastic is made. Neither the degradation rate nor the gas formation rate exceeds the rates given for bitumen.

Ion exchangers consist of a polymer, polystyrene, cross-linked with di-vinyl-benzene. Active groups are attached to the polymer skeleton and the porous structure increases the surface available to the microorganisms. No experimental data has been found, only the discussion by Rennerfelt /17/. Reported rates of microbial degradation of organic material under anaerobic conditions are presented in Table 16.

Table 16. Anaerobic degradation rates

Substance	Degradation rate moles total gas/kg,year			
	minimum	average	maximum	derived from Ref.
Cellulose				
Organic comp. (35% cellulose)	0.05	(0.1-0.4)	0.7	/25/
Plywood Box (mainly cellulose)	0.02	(0.04-0.2)	0.3	/25/
LASL comp.	0.01		0.4	/24/
Sawdust plywood (mainly cellulose)	0.03		0.2	/24/
CM-cellulose	0.0003		0.2	/24/
Bitumen				
Asphalt	0	(0.004-0.04)	0.05	/25/
Asphalt	0.002		0.04	/24/
Bitumen		(0.002-0.008)		/17/
Bitumen		(0.001)		/27/
Ion exchange resins				
		(0-0.01)		/17/

The rates from the Sandia reports /24,25/ are based on experimental investigations, while the references /17,27/ are not new research but judgements based on the Sandia investigations and other references.

3.3.4 Data used

For the calculation of the amount of gases generated by microbial degradation, the following data are needed:

- The total amount of each organic compound which will undergo degradation.
- The gas formation rate expressed as moles of total gas produced annually per kg substance.
- The distribution between different gaseous products.

The total amounts of organic materials present in the repository are presented in Table 17, which is based on the inventory of December 1984 /NTB 84-47/. This is different to the inventory of July 1984 which was used for the calculations in NGB 85-07 and NGB 85-08. The difference is that no cellulosic materials were assumed to be present in the earlier inventory.

The gas formation rates used are presented in Table 18. To indicate uncertainties in the used data also the maximum and minimum values are given.

Relative proportions of soluble (CO_2) and insoluble (H_2/CH_4) gases formed are given in the literature; see Section 3.3.2.3. The distribution is dependent on the chemical environment which is rather undefined in the waste. The assumption made about the partition is that equal amounts (moles) of soluble and insoluble gases are formed.

Table 17. Specification of total amounts (tonnes) of organic material for different waste categories

Waste category	Bitumen	Plastic	Ion exchange resin	Cellulose
Operational waste	300	100	12,200	0
Reprocessing waste	3,100	600	100	(5,300)*
Decommissioning waste	0	3,000	0	0
MIF waste	-	-	-	0
Whole repository	3,400	3,700	12,300	5,300

* The December 1984 inventory /NTB 84-47/.

Table 18. Anaerobic microbial gas formation rates used

Substance	Gas formation rate moles gas/(kg,year)		
	minimum	base case	maximum
Cellulose	0.0003	0.2	0.7
Bitumen	0	0.002	0.05
Plastics*	0	0.002	0.05
Ion exchangers*	0	0.002	0.05

* No gas formation rates are available; the same values as for bitumen have been assumed

3.3.5 Quantitative estimation of gas formation

The most important products formed by microbial degradation are the insoluble gases methane (CH_4) and hydrogen (H_2) and the soluble gas carbon dioxide (CO_2). The quantitative estimates are presented as follows:

- Table 19 presents the total amount of all these gases generated during 500 years.

- Figure 11 illustrates the rate of formation versus time for CH_4+H_2 for the different organic materials in the repository.

- Figure 12 illustrates the accumulated quantities of insoluble gases versus time for the base case and the minimum and maximum cases.

From Figure 11, the predominant role of cellulose is evident. The contributions from bitumen, plastics and ion exchange resins are minimal compared to the gas formation from the cellulose. The rate of gas formation from cellulose is also better supported by experiment.

The amount of gas formed due to degradation of cellulose is of the same order of magnitude as the amount of gas formed from the corrosion of aluminium and is therefore essential for the safety analysis.

The nuclide release calculations made for NGB 85-08 were based on an inventory in which the presence of cellulose was not yet identified. Consequently, the gas generation figures used were lower.

The carbon dioxide formed will first react with $Ca(OH)_2$ dissolved in the pore-water to form insoluble $CaCO_3$. The total quantity of CO_2 is, however, more than can react with the dissolved CaO in the pore-water present in the same part of the repository. It is, therefore, to be expected that part of the CO_2 will react with the solid concrete and cause changes in the matrix properties. These changes may result in decreased porosity and permeability and will also lower the pH.

The consequences of the rather high initial radiation level in some parts of the repository should be investigated further. It cannot be excluded that doses as high as 100 Mrad (Chapter 3.4.5) may delay the growth of some microorganisms. The decomposition will, however, only start later when the level of radiation has declined.

Table 19. Total amount of insoluble gaseous products formed by microbial degradation over a period of 500 years (Kmoles, m^3 (STP))

Waste category	(Kmoles)	m^3(STP)
Operational waste	6,300	140,000
Reprocessing waste	1,900(100,000)	43,000(2,200,000)*
Decomm. waste	1,500	34,000
MIF waste	0	0
Whole repository	9,700(108,000)	217,000(2,400,000)*

* The December 1984 inventory /NTB 84-47/

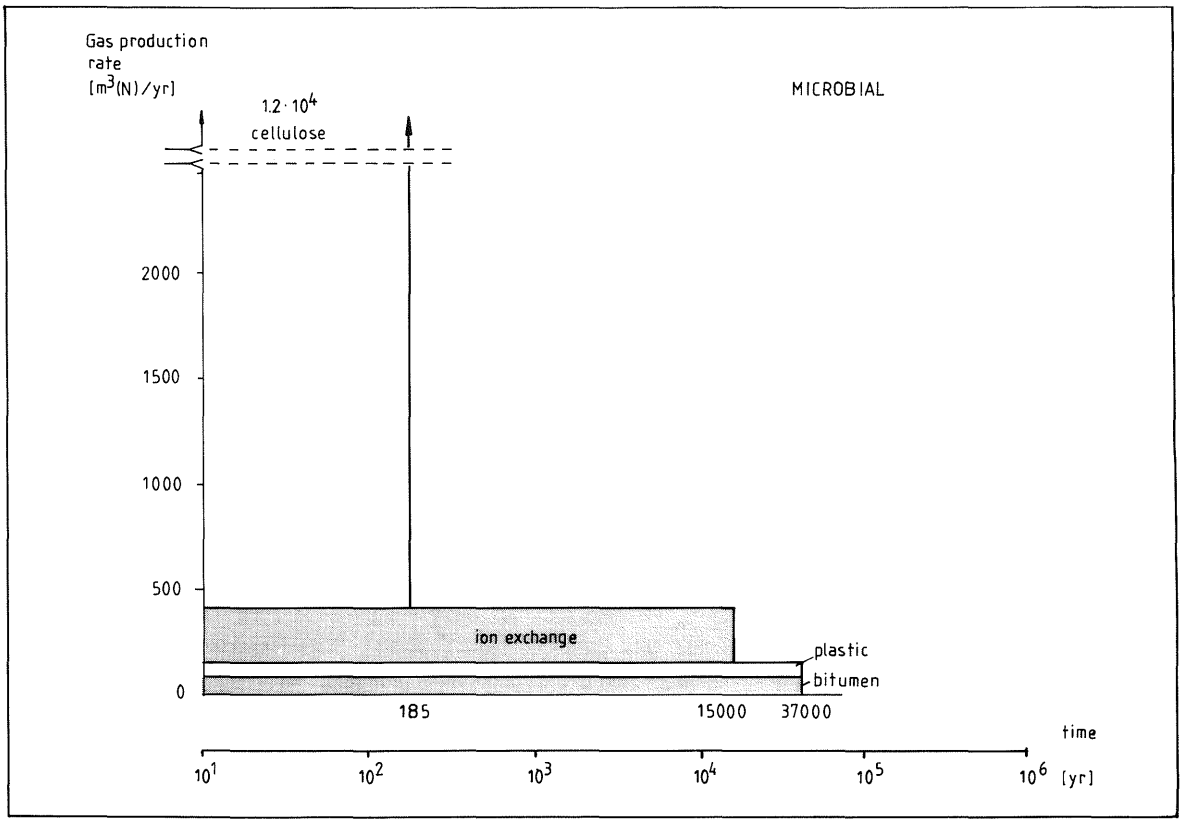

Figure 11. Annual rate of formation of insoluble gases from different organic compounds in the waste, base case. m^3(N) denotes normal cubic metres at STP

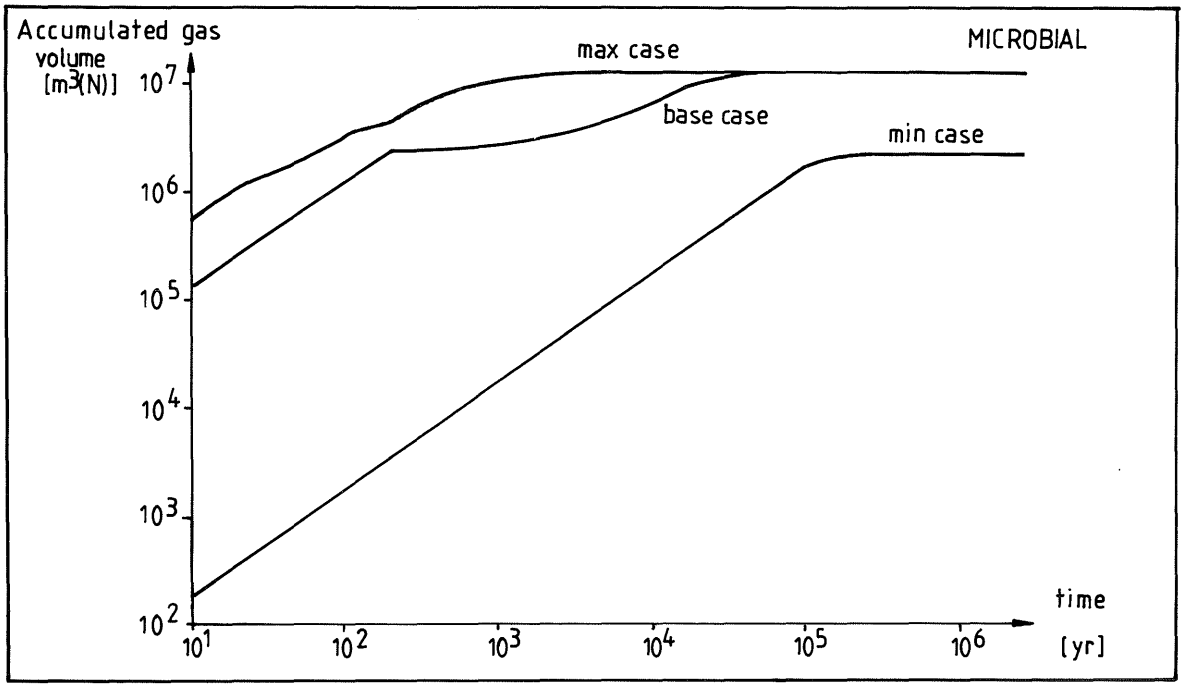

Figure 12. Accumulated gas formation caused by microbial processes for the whole repository. $m^3(N)$ denotes normal cubic metres at STP.

3.4 Radiolytic decomposition

3.4.1 General

The radionuclides present in the waste emit radiation which is absorbed by surrounding compounds. In general there are three distinct types of radiation: alpha, beta and gamma radiation. The penetrating power of each type of radiation is different. The alpha-particles will be absorbed within less than one mm in solid materials, beta-particles will reach up to 20 mm, whereas gamma-radiation will have a much greater range, somewhat dependent on its wavelength.

These types of radiation are also called ionizing radiation because they can remove electrons from an atom and, as a result, the atom is ionized. Therefore, materials which are exposed to radiation undergo a gradual change in their chemical composition. Inorganic materials are more resistant to such changes than most organic materials.

Typical chemical changes in organic ion exchange resins are that the chemical bonds in the functional groups are ruptured and groups of molecules are split off. The extent of these changes depends on both the energy of the absorbed radiation and the strength of the chemical bonds.

The materials present in the repository which could be influenced by radiation and form degradation products are water, ion exchange resins, bitumen, plastics and concrete (due to its water content). The presence of water will often increase the material degradation since radiation generates free radicals in the water which will also react with the organic molecules in this particular material.

Radiolytic decomposition has been studied experimentally for many compounds. These experiments give two pieces of information, which new compounds are formed and the quantitative relationship with absorbed energy. This relationship is called the G value and is defined as the number of species formed as a result of the absorption of 100 eV of ionizing radiation. G values can, for practical purposes, be converted into generation rates expressed as mole/Mrad,tonne. The conversion factor is close to unity.

G values have been determined experimentally and are available in the literature for most materials of interest. In Section 3.4.3, reported G values are listed with references to their origin. Unfortunately, the G values are valid only for the experimental conditions used and must therefore be applied with some caution.

The absorbed energy or dose must also be calculated for the different categories of waste. This is done by using a number of selected nuclides which contribute significantly to the dose.

The calculations show that a number of new compounds are formed. Hydrogen, H_2, is predominant among the gases but smaller amounts of SO_2, CO_2, CO and N_2 are also formed. Other products of interest are methylamines and sulphuric acid.

It is also important to observe that almost 90% of the radiolytic decomposition takes place during the first 50 years.

3.4.2 Radiolytic decomposition mechanisms

Ion exchange resin

The radiation from the incorporated waste will be absorbed by, and cause damage to, the materials present in the repository. The damage is proportional to the absorbed energy and depends upon the nature and composition of the material.

The water content in the different materials will also be of importance. During irradiation, excited and ionized water molecules are formed. The ionized water molecules then react to form hydroxyl radicals and hydrated electrons. The excited water molecules dissociate mainly into hydrogen and hydroxyl radicals. The reaction with organic materials in contact with the water is also possible.

Direct radiolysis of organic ion exchange resins causes changes which resemble effects observed in large organic polymers, as there is a basic similarity in chemical structure. Due to the presence of the ion exchanging functional groups, the similarities are, however, limited.

On exposure to ionizing radiation, macromolecular structures undergo changes such as bond breakages and bond formation. This will result in:

- changed swelling properties due to the loss or formation of bonds
- changed ion exchange properties due to the loss of functional groups
- formation of new compounds such as H_2, CO etc.

There is a difference in sensitivity to radiation between anion and cation exchangers. The percentage of active groups which are split off is smaller for cation exchange resins than for anion exchange resins, for the same absorbed radiation dose. The cation exchange resins in question are of the 'strong' type, with a sulphonate group as the active group. The radiolysis generates H_2SO_4, SO_2, H_2, CO_2 and CO as decomposition products.

The anion exchange resins are also of the 'strong' type with quarternary ammonium as the functional group. Radiolytic scission of the functional group generates mainly trimethylamine, but also lower amines and gases such as N_2, CO_2, CO and H_2. For OH^--form anion resins, trimethylamine is observed in the gas phase, while for resins in the Cl^--form and for mixed bed resins, trimethylamine is not observed as a gas, probably due to pH-dependent solubility effects. The irradiated OH^--form resin is quite alkaline, while the Cl^-, HOH and NaCl forms are acidic.

Chemical changes in ion exchange resins caused by radiation are a direct function of the total dose absorbed by the resin, but several other factors will also be of importance. These include the chemical composition of the resins, the ionic form in which they are exposed to radiation, the moisture content and the degree of cross-linkage of the macromolecular structure. This explains the lack of correlation between results from irradiation experiments.

The main experimental results are often presented in graphic form as shown in Figures 13, 14 and 15. Evidently, a straight line relationship exists up to doses much higher than those of interest for this evaluation. This allows the use of the G values. Hydrogen is the predominant gas formed (Figures 14 and 15), at least when wet products are irradiated. Other gases are usually formed at a lower yield.

The three Figures 13, 14 and 15 illustrate the importance of the water content in an ion exchanger for the amount of gas and its composition.

In sulphonic acid resin, $G(H_2)$ values for hydrogen generation in fully swollen resins are somewhat lower than would normally be expected on the basis of pure water radiolysis.

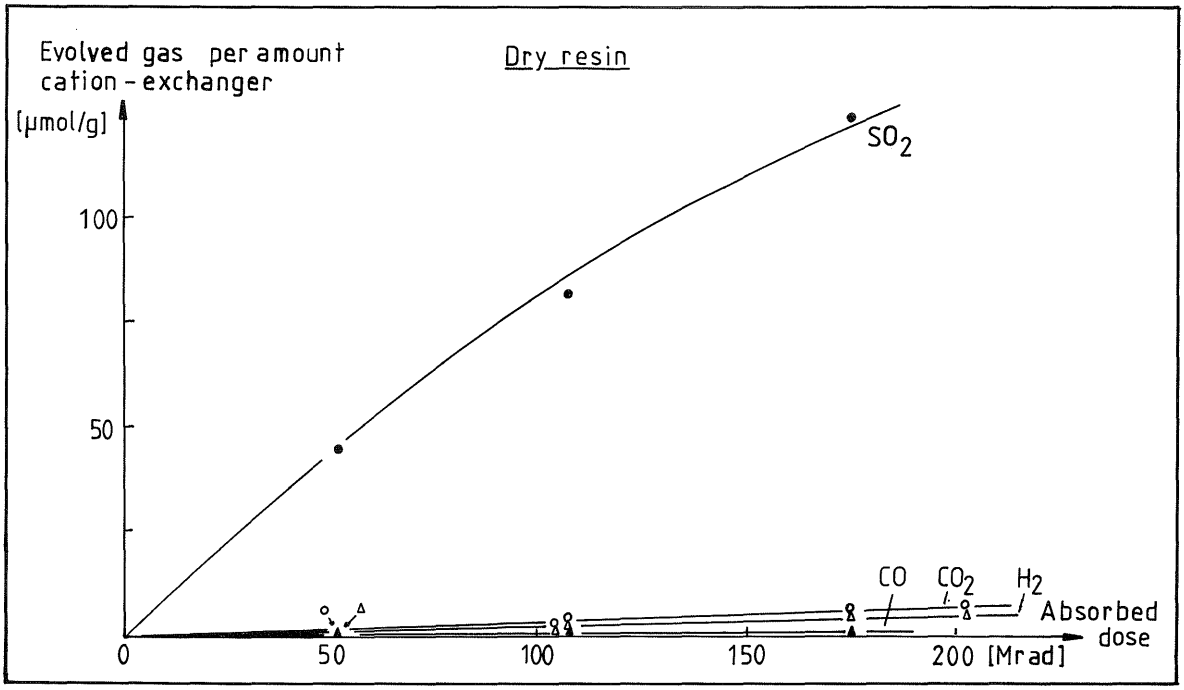

Figure 13. Gases evolved on irradiation of dry cation exchange resin. From Mohorcic et al. /28/

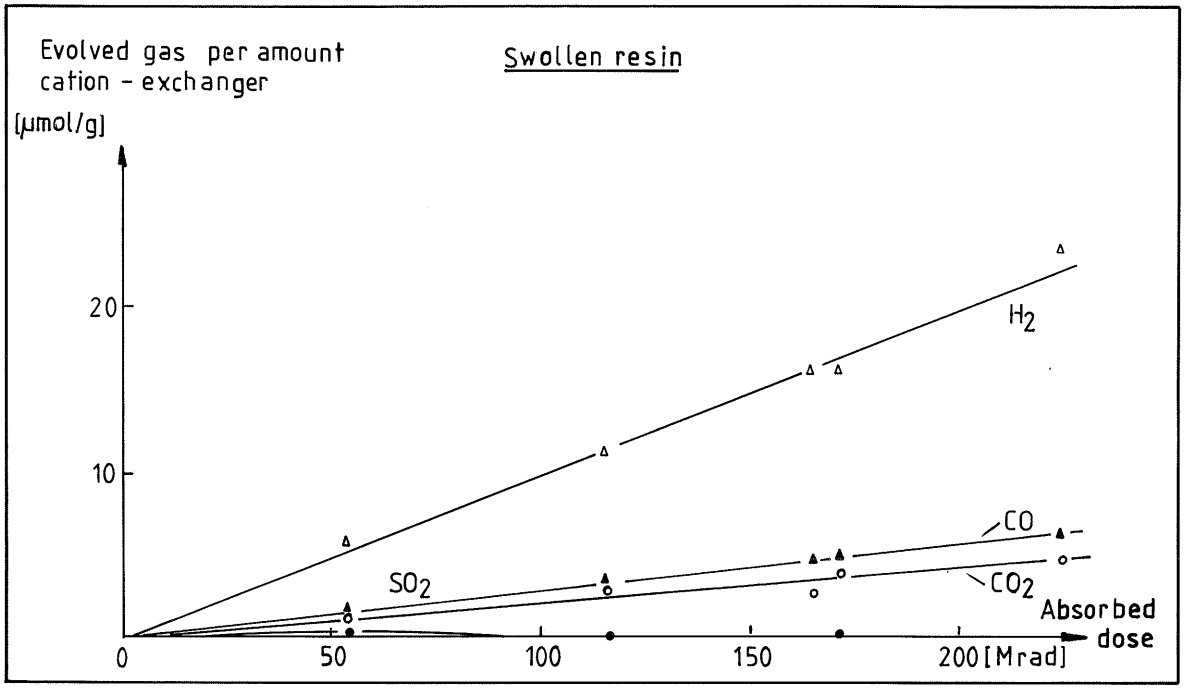

Figure 14. Gases evolved on irradiation of swollen cation exchange resin. From Mohorcic et al. /28/.

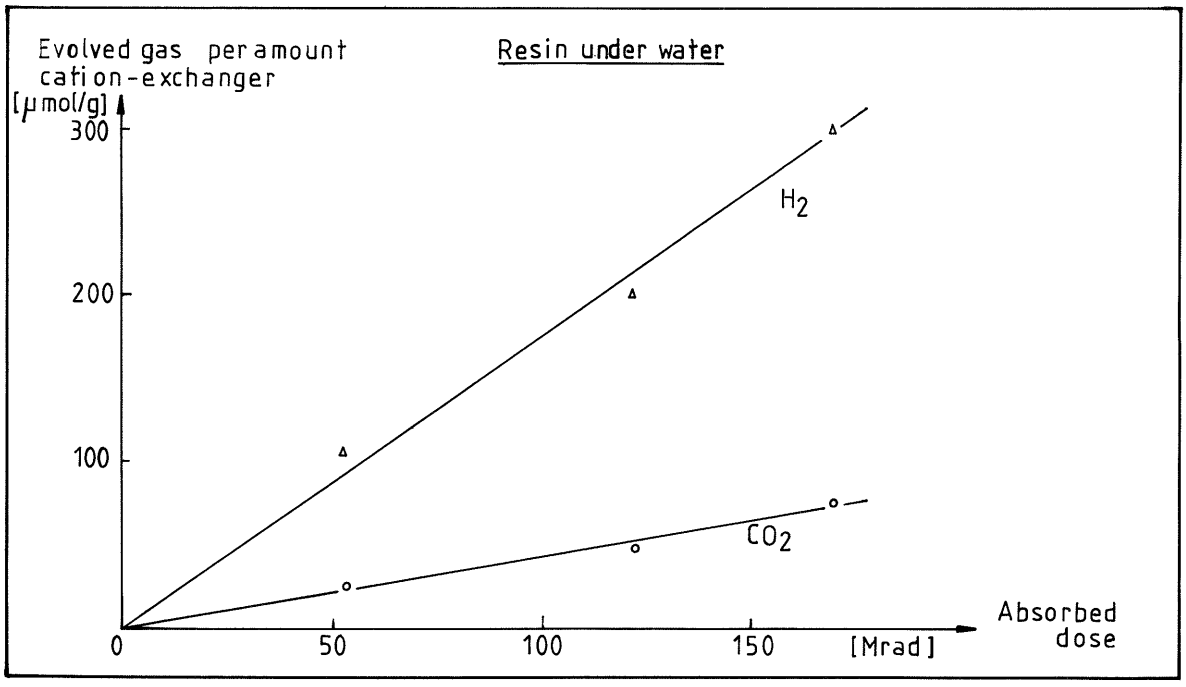

Figure 15. Gases evolved on irradiation of cation exchange resin under water. From Mohorcic et al./28/.

$G(H_2)$ for pure water is 0.45 /29/. For a resin containing 50% moisture, one would expect $G(H_2)=0.23$ from water radiolysis alone, but for swollen H^+-form resin $G(H_2)$ is 0.12 and does not vary with radiation dose rate /30/.

In resin water systems, some processes must therefore act to reduce the hydrogen production.

In some investigations of irradiated cation exchange resins immersed in water, $G(H_2)$ values of 1.3-1.7 have been found /28/. Under the same irradiation conditions, the $G(H_2)$ values for anion resins are greater than for cation resins and those expected for pure water radiolysis. The decomposition of functional groups may contribute to this /30/.

Sulphur dioxide is formed by the direct action of ionizing radiation on dry forms of sulphonic acid resins. In the presence of water, the SO_2 undergoes secondary reactions and for this reason very low SO_2 values are measured.

The rate of formation of carbon dioxide, carbon monoxide and hydrogen is directly proportional to the absorbed dose as seen in Figures 13-15.

Trimethylamine is the main decomposition product from the irradiation of strong-base anion-exchange resins. Also, quantitative yields of lower amines and ammonia are reported /31/. Trimethylamine is a gas at room temperature. It is, to a certain extent, soluble in water and reacts to form trimethylammonium ions. As a consequence, the solubility is high in acid solutions. At high pH, as for instance in a concrete-controlled environment, the solubility is again expected to be sufficiently high to dissolve all trimethylamine produced. More information is however needed to fully understand this situation.

Bitumen

Bitumen is slightly decomposed by radiolysis. Of the gases formed, hydrogen is predominant. According to Kosiewicz /32/ the gas composition is:

Hydrogen	97%
Methane	2%
Carbon oxides	1%
Other hydrocarbons	traces

Alpha radiation seems to give a higher yield than the same dose of gamma radiation. The yield is reported to decrease with increasing dose /32/. G values from 1.7 to 0.8 are reported, with the higher value for low doses /32/.

Concrete

Hydrogen was the only gas produced in gamma and beta irradiation of concrete. Hydrogen production is controlled by an equilibrium pressure which is proportional to dose rate. G values for hydrogen are in the range of 0.1-0.3 /33/.

In alpha irradiation of concrete, the hydrogen production is constant and no equilibrium pressure is obtained. Pressures of more than several thousands of atmospheres have been calculated. In most cases even oxygen is produced. $G(H_2)$ values in the range of 0.2-0.6 have been reported /33/.

$G(H_2)$ values can be diminished if the water is removed from the concrete and/or if nitrates are added to the concrete. The nitrates then cause an increased oxygen production.

3.4.3 Radiolytic decomposition rates

The following Tables list G values reported for the formation of gases such as H_2, SO_2, CO, CO_2 and for the formation of sulphate ions and trimethylamine.

Table 20. G values. Cation exchange resin, H-form

State gH_2O/ g resin	G values expressed in mole/Mrad, tonne H_2	SO_2	CO_2	CO	H_2SO_4	Irradiation condition	Ref.
Dry	0.1						/34/
Dry	0.026	0.87	0.035	0.009			/28/
Dry	0.051	0.001	0.19				/28/
Dry	1.1		0.06				/35/
0.15	0.039	0.06-0.22	0.034	0.024	0.67-0.72		/36/
0.32	0.059		0.02	0.029	1.32		/36/
0.68	0.082		0.015	0.018	1.27		/36/
0.88	0.12		0.022	0.015	1.21		/36/
1.35					2.4		/37/
1.38					2.4	In the	
1.39					2.7	absence	
1.39					2.7	of O_2	
1.4					25.1		
1.55					21.2		/37/
1.67					18.3		
2.20					19.8	In the	
3.23					17.0	presence	
5.36					16.1	of O_2	
6.82					17.2		
8.20					17.7		
Swollen					0.3-0.8	10^2-10^3	/30/
"	0.10					He-atmosphere	/30/
"	0.12					Air	/30/
"	0.12					Air and 6 psi O_2	/30/
"	0.17					Air and 17 psi O_2	/30/
"	1.22		0.60	0.39			/35/
24	0.095	0.006	0.019	0.027			/28/
36.8	0.12	0.005	0.046	0.005			/28/
164	1.7		0.41				/28/
320	1.7		0.43				/28/

Table 21. G values. Cation exchange resin,alkali-form

State gH_2O/ g resin	G-values expressed in mole/Mrad, tonne H_2	SO_2	CO_2	CO	Irradiation condition	Ionic form	Ref.
Dry	0.001	0.26	0.007	0.002		Li	/28/
Dry	1.0		0.03			Na	/35/
1	0.2					Na	/30/
23	0.11	0.50	0.008	0.19		Li	/28/
108	1.3		0.16			Li	/28/
Swollen	0.095	0.006	0.19	0.009		Na	/28/
Swollen	3.1		0.09			Na	/34/

Table 22. G values. Anion exchange resin

State gH_2O/ g resin	G values expressed in mole/Mrad, tonne H_2	CO_2	CO	$(CH_3)_3N$	Irradiation condition	Ionic form	Ref.
Dry				4.0-4.4	4.8 Mrad	Cl-and SO_4	/38/
Dry				4.0		NO_3	/38/
Air Dry	0.09		0.02			NO_3	/35/
Air Dry	0.10	0.06	0.01			NO_3	/35/
-				11.5-14	50-	OH	/39/
-				9-12.5	100 Mrad	SO_4	/31/
0.3				5		Cl	/38/
1	0.6					OH	/30/
1	0.3					Cl	/30/
2				3.2	4.8 Mrad	Cl- and SO_4	/38/

Table 23. G-values. Bitumen

State gH_2O/ g material	G-values expressed in mole/Mrad, tonne H_2	CH_4	Notes	Irradiation condition	Ref.
Dry	0.8-1.7		G(initial)		/32/
Dry	0.5-0.7				/32/
Dry	0.3-0.6	0.01			/40/
Dry	0.5				/41/
Dry	0.2		Bitumen/salt,50/50		/41/

Table 24. G-values. Concrete

State gH_2O/ g material	G-values expressed in mole/Mrad, tonne H_2	O_2	Note	Irradiation condition	Ref.
wet	0.6	0.1	Alpha radiation		/33/
wet	0.3	-	Beta radiation		/33/
wet	0.13	-	Gamma radiation		/33/
wet	0.086	0.28	Gamma radiation	with nitrate	/33/
wet	0.01	0.02	Gamma radiation	-"-	/33/

3.4.4 Data used

For the calculation of radiolytic decomposition the following information is needed:

- The G values for the compounds which will decompose.
- The quantities of these compounds divided into sub-categories of a reasonably uniform composition.
- The dose absorbed for each sub-category.

The materials which will undergo radiolytic decomposition are listed in Table 25 and the corresponding G values of importance are listed in Table 26. The intervals presented in Table 26 describe the highest and lowest values found in the basic Tables 20-24. The average values are selected in agreement with /NGB 85-07/, within the given intervals.

From the total inventory containing almost 200 waste types /NGB 85-02/, a list of about 100 sub-categories is extracted, each being more or less homogeneous in composition.

Table 25. Total amounts of materials of interest for radiolytic decomposition (tonnes)

Category	Concrete	Bitumen	Plastic	Ion-exch. resins
Operational	54,800	300	100	12,200
Reprocessing	9,100	3,100	600	100
Decommissioning	122,600	0	3,000	0
MIF-waste	8,400	-	-	-
Whole repository	194,900	3,400	3,700	12,300

The radiation dose in Mrad is calculated for each sub-category using the method described in /40/. In these calculations the primary quantity is the dose rate for each nuclide. It is calculated as a product of the specific activity, the average energy emitted per disintegration and a constant giving the ratio of the number of disintegrations and the activity. From the dose rate, the absorbed dose is calculated as an integral over the whole period of time.

The total absorbed dose should be the sum of the contributions from all nuclides present in the waste. For practical purposes a reduced list of nuclides is used. These nuclides are estimated to contribute more than 80% of the total absorbed dose.

The list comprises the following nuclides:

H-3	Ni-59	I-129
C-14	Ni-63	Cs-134
Mn-54	Zn-65	Cs-135
Fe-55	Sr-90	Cs-137
Co-60	Ag-110	Pu-239

The radiation dose generated in one waste container is assumed to be absorbed in the same container and divided among the contents in proportion to the weight percentage of the materials present. The following data are needed for all the ca. 100 sub-categories in these calculations:

- The total weight.
- The material composition.
- The content of the nuclides mentioned above.

These data are obtained from the waste inventory /NGB 85-02/.

Table 26. G values (mole/Mrad,tonne) used

Material	State water content	Ionic form	G values (mole/Mrad,tonne) (minimum - average - maximum) H_2SO_4	H_2	SO_2	CO_2
Ion exchange resin cationic	wet	Li+	0.7-1.3-25*	0.1 -1.3 -3.1	0.01-0.3-0.3	0.01 -0.2 -0.2
	dry	H+	0	0.03-0.03-1.1	0.001-0.9-0.9	0.004-0.04-0.2
Ion exchange resin anionic	wet	SO_4	0	0.3 -0.3 -0.6	0	0
	dry	SO_4	0	0.09-0.09-0.1	0	0.06
Bitumen	dry		0	0.2 -0.5 -1.7	0	0
Concrete	wet		0	0.01-0.03-0.6	0	0
Plastic**	dry/wet		0	0.2 -0.5 -1.7	0	0

Material	State water content	Ionic form	CO	$(CH_3)_3N$	N_2	O_2
Ion exchange resin cationic	wet	Li+	0.01-0.02-0.2	0	0	0
	dry	H+	0.009	0	0	0
Ion exchange resin anionic	wet	SO_4	0	9-12-14	0-0.13-0	0
	dry	SO_4	0.01-0.01-0.02	9-12-14	0	0
Bitumen	dry		0	0	0	0
Concrete	wet		0	0	0	0-0-0.3
Plastic**	dry/wet		0	0	0	0

* The same value as for wet cation exchange resin in H-form assumed, the highest value includes also the contribution from polysulphonic acids.

** The same value as for bitumen assumed.

3.4.5 Quantitative estimation of gas formation

The estimation of radiolytic decomposition is presented as follows:

- Table 27 gives an overview of the most important products which are formed.
- Figure 16 shows the rate of hydrogen formation during the first 500 years for the base case.
- Figure 17 gives the accumulated hydrogen formation for the base case compared with estimated maximum and minimum cases.

All the calculations are integrations over 500 years. This is obviously a sufficient time period, as seen from Figure 17. Almost all of the decomposition takes place during the first 50 to 100 years. In fact, much of the decomposition will take place before the waste is disposed of in the repository.

The calculations show that Co-60, Ni-63, Zn-65, Sr-90 and Cs-137 are the nuclides which contribute significantly to the dose. The average accumulated dose for the whole waste inventory during these first 500 years is $4 \cdot 10^7$ rad. It should be noted that the dose varies by orders of magnitude between the different waste sub-categories. For example, the accumulated absorbed dose in ion exchange resins in concrete is about $3 \cdot 10^8$ rad after 500 years for one of the reprocessing waste categories and about $1 \cdot 10^5$ rad for one of the operational waste categories. These variations have been accounted for by calculating the doses for each waste sub-category separately.

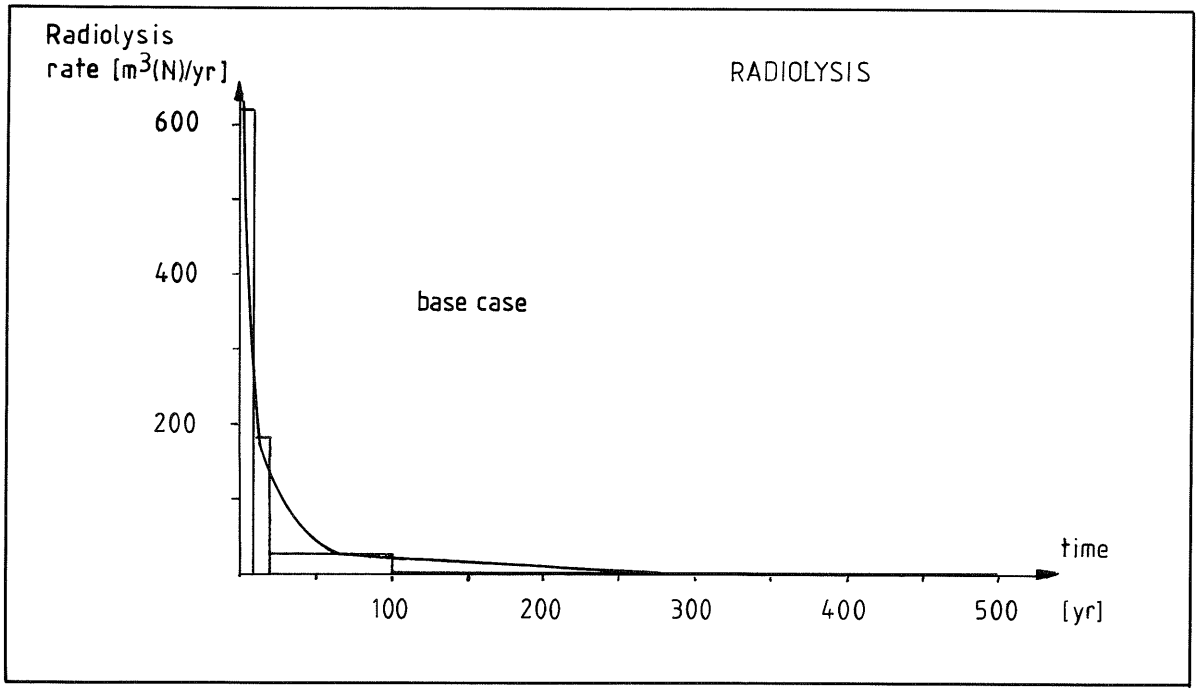

Figure 16. The H_2-gas formation rate during the first 500 years. The linedrawn is a smoothed integration. $m^3(N)$ denotes normal cubic metres at STP.

Table 27. Total amount of decomposition products formed in 500 years (Kmoles)

Waste category	Decomposition products						
	H_2SO_4	H_2	SO_2	CO_2	CO	$(CH_3)_3N$	N_2
Operational waste	9	24	6	2	2	130	1
Reprocessing waste	15	110	3	2	2	123	1
Decommissioning waste	-	315	-	-	-	-	-
MIF-waste	-	0.4	-	-	-	-	-
Whole repository	24	447	19	14	4	253	2

The amounts of gases generated are minimal compared with those generated by corrosion and microbiological processes.

The large quantity of methylamine produced (Table 27) is worth noticing. Its behaviour and consequences in a concrete environment have, however, not yet been fully investigated.

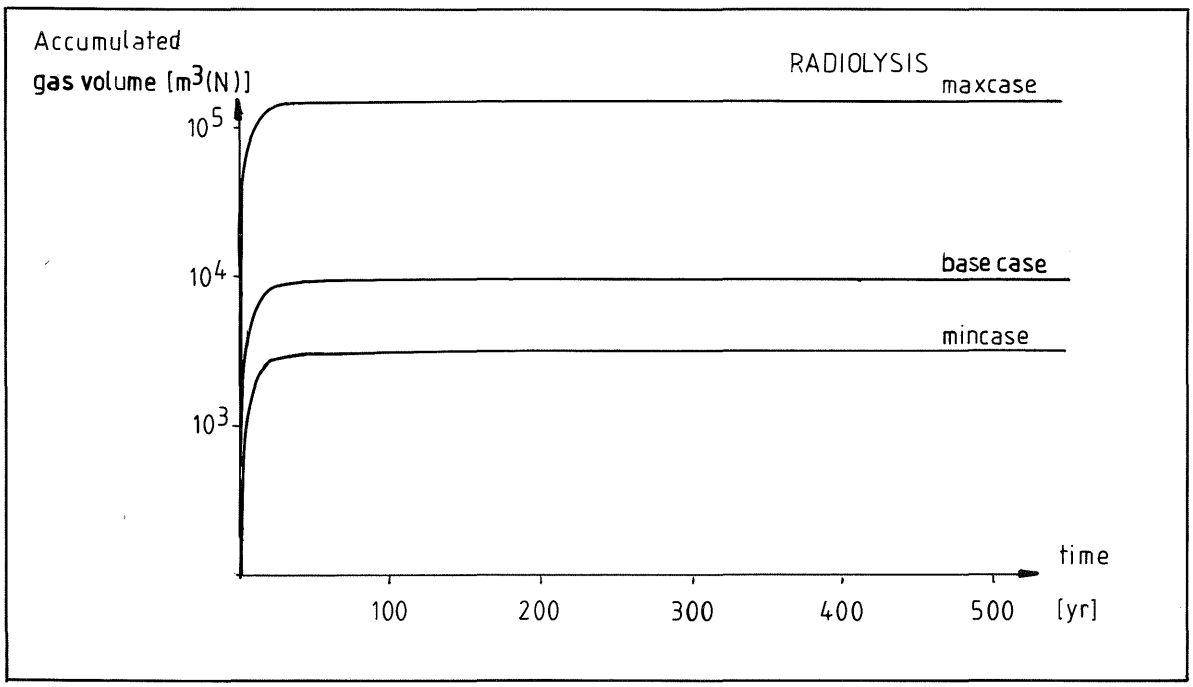

Figure 17. Minimum and maximum volumes of gases formed by radiolysis. $m^3(N)$ denotes normal cubic metres at STP.

3.5 Total gas formation in a type B repository

3.5.1 Results

The total gas formation (Figure 18) is the sum of gases from corrosion, microbial degradation and radiolytic decomposition. Of these three, the contribution from radiolytic decomposition is minimal. Microbial degradation predominates as a source of gases during the first 1000 years, while corrosion predominates on the long term.

As indicated in Figure 19, aluminium and cellulose contribute very highly during a short but important period of time. This must, however, be verified by further investigations, since the rates of gas formation under prevailing conditions could prove to be different from the rates derived from the literature, which have been used in the present calculation.

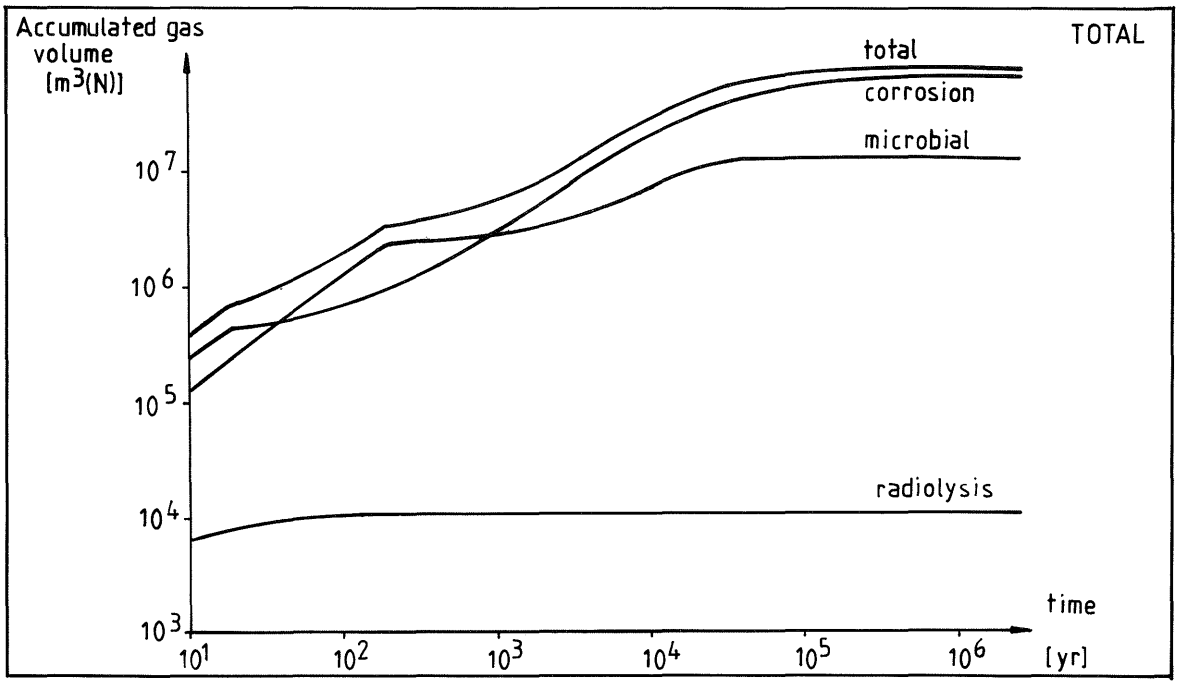

Figure 18. Accumulated gas volumes for the different gas-forming processes. $m^3(N)$ denotes normal cubic metres at STP.

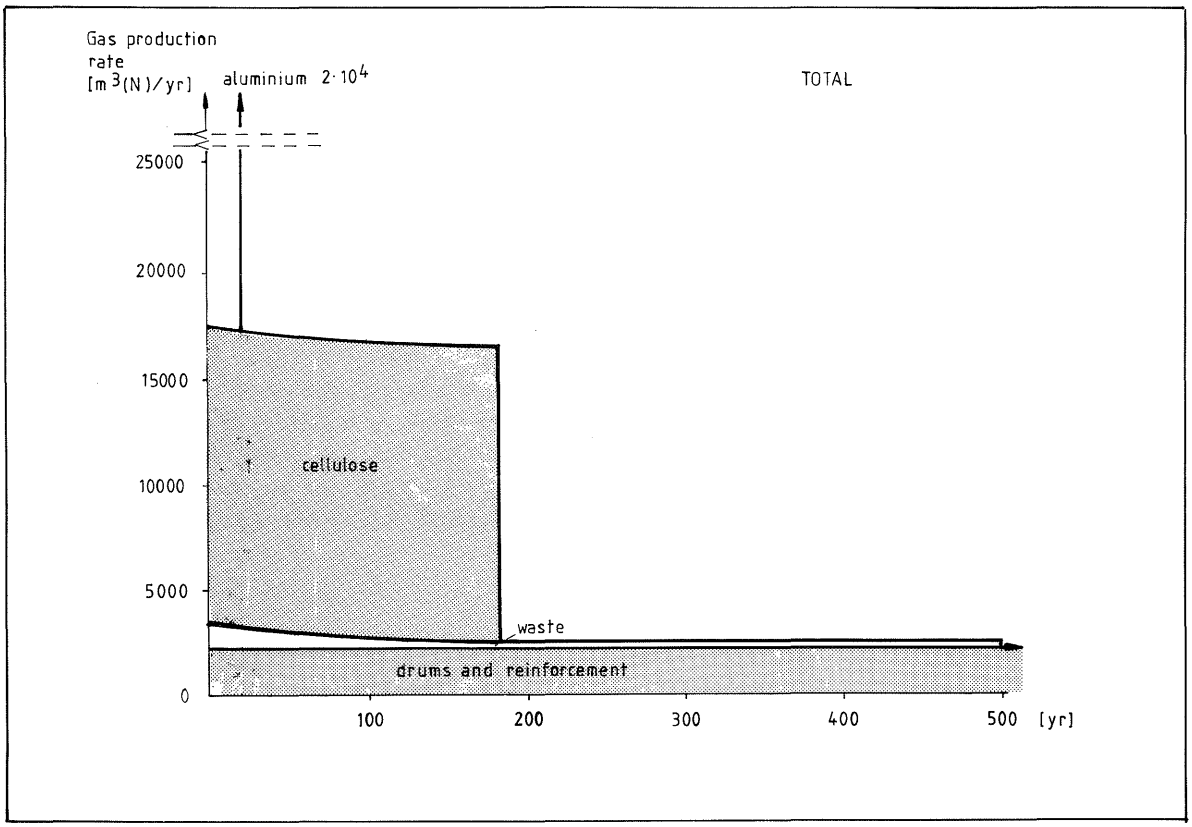

Figure 19. The contribution from different materials to the total rate of formation of insoluble gas during the first 500 years. $m^3(N)$ denotes normal cubic metres at STP.

For the gas migration calculations, the gas formation rate during the first twenty years after closure has been set at $5.7 \cdot 10^4$ m^3 (STP)/a ($1.8 \cdot 10^{-3}$ m^3(STP)/s), and during the following 730 years at $2.5 \cdot 10^4$ m^3 (STP)/a. ($8.0 \cdot 10^{-4}$ m^3 (STP)/s).

The assumed gas production rates in the gas migration calculations correspond to the values given in NGB 85-07 and NGB 85-08. The differences between these rates and the rates presented in this report are mainly:

the presence of cellulose in the updated waste inventory, the stoichiometric coefficient for the corrosion of steel which was conservatively rounded upwards in the NGBs and the assumptions made regarding the corrosion of aluminium and zinc as stated in Section 3.2.5.

In Figure 20, the accumulated gas production assumed for the gas migration calculations is shown together with the estimated total gas production for the minimum, base and maximum cases as presented in Sections 3.2.5, 3.3.5 and 3.4.5.

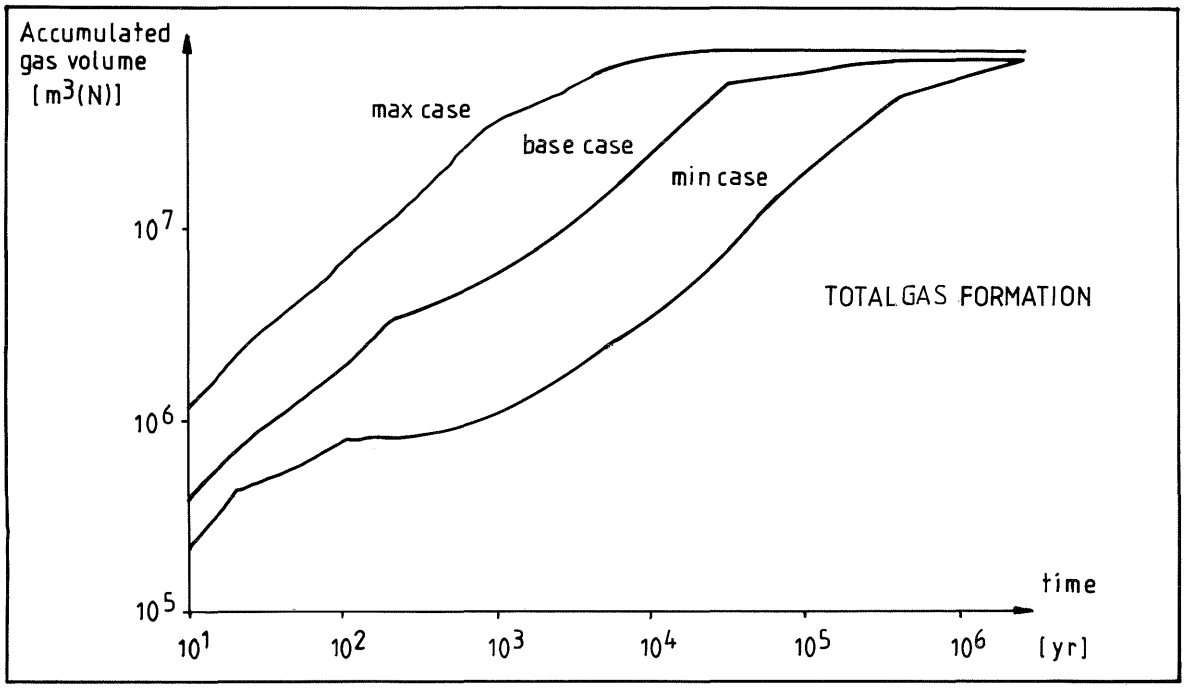

Figure 20. Accumulated gas production in the repository for different cases. $m^3(N)$ denotes normal cubic metres at STP.

4. GAS TRANSPORT

4.1 General

Chapters 4 to 6 of this report present a quantitative estimation of gas release from a repository for low-and intermediate-level radioactive waste.

The calculations are made under the assumption that the rock and the system of engineered barriers are either fractured or porous materials, with a certain low conductivity for gases. In the following, fractures and pores are called fractures and the term pores is used when the physical situation is applicable only to pores. Initially, the fractures are water-filled and no gases can be transported through the material. To enable gas transport, the water must first be displaced from the fractures. To start the displacement, the capillary pressure in the fracture and the hydrostatic pressure must be exceeded by the gas pressure and the first displacement of water will take place in the largest continuous fracture.

In the calculations of gas transport, the system of engineered barriers is assumed to have a sufficient number of fractures with low capillary pressure that the gases can easily escape from the near-field. The gases are assumed to be released from the near-field zone and to collect at the top of the decompressed zone. Here, a gas cushion will be formed and, as the volume of gas increases, water will be displaced from the decompressed zone. The solubility of the gas (mostly hydrogen) in the amount of water available is negligible in comparison with the large volume of gas.

The model used to calculate gas migration in the host rock assumes that, with continuous gas production, the pressure in the gas cushion rises until it exceeds the capillary pressure plus the hydrostatic pressure of the fractures in the rock; The gas then enters the fractures and water is displaced.

The hydraulic conductivities, i.e. the conductivity in a fully saturated material, have been estimated for "Project Gewähr" and are given as ranges. To obtain the conductivity for the gas it is necessary to determine also the relative conductivity for the

non-wetting phase. The conductivity of gas is given by the product of the hydraulic conductivity and a relative conductivity. The relative conductivity in a porous medium can be estimated as a function of the saturation degree. Methods can be found in the literature /42,43/. In this report, the relative conductivities for different rocks used in the calculations were calculated from mercury porosimetry data. It should be noticed that there are no data available for Valanginian marl.

Four different zones essential for gas transport, have been investigated; the host rock, the fracture zones, the decompressed zone around engineered tunnels and the system of engineered barriers.

The fact that there is no data available on the fracture aperture distribution in the rock means that it is difficult to evaluate the real gas flow in the rock. The calculations made so far are parameter studies using data selected within a range of best estimated values for similar rock materials (see Chapter 5).

4.2 Gas transport mechanisms

All transport mechanisms can be described by a transport coefficient and a driving force, e.g.:

Flow = (transport coefficient) x (driving force) (4-1)

For gas transport from an underground repository, the driving force is a pressure gradient determined by the gas production in the repository and the hydrostatic pressure. The transport coefficient is determined by the geometry of the fractures in the solid material through which the gas is transported.

The transport coefficient for flow in a fractured or a porous medium is usually expressed as the hydraulic conductivity of the material, i.e. the conductivity measured for water in a fully water-saturated material. The hydraulic conductivity depends on the structure of the porous medium and the characteristics of the fluid. The porous structure can theoretically be described by porosity, tortuosity and constrictivity. Usually the conductivity is measured directly by appropriate experiments.

For a fractured medium, fully or partially water-saturated, the transport of gases is restricted by the presence of water in the fractures. In a fully saturated medium, the water in the fractures is assumed to be displaced to such an extent that continuous gas-filled channels are formed before any continuous gas transport is possible. The higher the required gas transport capacity in the fractured material is, the larger the number of gas-filled channels must be. This can be expressed by the relative conductivity for the gas phase. The actual conductivity for the gas phase is then the product of the hydraulic conductivity at full saturation and the relative conductivity, i.e.:

$$K_{gas} = K_{saturation} \cdot K_{relative} \qquad (4\text{-}2)$$

For materials with distributed fracture/pore sizes, the relative conductivity can be calculated if the distribution of apertures is known. Calculation of the gas transport capacity of a porous medium is fairly simple for an unsaturated porous medium where continuous gas-filled channels already exist. When the initial water saturation is high and the properties of the host rock are such that the expected capillary pressure is significant, the calculation of the gas transport capacity is more complicated.

5. GAS TRANSPORT IN BARRIER MATERIALS

5.1 General

The tunnels excavated for the repository planned at the Oberbauen Stock model site have to be provided with linings of reinforced concrete.Due to the high plasticity of the Valanginian marl and to high lithostatic pressure, the marl may collapse if no mechanical support is provided around the tunnels.

The waste to be deposited in the repository is placed in 20 m^3 concrete containers and the empty space in the repository is filled with low viscosity concrete.

Due to various chemical processes in the waste, gases are formed in the repository. These processes are presented in Chapter 3. As a result, a pressure build-up can occur inside the repository if removal of gases through the technical barriers is not possible. A consequence of pressure build-up in the repository is that contaminated water can be displaced from the repository. This problem can be avoided by ensuring that the gases formed are able to escape from the repository. The capillary pressure of intact concrete and therefore the gas pressure that has to be applied to displace water from the pores of the concrete is very high. However, in a large concrete structure such as the repository lining, it is reasonable to assume that some small cracks are formed during construction, hardening etc. In these cracks, the capillary pressure will be lower than in the intact concrete. Thus, the gas could escape through the cracks without any significant pressure build-up.

On the other hand, if it can be shown that the presence of cracks in the concrete is not enough to release the gases from the repository, the repository lining may be provided with some sort of gas release device such as a zone of material characterized by low capillary pressure.

In this Chapter, the pressure build-up within the repository and the possibility of transporting gases through the concrete lining are quantified. In the next Chapter, however, the repository lining is

assumed to present no resistance to the transport of gases and hence the gases are assumed to be released from the system of engineered barriers without significant pressure build-up.

It has also been assumed throughout this report that all materials present inside the repository lining are more permeable to gases than the lining itself. Thus, the internal pressure build-up in the repository backfill material and in the concrete containers is assumed to be small compared to the pressure build-up caused by the resistance in the repository lining. This might be an unrealistic assumption and will be studied further when the planning of the actual repository proceeds.

5.2 Design and material properties of the barrier system

In NGB 85-06 and NGB 85-07, an extensive description of design and material properties is given. Only the data required in the calculations of gas transport in the barrier system are given here. The basic design of the system of engineered barriers is shown in Figure 21 and consists of the **waste matrix**, the **concrete container** with **backfill** and the **repository backfill** and the **lining**.

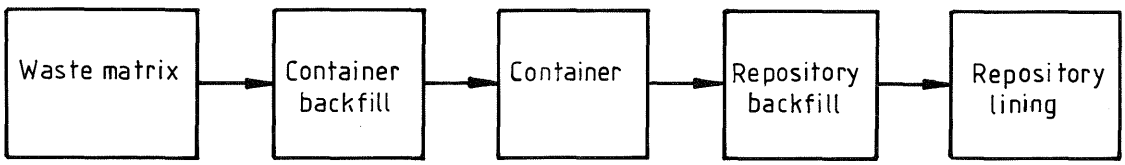

Figure 21. The sequence of engineered barriers around the waste

In this report, Only the influence of the repository lining on the overall capacity for transport of gases has been considered. The other barriers are represented in the calculations only by their pore volume.

The concrete lining is characterized by low conductivity and high capillary pressure. For concrete, the hydraulic conductivity is in the range of $8 \cdot 10^{-12}$-$3 \cdot 10^{-11}$ m/s /NTB 82-03/. The capillary pressure is represented by a pore size distribution curve. Figure 22 shows an example of a differential pore size distribution with the corresponding cumulative distribution.

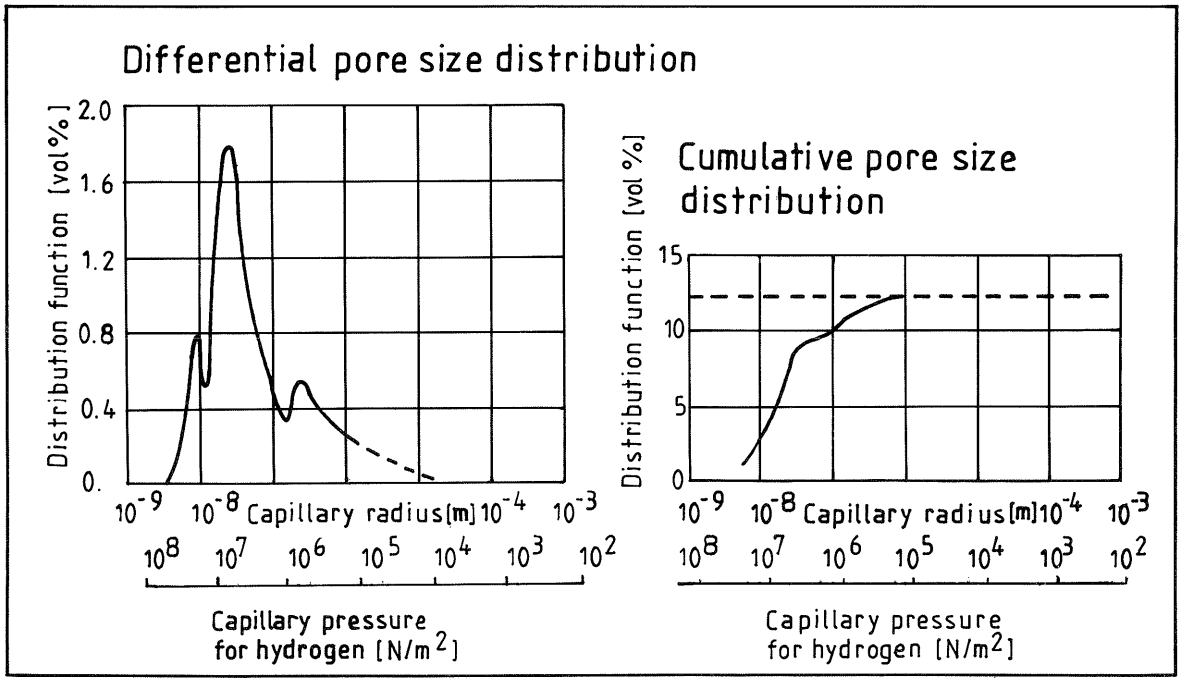

Figure 22. Differential pore size distribution, also showing the cumulative distribution for an ordinary concrete /44/

The pore size distribution depends on the water-cement ratio, ballast content, age, etc. Figure 23 shows the influence of the water-cement ratio on the pore size distribution. The Figure also indicates the largest continuous pore radius, which corresponds to the minimum capillary pressure. This, in turn, equals the minimum gas pressure that must be exceeded to induce gas transport through the barrier material.

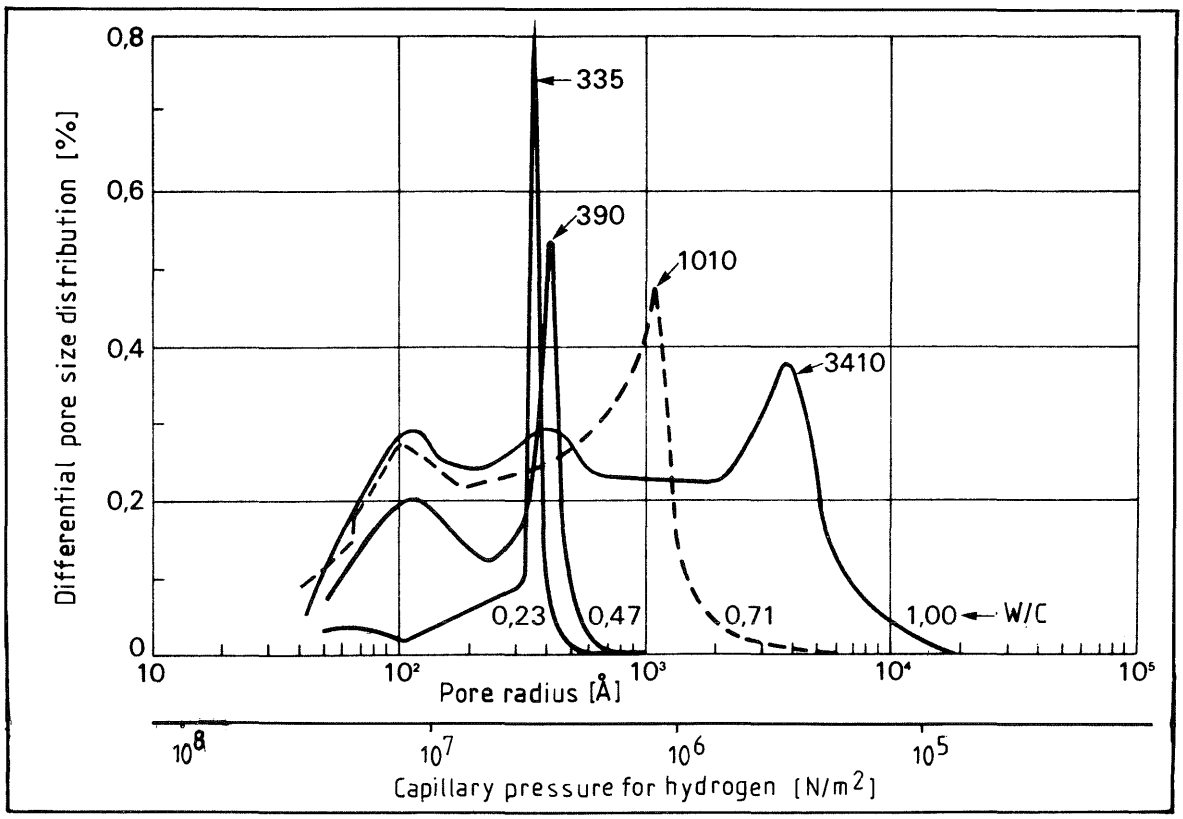

Figure 23. Differential pore size distribution for concretes with different w/c ratios. Numbers on the peaks indicate the maximum continuous pore radius (Å) /45/

Normal values for the water-cement ratio for construction concrete are in the range of 0.3-0.8. In this section the curves in Figure 23, corresponding to a w/c of 0.47 and 0.71, were used. For w/c = 0.47, the capillary pressure corresponding to the maximum continuous pore radius is 3.8 MPa, whereas for w/c = 0.71, the capillary pressure is 1.5 MPa. It must be stressed, however, that the occurrence of cracks with lower capillary pressures cannot be excluded, especially in the case of structures as large as those considered here. This is dealt with below.

5.3 Modelling and calculations

5.3.1 General

The gases may be released through the repository lining in three different ways.

Firstly, the lining may be equipped with gas release devices.

Secondly, small fractures may be formed in the concrete during construction or hardening (shrinkage). The capillary forces in these fractures in the concrete are then low enough to allow the gas to displace pore-water and form gas-filled channels through the lining.

Thirdly, if the concrete is unfractured a pressure build-up within the repository will take place. This will start a displacement of contaminated water through the bottom and walls of the repository lining. For low gas formation rates, the repository will be emptied of pore-water, whereas for high rates the pore-water cannot be displaced without a significant pressure build-up in the repository and, eventually, fractures may be formed in the lining.

In Section 5.3.2 the relationship between the required size and number of fractures able to balance the gas flow rate is given. The results of the gas transport calculations are presented in Section 5.3.5

In Section 5.3.3 the conditions for fracture formation in the repository lining due to internal overpressure are derived. The results of the calculations of the strength of the repository lining to internal overpressure are presented in Section 5.3.5.

In Section 5.3.4 the pressure difference required to displace water through the bottom of the repository lining is calculated. The results from these calculations for various combinations of hydraulic conductivities of the lining material and gas production rates are presented in Section 5.3.5.

5.3.2 The relationship between fracture sizes and gas flow

Consider the system presented in Figure 24 below.

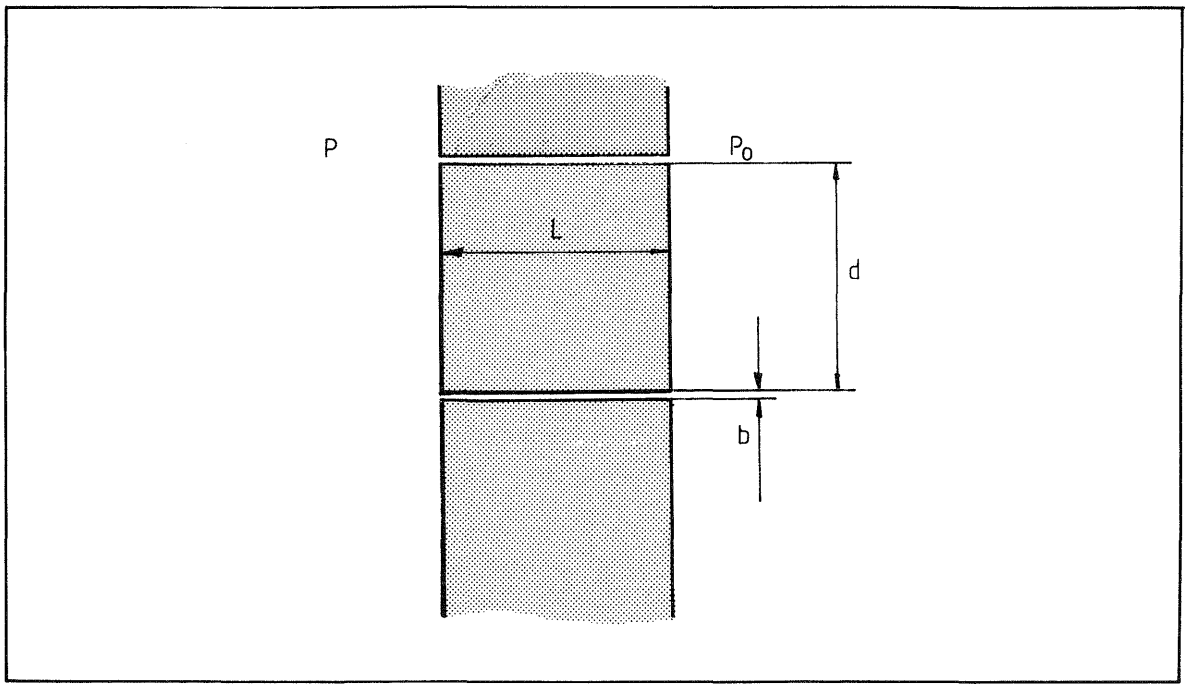

Figure 24. Schematic representation of a fractured barrier

Fracture spacing	d	(m)
Fracture width	b	(m)
Fracture frequency	$n=\frac{1}{d}$	(m^{-1})

For flow in a plane fracture, the conductivity is obtained from the Hagen-Poiseuille equation /46/;

$$K_{frac} = \frac{b^2}{12} \cdot \frac{\rho g}{\mu} \qquad (5\text{-}1)$$

The bulk conductivity is obtained by averaging the fracture conductivity and the conductivity of the unfractured material. For parallel fractures, the overall transport capacity is given by:

$$Q = \frac{A\, n\, b\, K_{frac}(P - P_o)}{\mu_g\, L} \qquad (5\text{-}2)$$

where

Q =	Capacity for transport of compressed gas	(m^3)
A =	Cross-sectional area	(m^2)
P =	Internal pressure	(Pa)
P_o =	Surrounding pressure	(Pa)
μ_g =	Dynamic viscosity of the gas	(Ns)
L =	Barrier thickness	(m)

For a 4,660 metre long tunnel with an elliptic cross-sectional area of about 180 m^2, the roof area can be estimated to 14,000-23,000 m^2. This range for the available cross-sectional area was used in the calculations presented in Section 5.3.5, Table 29.

5.3.3 Fracture formation in concrete lining due to internal overpressure

A short analysis is given of the internal pressure required to form cracks in a repository lining made of concrete. In the calculations, the presence of reinforcement bars in the concrete, i.e. the influence of the reinforcement bars on the distribution of fractures in the lining material and on the fracture pattern, is disregarded. This is a conservative assumption. In the analysis, a simplified geometry of the barrier system as shown in Figure 25 was assumed. Only the repository lining is considered and the influence of the other engineered barriers is disregarded. In Table 28, data collected from NGB 85-07 are summarized.

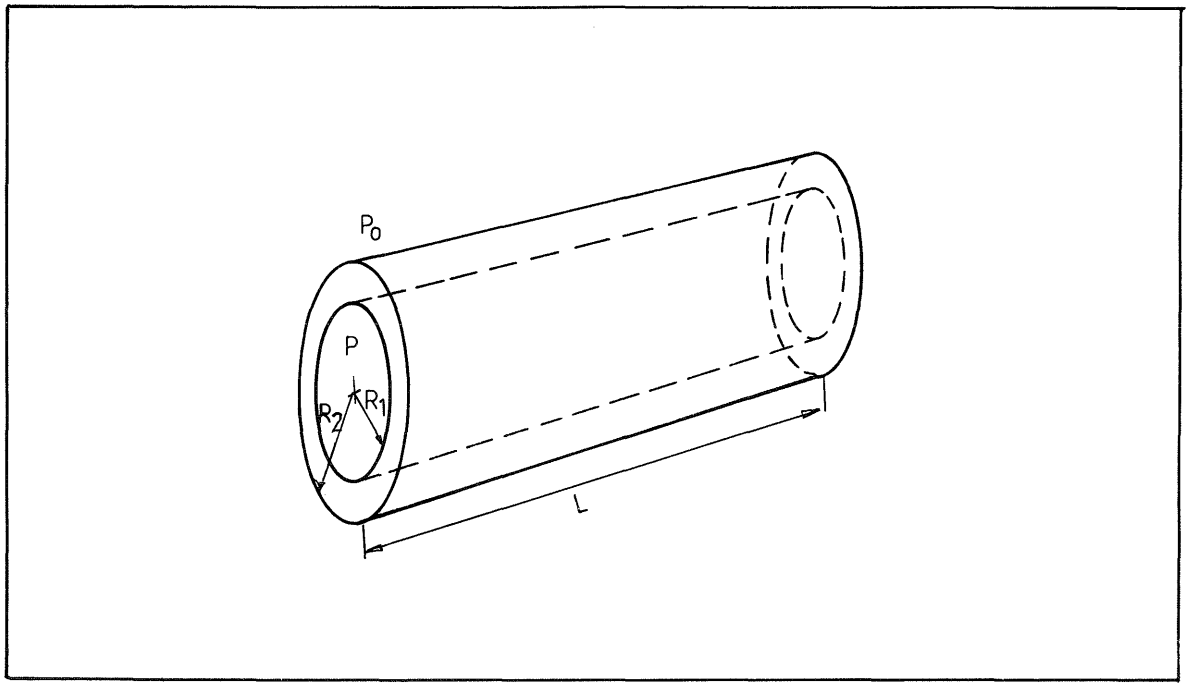

Figure 25. Schematic representation of the repository lining, assuming a cylindrical geometry

Table 28. Summary of relevant data collected from /NGB 85-07/ and /47/

Inner radius	R_1 = 6.5 m
Outer radius	R_2 = 7.4 m
Length	L = 4,660 m
Surrounding hydrostatic pressure	P_o = 1.5-2.0 MPa
Allowed tensile stress	σ_j = 1.8-3.0 MPa
Ultimate tensile stress	σ_j = 5.0 MPa

Assuming the lining to be a cylindrical tube with thin walls, the stress is evenly distributed over the cross-section of the walls. This simplified case is shown in Figure 26.

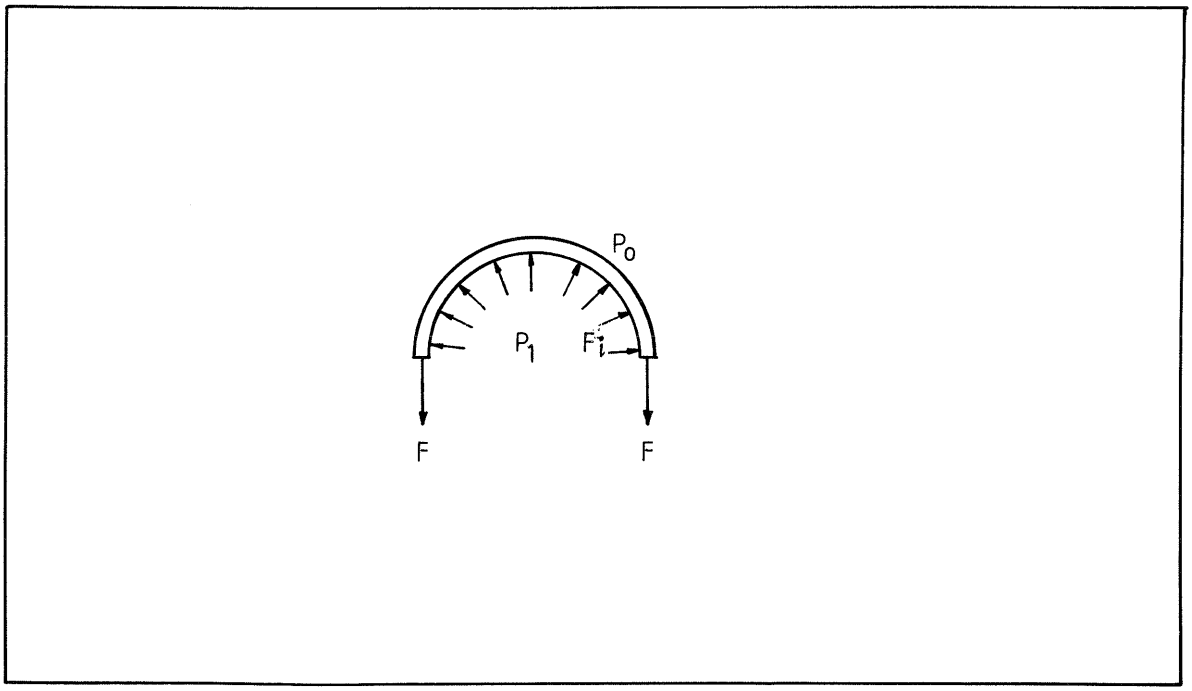

Figure 26. Internal pressure in a cylindrical tube with thin walls. For symmetry reasons, only one half is shown. Internal pressure P_1, surrounding pressure, P_o, and the resulting force, F, acting on the wall are indicated in the Figure

By the method of balancing between forces we obtain;

$$F = \frac{1}{2}(P_1A_1 - P_oA_o) \qquad (5\text{-}3)$$

$$F = \sigma_j A_{wall} \qquad (5\text{-}4)$$

(5-3) and (5-4) yield;

$$\Delta P = P_1 - P_o = \frac{2\sigma_j A_{wall} + P_oA_o}{A_1} - P_o \qquad (5\text{-}5)$$

Δp = pressure difference over the lining which would cause it to fracture

In the equations (5-3) to (5-5):

F = tangential force acting on the cylinder wall (N)

P_1 = internal pressure (N)

P_o = surrounding pressure (N/m^2)

A_1 = inner surface area of the lining (m^2)

A_o = outer surface area of the lining (m^2)

σ_j = allowed tensile stress in the lining wall (N/m^2)

σ_b = ultimate tensile stress (N/m^2)

A_{wall} = surface of a section through the wall (m^2)

Here, the allowed tensile stress has been used rather than the ultimate tensile stress to account for an early degradation of the lining material.

The results are presented in Section 5.3.5, Table 30.

5.3.4 Pressure difference required to displace water from the repository

In this Section, the pressure difference required to press out water at the same rate as the gas bubble in the repository grows is estimated. In the next Section, this is compared with the pressure required to cause formation of fractures in the lining due to internal overpressure.

In the following calculations, water is assumed to be pressed out through the bottom half of the repository lining; see Figure 27. The rate of water displacement corresponds to the volume of compressed gases produced in the repository.

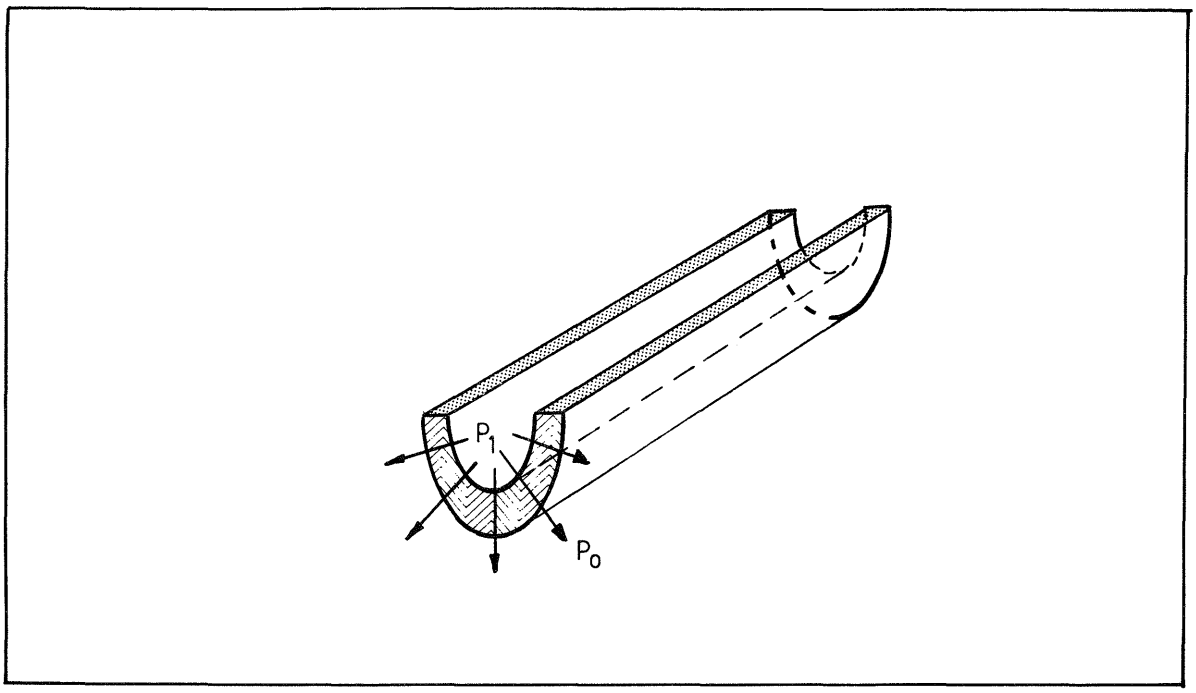

Figure 27. In the calculations a semi-cylindrical lining was assumed for displacement of water due to the formation of a gas bubble

The pressure difference can be estimated from (5-6) which is valid for incompressible flow of water through the lining.

$$\Delta P = P_1 - P_o = \frac{P_o^2 + 2\ \ln(R_2/R_1)\ \mu_w\ Q\ P_o}{K\ L\ \pi} - P_o \quad (5\text{-}6)$$

where:

P_o = hydrostatic pressure = 1.5-2.0 (MPa) /NGB 85-07/

P_1 = internal pressure

R_1 = inner radius = 6.5 (m)

R_2 = outer radius = 7.4 (m)

μ_w = dynamic viscosity of water = $1.307 \cdot 10^{-3}$ (Ns/m^2)

Q = rate of production of compressed gas (m^3/a)

K = hydraulic conductivity = $1 \cdot 10^{-13} - 3 \cdot 10^{-11}$ (m/s)

L = length of repository = 4660 (m)

The gas production inside the lining has been considered for the displacement of water from the repository. The pressure differences for various assumed hydraulic conductivities in the repository lining have been calculated for four cases of gas production.

Case N61 corresponds to a gas production rate of 1.0×10^{-3}. m^3(STP)/s and N62 to a gas production rate of 6.7×10^{-5} m^3(STP)/s both with hydrostatic pressure 2.0 MPa. Case N71 corresponds to a gas production rate of 1.5×10^{-3} m^3(STP)/s and case N72 to 5.4×10^{-4} m^3(STP)/s, both with hydrostatic pressure 1.5 MPa. These cases correspond to the near-field scenarios N6 and N7 described in NGB 85-08. The results for the different cases are presented in Section 5.3.5, Table 31.

5.3.5 Results

The escape of gases, primarily hydrogen, through the repository lining has been studied. The lining material is concrete with low conductivity for both water and gases. In addition, the capillary pressure of unfractured concrete is high. In order to escape from the repository, the gases must produce a pressure that exceeds the sum of the capillary pressure and the hydrostatic pressure. This pressure may be high enough to cause the lining to crack.

The results from calculations of gas transport in barrier materials are presented in the following order; firstly, the gas transport capacity in a fractured barrier is presented for a number of fracture apertures and frequencies; secondly, the combinations of pressure difference at which fractures are formed in the lining are presented and, thirdly, the possibility of such high pressure build-up in the repository prior to any significant displacement of water is estimated.

The required gas transport capacity is $1.5 \cdot 10^{-3}$ m^3(STP)/s and the hydrostatic pressure at repository level is 1.5 MPa /NGB 85-07/. By making reasonable assumptions regarding the range of pressure differences over the repository lining and the area available for gas transport, the values for the required fracture apertures and frequencies presented in Table 29 were calculated.

Table 29. Required fracture frequencies, n, and fracture apertures, b, for the given gas flow rate. Values in brackets indicate that the capillary pressure corresponding to the calculated fracture aperture exceeds the assumed pressure difference and should therefore be disregarded.

Roof area available for gas transport A (m^2)	Length of transport path i.e. lining thickness L (m)	Assumed pressure difference over the lining P (Pa)	Fracture frequency n (m^{-1})	Fracture aperture b (m)	Capill. pressure corr. to fracture aperture (Pa)
$1.4 \cdot 10^4$	0.9	$4 \cdot 10^3$	0.1	$6.7 \cdot 10^{-5}$	$1.1 \cdot 10^3$
			0.2	$5.3 \cdot 10^{-5}$	$1.4 \cdot 10^3$
			1	$3.1 \cdot 10^{-5}$	$2.4 \cdot 10^3$
			5	$(1.8 \cdot 10^{-5})$	$4.1 \cdot 10^3$
			10	$(1.5 \cdot 10^{-5})$	$4.9 \cdot 10^3$
$2.3 \cdot 10^4$	0.9	$1 \cdot 10^4$	0.1	$4.2 \cdot 10^{-5}$	$1.8 \cdot 10^3$
			0.2	$3.3 \cdot 10^{-5}$	$2.3 \cdot 10^3$
			1	$1.9 \cdot 10^{-5}$	$3.9 \cdot 10^3$
			5	$1.1 \cdot 10^{-5}$	$6.8 \cdot 10^3$
			10	$9.0 \cdot 10^{-6}$	$8.3 \cdot 10^3$
$1.4 \cdot 10^4$	1.5	$4 \cdot 10^3$	0.1	$6.1 \cdot 10^{-5}$	$1.2 \cdot 10^3$
			1	$2.8 \cdot 10^{-5}$	$2.7 \cdot 10^3$
			10	$(1.3 \cdot 10^{-5})$	$5.7 \cdot 10^3$
$2.3 \cdot 10^4$	1.5	$1 \cdot 10^4$	0.1	$5.0 \cdot 10^{-5}$	$1.5 \cdot 10^3$
			1	$2.3 \cdot 10^{-5}$	$3.2 \cdot 10^3$
			10	$1.1 \cdot 10^{-5}$	$6.8 \cdot 10^3$
$1.4 \cdot 10^4$	0.9	$4 \cdot 10^3$	$3 \cdot 10^4$	$(1 \cdot 10^{-6})$	$7.4 \cdot 10^4$
			$3 \cdot 10^7$	$(1 \cdot 10^{-7})$	$7.4 \cdot 10^5$

The results show that, for example, with 1 fracture every 0.1 metres, both the required fracture aperture and the required pressure difference are small. Hence, with a reasonable amount of very small fractures in the barrier material, the gas can be released from the repository without any significant displacement of contaminated water.

To predict the possibility of fracture formation in the repository lining, the mechanical stress in the material induced by an overpressure inside the repository was analysed. In Table 30 the maximum internal overpressure is presented for different allowed tensile stresses in the material.

Table 30. The maximum pressure difference over the repository lining as a function of the allowed tensile stress

Tensile stress σ_j (MPa)	Pressure drop ΔP_1 (MPa)
1.8	0.24
3.0	0.40

The results show that fracture formation in the repository lining can be expected if the internal overpressure, i.e. the pressure difference over the lining, exceeds 0.2-0.4 MPa.

Finally, it is essential to predict the sequence of events, i.e. whether or not fractures can be expected to be formed in the lining prior to a displacement of contaminated water from the repository. In the calculations, the displacement of contaminated water is assumed to take place at a rate corresponding to the production of compressed gases. When water is pressed out through the lining, a considerable pressure drop over the lining will occur. At high rates of displacement, this pressure difference will be sufficient to form fractures in the lining. In Table 31 the pressure difference is calculated for various combinations of hydraulic conductivities in the lining material and gas production rates.

Table 31. Pressure difference for various assumed conductivities in the repository lining and various gas production rates. Shaded areas indicate the range of pressure difference for which fracture formation in the repository lining is expected

Concrete conductivity	Pressure differ.(Cases N61,N62,N71,N72 are presented in Section 5.3.4)			
K (m^3)	P_{N61} (MPa)	P_{N62} (MPa)	P_{N71} (MPa)	P_{N72} (MPa)
$1 \cdot 10^{-10}$	0.06	0.003	0.13	0.06
$7 \cdot 10^{-11}$	0.09	-	0.18	0.09
$6 \cdot 10^{-11}$	0.10	-	0.21	0.10
$5 \cdot 10^{-11}$	0.12	-	0.25	0.12
$3 \cdot 10^{-11}$	0.20	-	0.40	0.19
$1 \cdot 10^{-11}$	0.55	0.09	1.0	0.53
$5 \cdot 10^{-12}$	-	0.18	-	-
$4 \cdot 10^{-12}$	-	0.22	-	-
$3 \cdot 10^{-12}$	-	0.29	-	-
$1 \cdot 10^{-12}$	3.4	0.78	5.1	3.1
$1 \cdot 10^{-13}$	14.0	4.4	18.8	12.2

By comparing the results presented in Table 31 with those given in Table 30, it can be concluded that fractures will be formed in the concrete lining prior to any significant displacement of water if the hydraulic conductivity is less than $3 \cdot 10^{-11}$-$7 \cdot 10^{-11}$ m/s at the given rate of gas production (N61 and N62). If we disregard the contribution from radiolysis and corrosion of aluminium to the total gas production rate, the crack formation will occur if the conductivity is less than $5 \cdot 10^{-12}$-$3 \cdot 10^{-11}$ m/s. (N71 and N72). By comparison, normal values for concrete conductivities are $8 \cdot 10^{-12}$-$3 \cdot 10^{-11}$ m/s /NTB 82-03/.

To summarize the results, it can be concluded that, for normal concrete hydraulic conductivities, the displacement of water will result in a pressure difference which is sufficient to form fractures in the repository lining. Once small fractures are formed, the gas can be released from the repository without any significant displacement of contaminated water.

6. GAS TRANSPORT IN THE HOST ROCK

6.1 Description of the geology

Oberbauen Stock has been chosen as the model reference site for "Project Gewähr". The site was selected under consideration of numerous criteria for the suitability of the repository location. One reason for choosing Oberbauen Stock as a reference site was the data available from the construction of the Seelisberg tunnel situated not far from the planned location of the repository. For more detailed information, see NTB 84-20 and NGB 85-07.

6.1.1 Location of the repository and tunnels

The repository has a 200-450 m rock overburden of Valanginian marl followed by a layer of Valanginian limestone and various layers of lime and shale. The total overburden is 750-1,500 m. In the calculations, the highly permeable layer on top of the marl has been considered as a chimney for the gas. A description of the various layers of rock materials is given in Figure 28.

The connecting tunnel has a total rock overburden of, at most, 300 m.

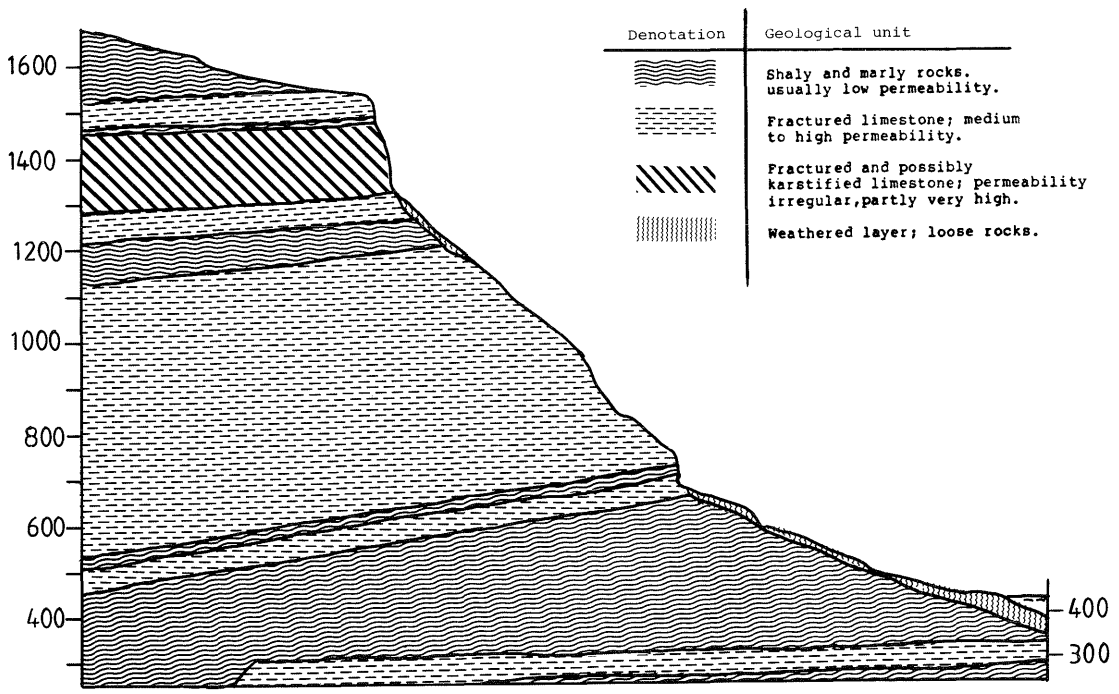

Figure 28. A section through the host rock showing the different layers of material /NTB 84-20/

6.1.2 Lineaments in the marl

In the Valanginian marl, some fracture zones with higher conductivities occur. Throughout this report these fracture zones are called lineaments. In the lineaments, the hydraulic conductivity may be 10-100 times higher than the hydraulic conductivity in the dense marl. These lineaments are reported to occur with 5 m mean spacing and have a width of 0.02-0.05 m each. A statistical inventory of these lineaments is given in /NTB 84-20/.

6.1.3 Decompressed zone around engineered tunnels

When constucting the transport tunnels and the repository caverns, the stress field in the rock is altered /NTB 85-30/. This results in a concentric zone around the tunnels with increased hydraulic conductivities. This zone can be divided into an inner and outer decompressed zone.

In this report, the inner zone has been neglected as its dimension are of lesser significance.

6.2 Description of possible pathways

6.2.1 General

The gases produced in the repository can be transported through the rock in three different zones - the dense marl, the lineaments in the marl and the decompressed zone around engineered tunnels. The gas might also accumulate in the decompressed zone; see Figures 29,30. The transport capacity of the different zones is determined by their conductivity and the cross-sectional area available for gas transport. The potential gradient is then the driving force.

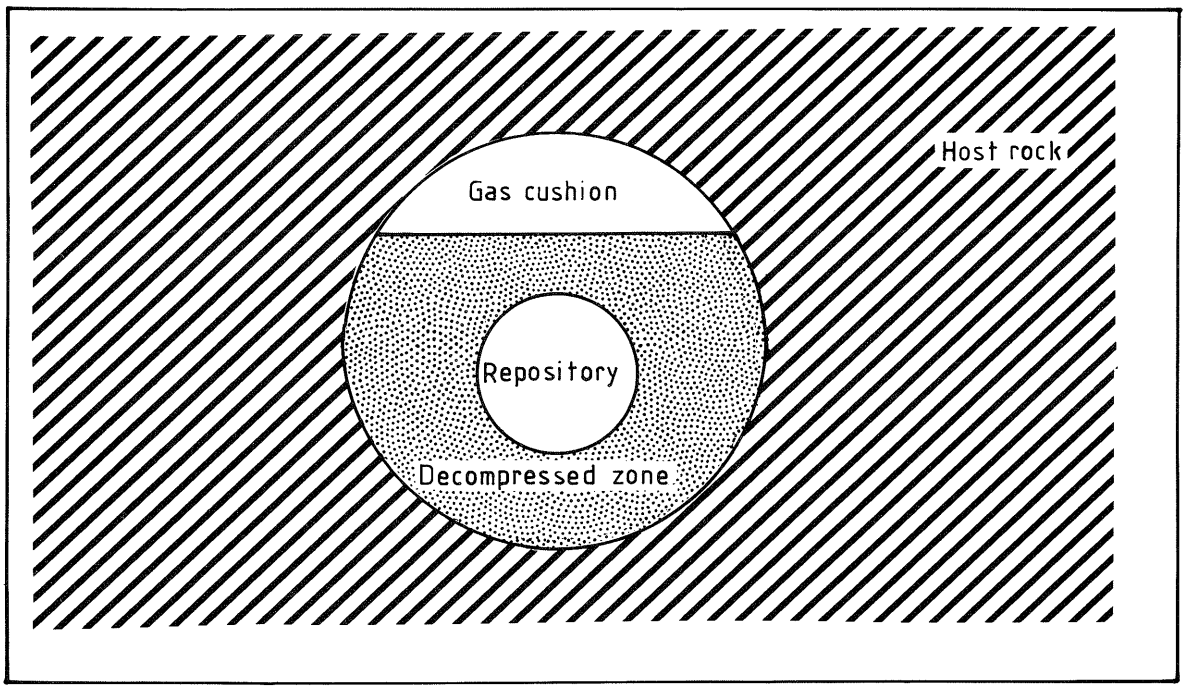

Figure 29. Schematic representation of the formation of a gas cushion at the top of the decompressed zone around the repository caverns

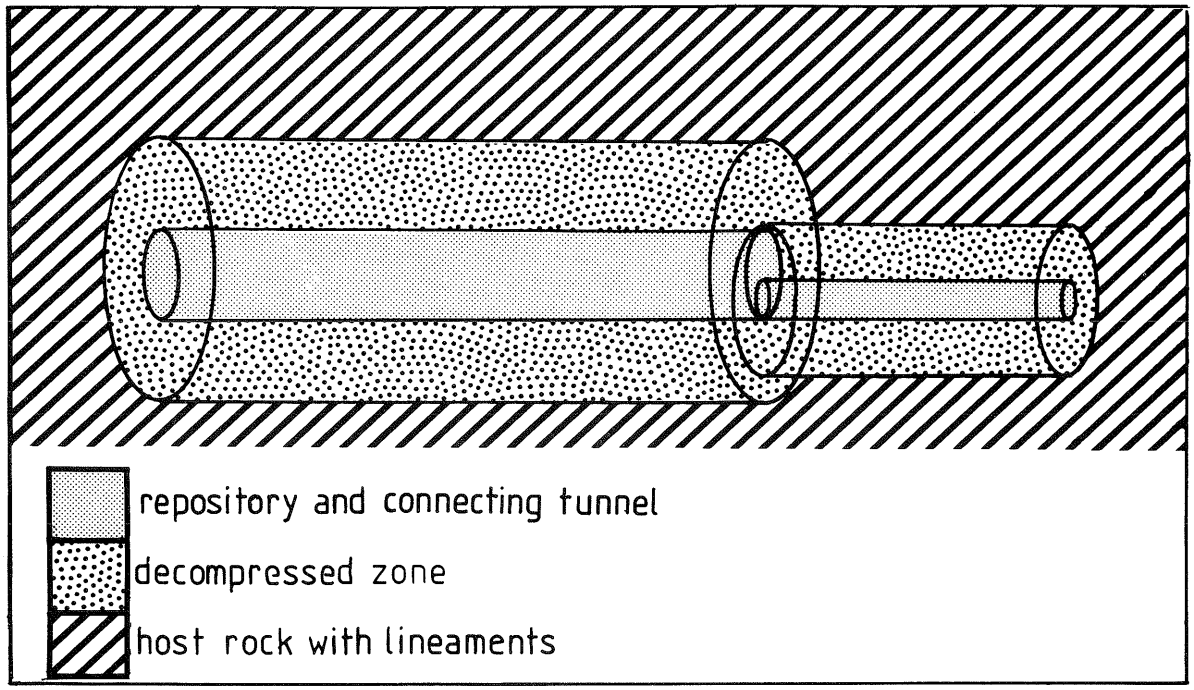

Figure 30. Principal paths for gas transport in the host rock

The hydraulic conductivities for the different zones are given as intervals in Table 32.

Table 32. Hydraulic conductivities for the different zones in the host rock

Zone	Hydraulic conductivity (m/s) Ref. /NTB 84-20, NGB 85-07/
Dense marl	$1 \cdot 10^{-12}$–$1 \cdot 10^{-8}$
Lineaments in the marl	$1 \cdot 10^{-9}$–$1 \cdot 10^{-7}$
Decompressed zones (inner)	$1 \cdot 10^{-8}$–$1 \cdot 10^{-6}$ (Not used in calculations)
Decompressed zones (outer)	$1 \cdot 10^{-9}$–$1 \cdot 10^{-7}$

6.2.2 Gas transport in dense marl and in lineaments

The difference in transport capacity for these two zones depends on the conductivity and the cross-sectional area available for gas transport. The lineaments constitute only about one per cent of the total area.

No data are available on the pore size distributions for either the dense marl or the lineaments. Therefore it has been decided to use the same pore size distribution for both. This means that, in the lineaments where the conductivity is higher, the pore size distribution is the same as for the dense marl but the number of pores is greater. (This assumption is in contradiction with the hydraulic assumptions where the same porosity in both zones is assumed).

6.2.3 Gas transport in the decompressed zones

When building the connecting tunnel and the repository, the stress field in the rock material is altered. This results in a zone with increased conductivity around the tunnels. The conductivity increase has been estimated to be 10-1,000 times the conductivity of the undisturbed marl /NTB 85-30/.

The estimated radius of the decompressed zone around the repository is 25-35 metres and 5-10 metres around the tunnels /NTB 85-30/.

The possibility of gas transport in the decompressed zone along the transport tunnel was investigated but was found to be of minor importance. This is due to the fact that the area available for gas transport in the axial direction of the transport tunnel is very small compared with the area of the cavern roof. Before closing the repository, cement might be injected into the decompressed zone around the tunnel at certain places to prevent migration of nuclides along the tunnel /NTB 84-33/. These barriers will also hinder gas transport along the tunnels.

The decompressed zone around the repository can also be of great importance as a zone in which the gas will accumulate. The gas is assumed to penetrate the repository lining easily, either through specially designed gas release devices or through fractures in the concrete. The decompressed zone is assumed to include rather wide fractures or pores, so that the capillary pressure within this zone is small and gas penetration is readily possible. If the gas cushion is built up in the decompressed zone instead of in the repository cavern, the amount of contaminated water displaced from the repository is very much reduced.

6.3 Material properties

6.3.1 Capillary pressure

To enable gas transport through a fractured or porous medium, the gas pressure has to exceed the capillary pressure /48/. This means that a pressure build-up must occure before any gas can penetrate the porous or fractured material. The relationship between capillary pressure and pore size (i.e. the radii of the curvature of the interface, R_1 and R_2) is given by the Laplace formula;

$$P_c = \sigma(\frac{1}{R_1} + \frac{1}{R_2}) \cos\theta \qquad (6\text{-}1)$$

Where

P_c = capillary pressure	(N/m^2)
γ = surface tension for the hydrogen-water interface	(N/m)
θ = contact angle between interface and rock wall	(^{0})
R_1, R_2 = radius of the curvature of the interface	(m)

In Figure 31, an illustration of a gas-water interface in a capillary pore is given.

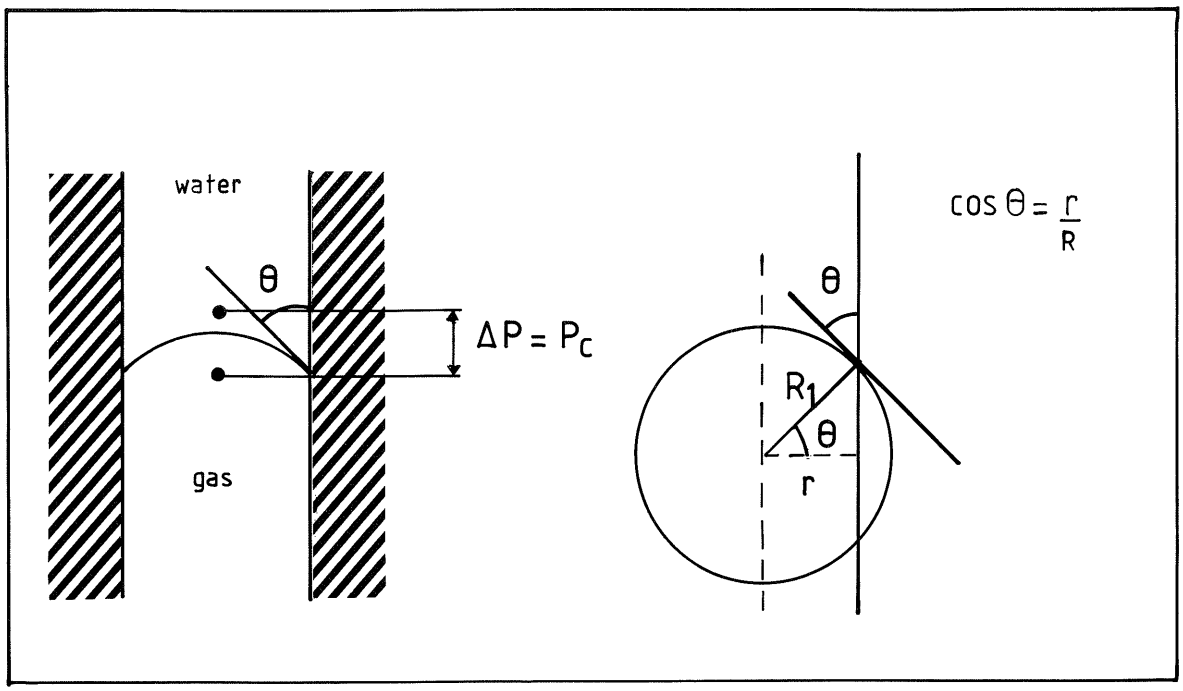

Figure 31. Schematic representation of a capillary tube showing the curvature R_1 of the interface between gas and water; r is the pore radius. For a fully wetted system, the contact angle θ is zero and $r=R_1$

If we assume a rock material with distributed fracture or pore sizes, only the water in the largest fractures will be displaced when the gas pressure applied just exceeds the minimum capillary pressure and the hydrostatic pressure. To displace the water in smaller fractures or pores, a higher pressure must be built up.

Experimental methods exist for measuring the capillary pressure and the pore size distribution of porous materials. From these measurements, capillary pressure curves as a function of the degree of volumetric water saturation are obtained. A number of curves for different geological materials are presented in Figure 32. Capillary pressure curves can be used to calculate the relative conductivity for the gas in an unsaturated fractured or porous material as a function of the gas pressure applied or the degree of water saturation; see next Section.

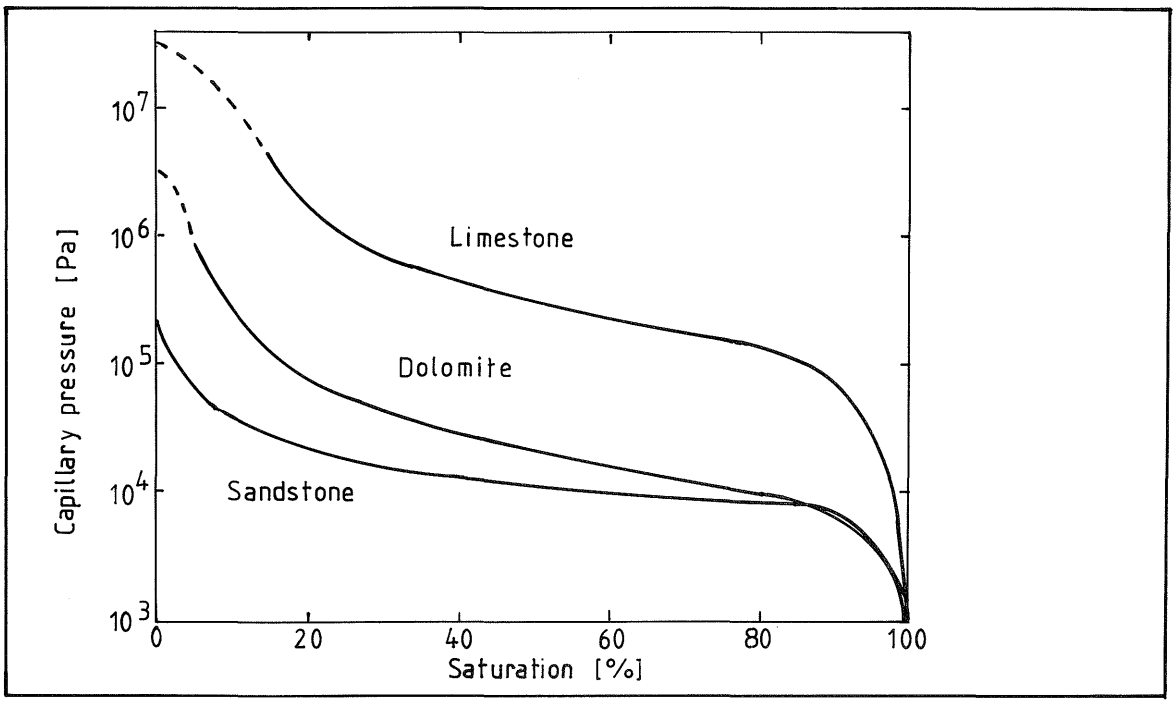

Figure 32. Capillary pressure versus saturation with water for three different rock materials. Compilation of data from /49,50/

6.3.2 Conductivity

To characterize the transport capacity of a geological medium, the permeability is conveniently used. The permeability is a material constant determined only by the porous structure and does not depend on the fluid being transported. Various experimental methods exist for measuring the permeability in rock materials. For example, the permeability may be obtained from measurements of hydraulic conductivity, by measuring the water loss in a borehole (so-called packer tests).

To estimate the transport capacity of an in water insoluble fluid or gas in the porous material, the conductivity must be corrected for pores filled with water since they do not contribute to the gas transport capacity.

Thus, only those pores which are not water-filled are available for gas transport. This correction is expressed as the relative conductivity (K_{rnw}) of the gas phase. The relative conductivities corresponding to the capillary curves given in Figure 32 are calculated using the method described below and are presented in Figure 33.

In the gas transport calculations, the effective conductivity is used. The effective conductivity is the product of the relative conductivity and the hydraulic conductivity at saturation.

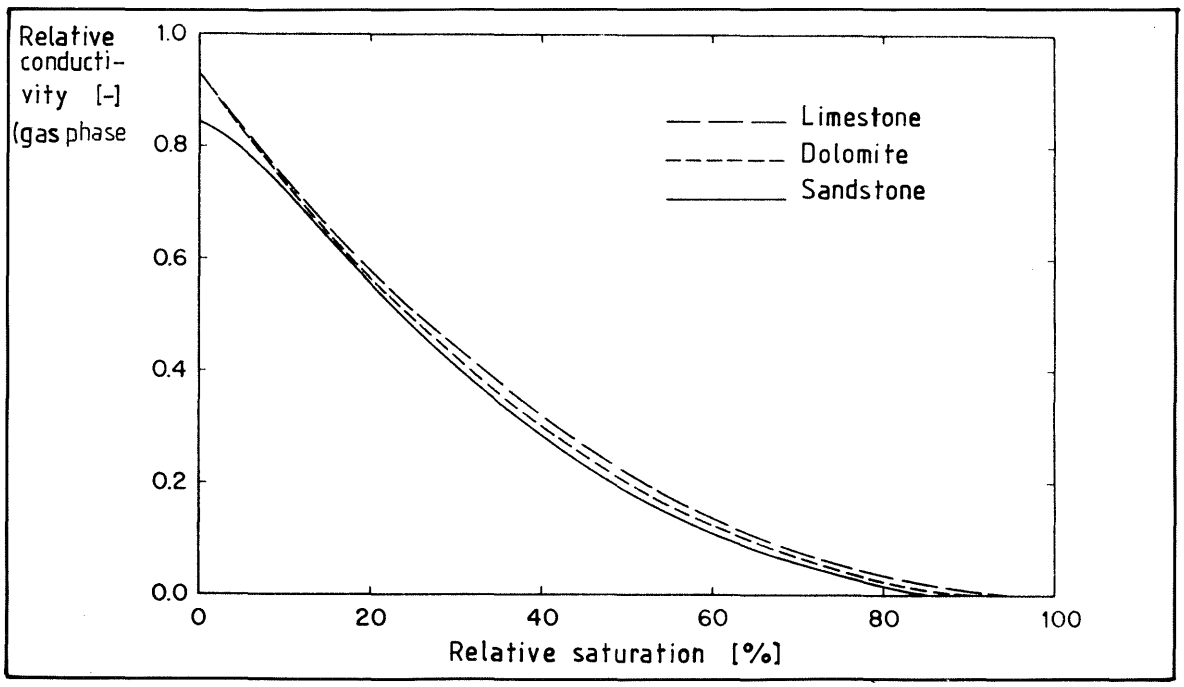

Figure 33. Relative conductivities versus saturation for the three different rock materials

In the literature, various methods are proposed for estimating the relative conductivity in a porous medium /42, 43/.
The relative conductivity can be calculated in the following way, assuming a boundle of capillary tubes. The value of the degree of saturation, S_w, should be corrected for the irreducible wetting phase saturation, S_{wi}, /42, 43/;

$$S_{wi} = 1 - \frac{\varepsilon_{eff}}{\varepsilon} \qquad (6\text{-}2)$$

where
$\varepsilon_{effective}$ is the drainable porosity, and ε is the total porosity. The drainable porosity is determined by direct measurements.

This correction for the irreducible wetting phase saturation is made to account for water being strongly bound in the thinnest capillaries, for example by adsorption.

The effective saturation, S_{eff}, also called reduced saturation, can be calculated by the method proposed by /43/;

$$S_{eff} = \frac{S_w - S_{wi}}{1 - S_{wi}} \qquad (6\text{-}3)$$

If the pore size distribution function, (D), is known, the effective saturation as a function of the pore diameter, D, can be evaluated;

$$S_{eff} = \frac{\int_{D_1}^{D} D^2 \gamma(D)\, dD}{\int_{D_1}^{D_2} D^2 \gamma(D)\, dD} \qquad (6\text{-}4)$$

where D_1 and D_2 are lower and upper limiting pore diameters in the porous material respectively.

The relative conductivity for the gas phase, K_g, is given by /43/; When the value of the effective saturation is known;

$$K_g = (1 - S_{eff})^2 \frac{\int_{S_{eff}}^{1} \frac{dS_{eff}}{(P_c(S_{eff}))^2}}{\int_{0}^{1} \frac{dS_{eff}}{(P_c(S_{eff}))^2}} \qquad (6\text{-}5)$$

where P_c is the capillary pressure. Except for very simple cases, these calculations are best performed using numerical methods.

The method outlined above has not been used in detail in the present report due to lack of information regarding the irreducible wetting phase saturation and the pore size distribution function. However, with the assumption that S_{eff} equals S_w, the equation (6-5) was numerically integrated using the capillary pressure curves in Figure 32 as $P_c=f(S_w)$. The results are presented in Figure 33.

6.3.3 Estimation of conductivities by the use of ventilation calculations

In geological formations where no direct measurements have been performed, the conductivities are unknown and must be estimated. Before the construction of the motorway tunnel, two pilot tunnels were built. Because of the possibility of methane gas formation within the tunnels, ventilation was necessary. From observations in existing tunnels, the tunnel walls are reported to be dry. Since the tunnels are ventilated, the necessity for estimation of water transport by ventilation air was obvious. In addition, it was found that this is a good experimental method for obtaining the large scale conductivity in a tunnel using very simple techniques. Further, it was possible to calculate a maximum value for the large scale conductivity of the rock from the available information.

The general principle for the calculations was to estimate the amount of water that can be evaporated from the tunnel walls and transported out by the air stream. Due to conservation of mass, this amount of water must then also be transported into the tunnel through the rock. A high conductivity compared to the transport capacity of the ventilation air stream would result in wet walls in the tunnel, whereas a low conductivity would result in the formation of a dry zone in the rock walls. The results can be compared with reports from visual inspections of the tunnel.

In the tunnel studied the walls are reported to be dry or partly moist /1/. This means that the calculations can be used directly to predict a maximum large scale conductivity of the rock if the hydraulic gradient is known. In this report, different values for the hydraulic gradient were assumed, giving a range for the maximum value of the large scale conductivity.

The calculations are to be regarded as a parametric study. The data assumed in the calculations cover a wide range but the results can be used to make better estimates of the conductivity and to draw conclusions on whether the rock is water-bearing or dry.

The amount of water transported into a tunnel through the rock is obtained by the hydraulic conductivity and the hydraulic gradient in the rock (Darcy's law);

$$q = K_p \cdot i \qquad (6\text{-}6)$$

where:

q	=	water flow per unit area	$(m^3/m^2,s)$
K_p	=	hydraulic conductivity	(m/s)
i	=	hydraulic gradient	(m/m)

Total water flow into the tunnel;

$$G_w = q\ \rho_w\ A \qquad (6\text{-}7)$$

where:

G_w =	total water flow	(kg/s)
A =	total area of rock walls	(m^2)
S_w =	density of water	(kg/m^3)

The amount of water evaporated and ventilated out is calculated from the air flow and the difference in moisture content between the incoming and the outgoing air stream; see Figure 34.

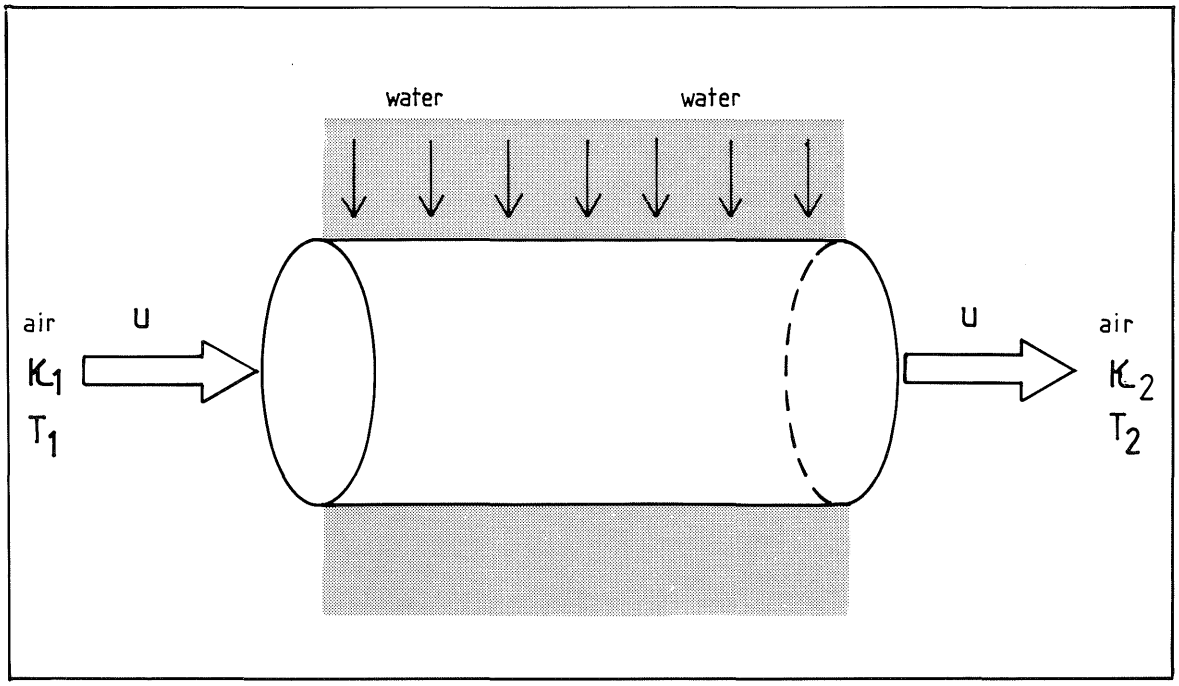

Figure 34. A ventilated tunnel. Incoming air has temperature T_1 and relative humidity H_1, outgoing air has temperature T_2 and relative humidity H_2. The velocity of the air stream is u

The amount of air is;

$$V = u\ A_c \qquad (6\text{-}8)$$

where:

V =	volumetric flow of air	(m^3/s)
u =	velocity of the air stream	(m/s)
A_c=	cross-sectional area of tunnel	(m^2)

The change in water content between the incoming and the outgoing air stream with steady-state conditions is given by;

$$G_a = V(\xi_2 W(T_2) - \xi_1 W(T_1)) \qquad (6\text{-}9)$$

where:

G_a = amount of water transported by air (kg/s)

H_1, H_2 = relative humidity of air entering and leaving the tunnel respectively

$W(T)$ = water content in saturated air at temperature T (kg/m^3)

T_1, T_2 = temperature of air at tunnel entrance and exit respectively

In addition, for low conductivities, the water transport capacity of the air may be higher than the water transport capacity in the rock. In such cases, a dry zone is developed in the rock wall.

The water transport through the dry zone will be determined by diffusion. Using a steady-state formula, the maximum thickness of the dry zone can be calculated

$$Z = \frac{D_e A \Delta C}{G_w} \qquad (6\text{-}10)$$

where:

Z = thickness of the dry zone (m)

D_e = $D G_f \varepsilon$ = effective diffusivity of water vapour (m^3/s)

A = rock wall area (m^2)

C = concentration difference of water vapour over the dry zone (kg/m^3)

G_w = flow of water (kg/s)

D = diffusivity of water vapour in air (m^2/s)

G_f = a geometric factor describing tortuosity and constrictivity of the pores

ε = porosity of the rock (gas-filled porosity)

If the rock is water-bearing it should be possible to measure an increase in the air humidity as it passes through the tunnel. However, since no such data are available, assumptions must be made regarding moisture content and temperatures. In addition, the hydraulic gradient is unknown and has, therefore, been varied within a large interval in the calculations. By assuming a constant temperature of 10°C in the air stream and an increase in the relative humidity from 60 to 80 percent as the air flows through the tunnel, the possible water transport was estimated to be about 600 tonnes per year from a 1 km tunnel with an air flow of 5 m^3 (STP)/s. This corresponds to a rock hydraulic conductivity of $1 \cdot 10^{-9}$ m/s for an assumed hydraulic gradient of 2 m/m and to a conductivity of $1 \cdot 10^{-8}$ m/s for an assumed hydraulic gradient of 0.2 m/m. This corresponds in turn to the maximum conductivities which can be expected.

If it is assumed that there is an increase in humidity in the ventilation air stream and that a dry zone of finite thickness in the rock wall is observed, one can also estimate the minimum value of the conductivity. This value should correspond to the measured increase in the humidity of the ventilation air stream as well as to the transport rate of water vapour through the dry zone. For a conductivity of $1 \cdot 10^{-12}$ m/s, the estimated dry zone is 0.2-3.1 m thick. If the dry zone observed in the rock wall is 0.2 m or less, this would then give a minimum hydraulic conductivity of 10^{-12} m/s. This serves only as an example.

The results from the calculations are presented in detail in Tables 33 and 34. Basic data and nomenclature can be found in Table 34.

From the results it can be concluded that the ventilation air can carry large amounts of water out of the tunnel. The consequence is that the rock wall may be dry while the rock itself is water-filled. The estimated maximum conductivity is $1 \cdot 10^{-8}$ m/s. It should be possible to estimate the minimum permeability but this requires observation of relative humidities and dry zones.

Table 33. Results from the ventilation calculations for a hydraulic gradient of 1 and 2 m/m (G_f=0.05)

Kp m/s	i m/m	K_1 Relative-%	K_2	ε	D_e m^2/s	L m	Gw kg/s	Ga kg/s	Tr °C	Ta	Z m	Remarks	Ga kg/s	Tr °C	Ta	Z m	Remarks
10^{-8}	1	60	100	0.03	$2.3\cdot10^{-7}$	1000	0.11	$3.8\cdot10^{-2}$	10	10	-	Wet wall	$5.3\cdot10^{-2}$	15	15	-	Wet wall
10^{-8}	2	60	100	0.03	$2.3\cdot10^{-7}$	1000	0.22	$3.8\cdot10^{-2}$	10	10	-	Wet wall	$5.3\cdot10^{-2}$	15	15	-	Wet wall
10^{-10}	1	60	100	0.03	$2.3\cdot10^{-7}$	1000	$1\cdot10^{-3}$	$3.8\cdot10^{-2}$	10	10	$4\cdot10^{-3}$	Wet/dry	$5.3\cdot10^{-2}$	15	15	$6\cdot10^{-3}$	Wet/dry
10^{-10}	2	60	100	0.03	$2.3\cdot10^{-7}$	1000	$2\cdot10^{-3}$	$3.8\cdot10^{-2}$	10	10	$2\cdot10^{-3}$	"	$5.3\cdot10^{-2}$	15	15	$3\cdot10^{-3}$	"
10^{-12}	1	60	100	0.03	$2.3\cdot10^{-7}$	1000	$1\cdot10^{-5}$	$3.8\cdot10^{-2}$	10	10	0.43	Dry	$5.3\cdot10^{-2}$	15	15	0.63	Dry
10^{-12}	2	60	100	0.03	$2.3\cdot10^{-7}$	1000	$2\cdot10^{-5}$	$3.8\cdot10^{-2}$	10	10	0.22	"	$5.3\cdot10^{-2}$	15	15	0.31	"
10^{-10}	1	60	100	0.02	$1.6\cdot10^{-7}$	1000	$1\cdot10^{-3}$	$3.8\cdot10^{-2}$	10	10	$3\cdot10^{-3}$	Wet/dry	$5.3\cdot10^{-2}$	15	15	$4\cdot10^{-3}$	Wet/dry
10^{-10}	1	60	100	0.04	$3.1\cdot10^{-7}$	1000	$1\cdot10^{-3}$	$3.8\cdot10^{-2}$	10	10	$6\cdot10^{-3}$	"	$5.3\cdot10^{-2}$	15	15	$8\cdot10^{-3}$	"
10^{-10}	1	60	80	0.03	$2.3\cdot10^{-7}$	1000	$1\cdot10^{-3}$	$2.0\cdot10^{-3}$	10	10	$7\cdot10^{-3}$	"	$2.7\cdot10^{-2}$	15	15	$9\cdot10^{-3}$	"
10^{-10}	1	50	100	0.03	$2.3\cdot10^{-7}$	1000	$1\cdot10^{-3}$	$4.4\cdot10^{-2}$	10	10	$6\cdot10^{-3}$	"	-	-	-	-	-
10^{-10}	1	70	100	0.03	$2.3\cdot10^{-7}$	1000	$1\cdot10^{-3}$	$2.8\cdot10^{-2}$	10	10	$3\cdot10^{-3}$	"	-	-	-	-	-
10^{-10}	1	60	100	0.03	$3.5\cdot10^{-8}$ *)	1000	$1\cdot10^{-3}$	$3.8\cdot10^{-2}$	10	10	$7.5\cdot10^{-4}$	"	$5.3\cdot10^{-2}$	15	15	$1\cdot10^{-3}$	Wet/dry

Table 33 Numerical values of the calculations for a hydraulic gradient of 1 and 2. (G_f=0.05)

* G_f=0.3

Table 34. Results from the ventilation calculations for a hydraulic gradient of 0.2 and 0.4 m/m (G_f = 0.05)

Kp m/s	i m/m	K_1 Relative-%	K_2 Relative-%	ε	D_e m^2/s	L m	Gw kg/s	Ga kg/s	Tr °C	Ta °C	Z m	Remarks	Ga kg/s	Tr °C	Ta °C	Z m	Remarks
10^{-8}	0.2	60	100	0.03	$2.3 \cdot 10^{-7}$	1000	$2 \cdot 10^{-2}$	$3.8 \cdot 10^{-2}$	10	10	$2 \cdot 10^{-4}$	Wet wall	$5.3 \cdot 10^{-2}$	15	15	$3 \cdot 10^{-4}$	Wet wall
10^{-8}	0.4	60	100	0.03	$2.3 \cdot 10^{-7}$	1000	$4 \cdot 10^{-2}$	$3.8 \cdot 10^{-2}$	10	10	$1 \cdot 10^{-4}$	Wet wall	$5.3 \cdot 10^{-2}$	15	15	$2 \cdot 10^{-4}$	Wet wall
10^{-10}	0.2	60	100	0.03	$2.3 \cdot 10^{-7}$	1000	$2 \cdot 10^{-4}$	$3.8 \cdot 10^{-2}$	10	10	$2 \cdot 10^{-2}$	Wet/dry	$5.3 \cdot 10^{-2}$	15	15	$3 \cdot 10^{-2}$	Wet/dry
10^{-10}	0.4	60	100	0.03	$2.3 \cdot 10^{-7}$	1000	$4 \cdot 10^{-4}$	$3.8 \cdot 10^{-2}$	10	10	$1 \cdot 10^{-2}$	"	$5.3 \cdot 10^{-2}$	15	15	$2 \cdot 10^{-2}$	"
10^{-12}	0.2	60	100	0.03	$2.3 \cdot 10^{-7}$	1000	$2 \cdot 10^{-6}$	$3.8 \cdot 10^{-2}$	10	10	2.2	Dry	$5.3 \cdot 10^{-2}$	15	15	3.1	Dry
10^{-12}	0.4	60	100	0.03	$2.3 \cdot 10^{-7}$	1000	$4 \cdot 10^{-6}$	$3.8 \cdot 10^{-2}$	10	10	1.1	"	$5.3 \cdot 10^{-2}$	15	15	1.6	"
10^{-10}	0.2	60	100	0.02	$1.6 \cdot 10^{-7}$	1000	$2 \cdot 10^{-4}$	$3.8 \cdot 10^{-2}$	10	10	$1 \cdot 10^{-2}$	Wet/dry	$5.3 \cdot 10^{-2}$	15	15	$2 \cdot 10^{-2}$	Wet/dry
10^{-10}	0.2	60	100	0.04	$3.1 \cdot 10^{-7}$	1000	$2 \cdot 10^{-4}$	$3.8 \cdot 10^{-2}$	10	10	$3 \cdot 10^{-2}$	"	$5.3 \cdot 10^{-2}$	15	15	$4 \cdot 10^{-2}$	"
10^{-10}	0.2	60	80	0.03	$2.3 \cdot 10^{-7}$	1000	$2 \cdot 10^{-4}$	$2.0 \cdot 10^{-2}$	10	10	$3 \cdot 10^{-2}$	"	$2.7 \cdot 10^{-2}$	15	15	$5 \cdot 10^{-2}$	"
10^{-10}	0.2	50	100	0.03	$2.3 \cdot 10^{-7}$	1000	$2 \cdot 10^{-4}$	$4.4 \cdot 10^{-2}$	10	10	$3 \cdot 10^{-2}$	"	-	-	-		-
10^{-10}	0.2	70	100	0.03	$2.3 \cdot 10^{-7}$	1000	$2 \cdot 10^{-4}$	$2.8 \cdot 10^{-2}$	10	10	$2 \cdot 10^{-2}$	"	-	-	-		-
10^{-10}	0.2	60	100	0.03	$3.5 \cdot 10^{-8}$ *)	1000	$2 \cdot 10^{-4}$	$3.8 \cdot 10^{-2}$	10	10	$3 \cdot 10^{-2}$	"	$5.3 \cdot 10^{-2}$	15	15	$5 \cdot 10^{-2}$	Wet/dry

Table 34 Numerical values of the calculations for a hydraulic gradient of 0.2 and 0.4. (G_f=0.05)

*G_f=0.3

Table 35. Basic data and assumptions. Symbols used

The tunnel is assumed to be a cylinder.	
Tunnel cross-section area	A_C = 10 m^2
Hydraulic conductivity	Kp = 10^{-8},10^{-10},10^{-12} m/s
Hydraulic gradient	i = 0.2-2 m/m
Velocity of air	u = 0.5 m/s
Length of tunnel	L = 1,000 m
Rock wall area	A_w= 11,200 m^2
Density of water	S_w= 1,000 kg/m^3
Mean temperature of rock wall	Tr = 10, 15°C
Mean temperature of air	Ta = 10, 15°C
Humidity of air, incoming	H_1 = 50,60,70%-rel.
" " " , outgoing	H_2 = 80,100%-rel.
Rock porosity	ε = 0.02,0.03,0.04
Geometric factor	Gf = 3-20
Diffusivity of water vapour in air	D = $2.4 \cdot 10^{-5}$ m^2/s
Heat of evaporation	H = 2,500 kJ/kg H_2O
Heat conductivity of rock	λ = 1 W/m, °C
Moisture content of saturated air	W(10°)=$9.40 \cdot 10^{-3}$ kg/m^3 W(15°)=$12.8 \cdot 10^{-3}$ kg/m^3

Table 35. continued

Darcy velocity of water	q	(m^3/ m^2 s)
Flow of air	V	(m^3/s)
Distance	x	(m)
Temperature gradient	$\frac{\partial T}{\partial X}$	(^oC/m)
Depth of the dry zone	Z	(m)

Remark The geometric factor Gf is defined as the constrictivity divided by the tortuosity squared.

When water is evaporated, heat must be supplied by the rock to maintain a constant temperature in the rock wall. The major contribution to the heat supply is by conduction in the rock material, assuming that no heat is supplied by the air. The required amount of heat is given by;

$$Q = H\ G_w \qquad (6\text{-}11)$$

where:

Q = heat flow (J/s)

H = heat of evaporation (J/kg)

G_w = water flow (kg/s)

Assuming steady-state conditions, the thermal gradient in the rock required to maintain a balance between heat supply and evaporation can be calculated;

$$Q = \lambda\ A\ \frac{\partial T}{\partial X} \qquad (6\text{-}12)$$

where:

λ = heat conductivity of rock material (J/s/m/^{o}C)

A = rock wall area (m^2)

$\frac{\partial T}{\partial X}$ = thermal gradient in rock material (^{o}C/m)

The energy needed to evaporate the water was roughly estimated using the data presented in Table 30. The results show that the heat can be supplied by the rock without any significant decrease in temperature. The necessary thermal gradient was calculated to be 0.02 ^{o}C/m, which is about the same as a normal geothermal gradient.

6.4 Gas and water transport in a water-bearing fissured rock

To enable gas transport in a water-bearing fissured rock, the water in the major fissures must be displaced by the gas to open transport channels. Displacement of water from a fissure can only take place when the pressure of the gas exceeds the sum of the capillary pressure and hydrostatic pressure in the fissure.

The capillary pressure for a fissure was defined in Section 6.3.1:

$$P_c = \sigma(\frac{1}{R_1} + \frac{1}{R_2}) \cos\Theta \qquad (6\text{-}13)$$

The permeability in a single fissure is given by the solution to the Navier-Stokes equation for the flow of an incompressible fluid between parallel plates:

$$k_f = \frac{b^2}{12} \qquad (6\text{-}14)$$

The displacement of water from the fissure is assumed to take place by the gas pushing the gas-water interface. At all times, the velocity in both the gas phase and in the water phase equals the velocity of the moving interface. Here, the gas has been treated as incompressible during the time of displacement of the water. In addition, the rock surfaces of the fissure are assumed to be impermeable.

From the conservation of mass equations and the equations of motion for both the gas phase and the water phase, an expression for the velocity of the gas - water interface during displacement can be derived /48/:

$$V = \frac{k_f}{\mu_g} \frac{g H_g(\rho_w - \rho_g) - P_c}{x + \frac{\mu_w}{\mu_g}(L - x)} \qquad (6\text{-}15)$$

where:

$H_g = f(t)$ = vertical height of the gas cushion (m)

x = spatial coordinate, length of displacement (m)

t = time (s)

k_f = fracture permeability (m^2)

μ_g = dynamic viscosity of the gas (Ns/m^2)

μ_w = ditto for the wetting fluid, i.e. water (Ns/m^2)

g = gravitation (m/s^2)

ρ_w = density of water (kg/m^3)

ρ_g = density of gas (kg/m^3)

P_c = capillary pressure (Pa)

L = length of fracture (m)

Since the gas cushion height is a function of time, the equation (6-15) must be integrated numerically to obtain the required time for displacement of the water.

6.5 Gas transport in an unsaturated porous material

The transport of gases in an unsaturated porous material can be calculated by the generalised Darcy equation /51/. See also Figure 35:

$$q = - \frac{k_{eff}}{\mu_g} (\nabla P + \rho g \cos\Theta) \qquad (6\text{-}16)$$

where:

q	=	volumetric flow rate of gas	(m^3(STP)/m^2,s)
k_{eff}	=	effective permeability	(m^2)
μ_g	=	dynamic viscosity of the gas, assumed constant	(Ns/m^2)
∇P	=	pressure gradient	(Pa/m)
ρ	=	density of the gas	(kg/m^3)
g	=	gravitation	(m/s^2)
Θ	=	angle between flow direction and gravitational vector, assumed constant	(^{o})

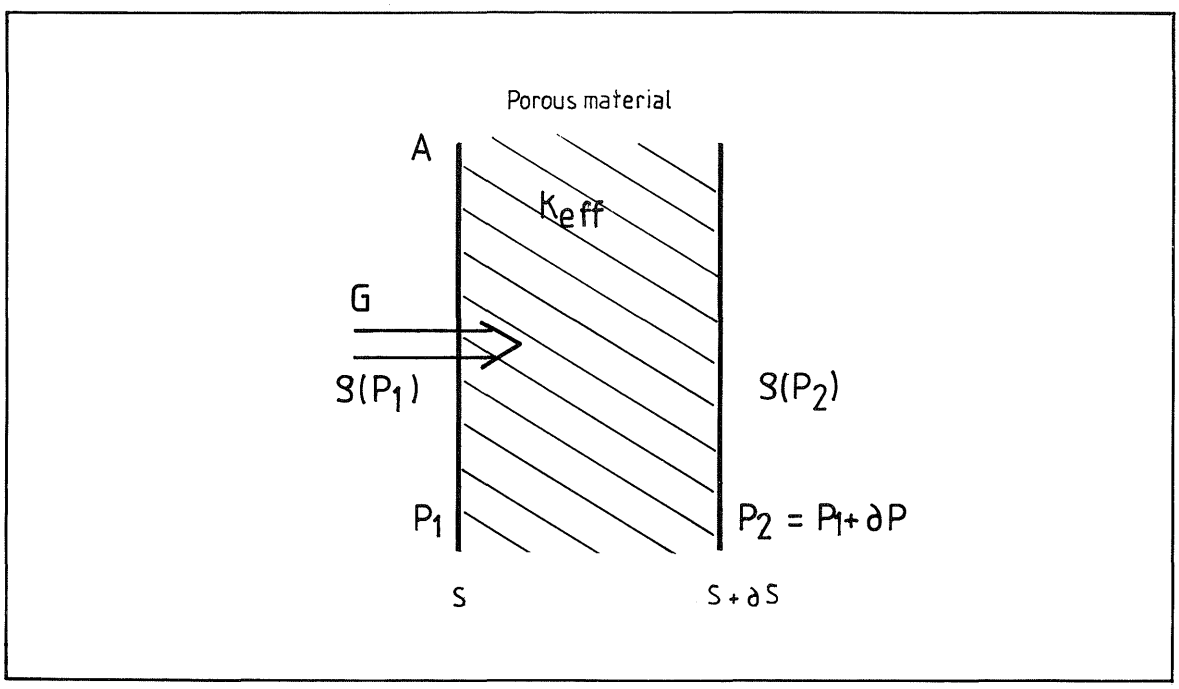

Figure 35. Gas transport in an unsaturated porous medium. symbols used are explained in the text

Here the effective permeability is used as it is independent of the properties of the fluid. The relationship between the effective permeability and the effective conductivity is:

$$K_{eff} = k_{eff} \frac{\rho g}{\mu_g} \qquad (6\text{-}17)$$

Estimation of the effective conductivity, K_{Eff}, was treated in detail in previous sections.

When the pressure drop is significant, Eq. (6-16) must be corrected for the compressibility of the gas. The treatment is simplified by introducing the mass flow rate of gas instead of the volumetric flow rate. Thus:

$$G = q\, \rho(P) \qquad (6\text{-}18)$$

for an ideal gas

$$\rho(P) = \frac{M P}{R T} \qquad (6\text{-}19)$$

where:

G = mass flow rate (kg/m^2,s)

M = molar weight of gas (kg/kmole)

P = pressure (Pa)

R = gas constant (Pa·m^3/kmole,K)

T = absolute temperature (K)

Introducing (6-18) and (6-19) in (6-16) gives:

$$G = - \frac{k_{eff}}{\mu_g} \frac{M}{R T} \left(P \nabla P + \frac{M P^2}{R T} g \cos\Theta \right) \qquad (6\text{-}20)$$

Since G is constant (no production of gas in the fissures), (6-20) is separable and may be integrated for a one-dimensional flow in the S-direction:

$$\int_{P_1}^{P_2} \frac{P\, dP}{- G \frac{\mu_g}{k_{eff}} \frac{R T}{M} - \frac{M P^2}{R T} g \cos\Theta} = \int_{S_1}^{S_2} dS \qquad (6\text{-}21)$$

Integrating and rearranging gives

$$G = \frac{k_{eff}}{\mu_g}\left(\frac{M}{R\,T}\right)^2 g\cos\Theta \quad \frac{\left(\exp\left(2\,\frac{M}{R\,T}\,g\cos\Theta(S_2 - S_1)\right)\right) P_2^2 - P_1^2}{1 - \exp\left(2\,\frac{M}{R\,T}\,g\cos\Theta(S_2 - S_1)\right)} \qquad (6\text{-}22)$$

The calculation of the gas transport capacity in the lineaments and host rock starts with an estimation of the effective gas conductivity and the pressure build-up in the decompressed zone around the repository. Using the results from these calculations, the gas transport capacity has been calculated by equation (6-22). The procedure was iterated until the calculated gas transport capacity was equal to the rate of gas production in the repository.

An alternative form of equation (6-22) can be found in literature /43/ if the term $\rho g \cos\Theta$ in equation (6-16) is disregarded. For this case:

$$q_2 = - \frac{k_{eff}}{\mu_g} \quad \frac{P_2^2 - P_1^2}{2P_2(S_2 - S_1)} \qquad (6\text{-}23)$$

and

$$G = q_2\ \rho(P_2) \qquad (6\text{-}24)$$

gives

$$G = - \rho(P_2)\ \frac{k_{eff}}{\mu_g} \quad \frac{P_2^2 - P_1^2}{2P_2(S_2 - S_1)} \qquad (6\text{-}25)$$

The calculated massflow using equations (6-22) and (6-25) respectively differs by less than 8 percent.

6.6 Modelling strategy

The calculations of gas transport from the underground repository through the host rock are based on a number of simplifications and assumptions.

The real repository is designed with a complicated system of barriers. The repository cavern is surrounded by a concrete lining and the space between this and the container pile is filled with concrete. It is assumed that the gas produced can penetrate these barriers easily. The repository lining can either be cracked or, if necessary, will be equipped with gas-release devices. The devices can be constructed with channels filled with a highly permeable porous medium, through which the gas can escape even at a low overpressure.

The repository cross-section, which is elliptical, is approximated as a square in the model.

The hydrostatic pressure taken into consideration corresponds to the overburden of marl. The layer on top of the marl is very permeable, with higher conductivity and low capillary pressure and therefore offers no resistance to gas transport.

The structure of the marl overburden is characterized by discontinuous zones called lineaments. In the calculations, it has been assumed that these zones have a width of 0.05 m and a frequency of 0.2 m^{-1} /NGB 85-07/. The lineament is also assumed to form an angle of 45 degrees with the horizontal plane.

In the calculations, the gases formed are assumed to accumulate in the decompressed zones around the caverns.

Since it has been impossible to find capillary pressure data for Valanginian marl, it was decided to use literature data for other similar rock materials, i.e. dolomite, sandstone and limestone (see Figure 32).

In the calculations, gases are assumed to be transported in both the host rock and in the lineaments, simultaneously. The transport in the decompressed zone along the transport tunnel is of less importance and has not been taken into account.

To simplify the calculations, steady-state transport was assumed by equalling the gas transport rate to the gas production rate.

6.7 Data used

The gas formation rates used in the calculations are presented in Table 36. Different configurations of the decompressed zone around the repository are given in Table 37 and are illustrated in Figure 36.

Capillary pressure and relative conductivity as a function of saturation degree are presented in Figures 32 and 33, Section 6.3. Data used are from the literature and refere to three different rock types - sandstone, dolomite and limestone.

Hydraulic conductivities in the host rock (K_H) and in the lineaments (K_L) are given as intervals with a most probable value specified in Table 38.

Table 36. Gas formation rates and hydrostatic pressures

Notation	Gas formation rate m^3(STP)/s	Time period yr	Hydrostatic pressure (MPa)
N71	$1.8 \cdot 10^{-3}$	0-20	1.5
N72	$8.0 \cdot 10^{-4}$	20-750	1.5
N61	$1.1 \cdot 10^{-3}$	0-20	2.0
N62	$1.6 \cdot 10^{-4}$	20-750	2.0

Table 37. Different configurations of the decompressed zone around the repository

Case	Height x Width (m)	Height of decompressed zone (m)
D1	40x40	13
D2	36x35	11
D3	27x27	6
D4	33x33	10
D5	12x14	*)

*) In this case, gases are assumed to accumulate inside the repository lining.

Table 38. Hydraulic conductivity at saturation in the host rock (K_H) and in the lineaments (K_L)

	Hydraulic conductivity (m/s) minimum	average	maximum
Host rock	10^{-10}	$2 \cdot 10^{-9}$	10^{-8}
Lineaments	10^{-9}	$3 \cdot 10^{-9}$	10^{-7}

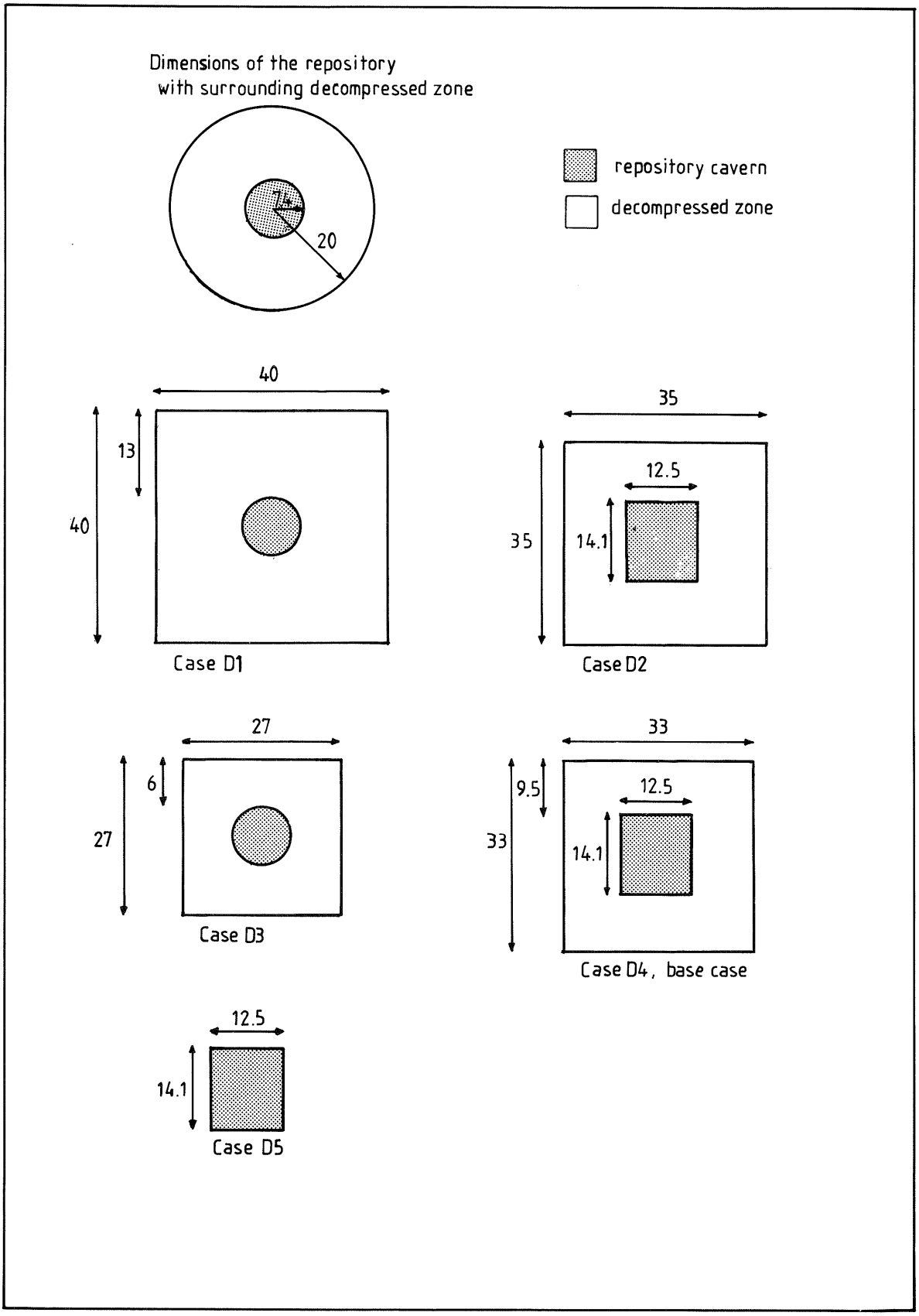

Figure 36. Assumed configurations of the decompressed zone around the repository. In Cases D1 to D4 the gas is assumed to accumulate in the surrounding decompressed zone, while in Case D5 the gas is assumed to accumulate in the repository

Basic data

Acceleration of gravity	$g = 9.8\ ms^{-2}$
Interfacial tension (hydrogen/water)	$\gamma = 0.07422\ N\ m^{-1}$
Density, non-wetting phase	$\rho_{nw} = 0.087\ kg\ m^{-3}$
Viscosity, non-wetting phase	$\mu_{nw} = 8.5 \cdot 10^{-6}\ Ns\ m^{-2}$
Viscosity, wetting phase	$\mu_w = 1.3\ 10^{-3}\ Ns\ m^{-2}$
Rock temperature	$T = 10\text{-}15^{o}C$
Gas constant	$G = 8314.34\ J\ K^{-1}kmole^{-1}$
Molecular weight, non-wetting phase	$M_{nw} = 2kg\ kmole^{-1}$
Repository volume	$820\ 000\ m^3$
Repository length	4 660 m
Repository location	450 m.a.s.l

6.8 Results and discussion

The possibility of gas transport from the Type B repository through the surrounding rock has been calculated and the results are presented below. The Oberbauen Stock model site has been considered.

The gases produced in the repository have been assumed to escape from the repository barriers and be collected in the decompressed zone which may be formed around the repository during tunnel excavation. The accumulated gas will form a gas cushion at the top of the decompressed zone. The pressure in the gas cushion will continue to rise as more gas is accumulated. When the gas pressure exceeds the sum of the hydrostatic pressure and the capillary pressure in the overlying rock, gas will displace water from the fissures in the rock.

Water will first be displaced from the major fissures with the lowest capillary pressure, and if necessary, water from smaller fractures will be displaced until a steady-state situation is obtained, in which the gas transport capacity equals the gas production rate.

In the calculations, the gases have been assumed to be transported in both the host rock and in the lineaments simultaneously.

The results from the calculations are presented in the following way:

- the time required to obtain a steady-state situation with respect to gas transport, here denoted release time
- the height of the gas cushion at steady-state, denoted Hg
- the calculated degree of water saturation in the host rock and lineaments at steady-state, denoted saturation degree. The degree of water saturation is, in principle, the quotient of the volume of water-filled pores and the total volume of pores in the rock material.

In Figure 37, a schematic picture of the formation of a gas cushion in the decompressed zone around the repository and the approach to a steady-state situation is shown.

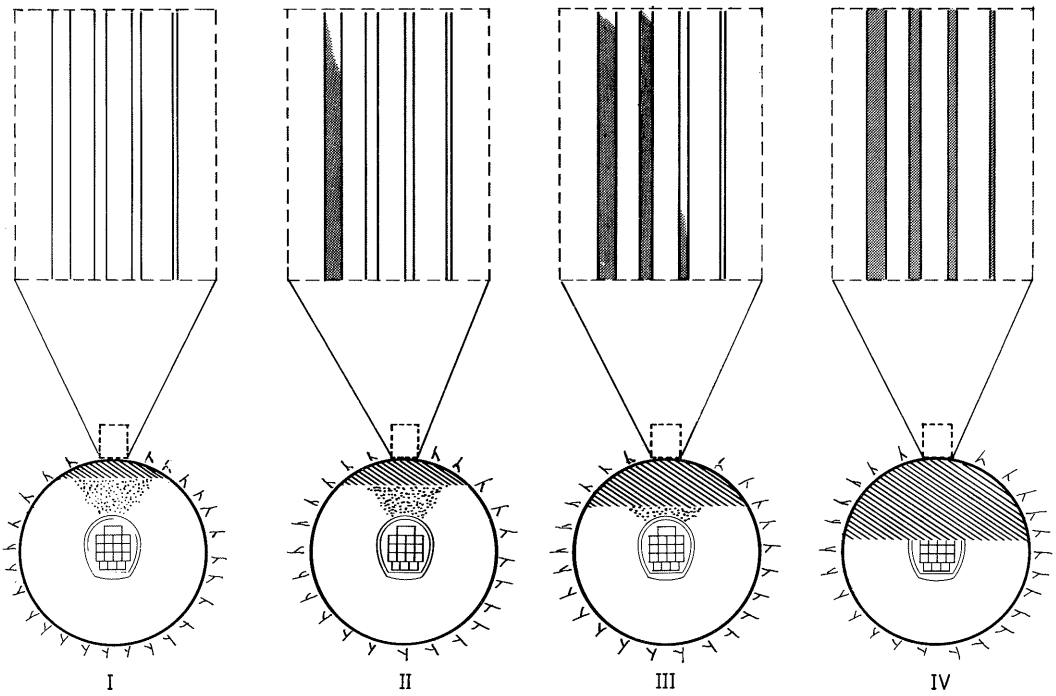

Figure 37. The picture illustrates schematically the formation of a gas cushion in the decompressed zone (I), the displacement of water from fissures as the size of the gas cushion increases (II), and the steady-state situation for most calculated cases (III). The situation in an unfavourable case with too low rock conductivity is outlined in (IV)

The important consequences of the assumption that gases are accumulated in the decompressed zone instead of inside the repository lining, are that the storage volume for the gases as well as the cross-sectional area available for gas transport are increased. Therefore, the amount of water being displaced from the repository itself during formation of the gas cushion is decreased, and, instead of radionuclide-contaminated pore-water, mainly non-contaminated ground-water is displaced.

The gas transport has been calculated for a number of parameter value combinations. In Figures 36-40 the calculated gas cushion height with steady-state conditions is shown for three different rock materials. The different rock materials are represented by capillary pressure curves found in the literature /49,50/, and applied to dolomite, sandstone and limestone.

In the calculations, the capillary pressure curves are assumed to be the same for different conductivities. This means that only the number of fissures varies with the conductivity.

In Figure 38, the results for a dolomite rock are presented. The major parameters are the hydraulic conductivities of the host rock and of the lineaments. It can be concluded that, for hydraulic conductivities higher than 10^{-9} m/s in the host rock, the transport capacity is high and the gas cushion height is independent of the conductivity in the lineaments. It can also be concluded that the gas transport capacity has been found to be sufficiently high for all calculated cases where the host rock conductivity is higher than $4 \cdot 10^{-11}$ m/s. For host rock conductivities less than 10^{-10} m/s, the calculated gas cushion height is very dependent on the conductivity in the lineaments.

This effect can be explained by the non-linear relationship between the calculated gas cushion height and the calculated relative conductivity which becomes important for low conductivities; for details see Section 6.3.1.

As an example, if we assume a host rock conductivity of 10^{-11} m/s, the hydraulic conductivity in the lineaments must be higher than about $5 \cdot 10^{-9}$ m/s to avoid displacement of pore-water from the repository. Here, the height of the decompressed zone above the repository is assumed to be 10 metres, as is indicated by the dashed line in Figures 38 and 40.

In Figure 39, the calculation results for sandstone are presented.

In all calculated cases, the gas cushion height is lower than for dolomite. In this case too, a non-linear behaviour is observed for low conductivities, the reason being the same as in the dolomite case. For all calculations where the conductivity of the host rock is higher than $5 \cdot 10^{-11}$ m/s, the gas cushion height is less than 2.5 metres. As a consequence, no displacement of water from the repository contaminated with radionuclides will take place in these cases.

Figure 40 shows the calculated gas cushion height, Hg, corresponding to the capillary pressure curve for limestone. The results differ significantly from those previously presented for dolomite and sandstone. This is shown by the comparatively high values for Hg. The non-linear behaviour of Hg as a function of the conductivities, which was discussed for dolomite, can also be observed here. The results show that, except for very high host rock conductivities(higher than 10^{-8} m/s), the calculated gas cushion height is larger than the height of the decompressed zone above the repository.In this case, radionuclide-contaminated water will be displaced from the repository.

The calculated release times for gases given in Table 39 are less than 20 years in all cases except for host rock conductivities less than $1 \cdot 10^{-12}$ m/s. It should be noted that the rate of gas production slows down after 20 years and thereafter the required gas transport capacity is somewhat lower. The release times for sandstone and limestone are also given in Table 39. The release time for sandstone is less than 20 years, except for cases with host rock conductivities less than $1 \cdot 10^{-12}$ m/s and conductivities in the lineaments less than $2 \cdot 10^{-9}$ m/s.

In these cases, the calculated degree of water saturation is below about 20%; see also Table 40. It is believed that at such low saturations other effects such as adsorption phenomena may appear, which make the model less reliable. Therefore, these results should be disregarded. The results for limestone show that the release time is less than 20 years only for those cases where the host rock conductivity is higher than 10^{-8} m/s.

To estimate the effect of the assumptions made regarding the geometry and volume of the decompressed zone around the repository a number of calculations assuming different geometric configurations of this zone were made. The assumed geometric data for the different cases are presented in Table 37 and in Figure 36 in Section 6.7. The results are presented in Figure 41.

The results refer to the dolomite rock type with a fixed conductivity in the lineaments of $3 \cdot 10^{-9}$ m/s and show that the assumptions made regarding the geometry of the decompressed zone are important but not critical for the gas transport capacity. However, the same Figure also shows the effect of all gases being accumulated inside the repository, i.e. curve D5. In this case, the value Hg refers to the height of the gas cushion inside the repository and corresponds implicitly to the volume of radionuclide-contaminated water that is displaced from the repository. It can also be noted that, for host rock conductivities less than $3 \cdot 10^{-11}$ m/s, the release time exceeds 20 years, which results in a knee on the curve D5.

In Figure 42 the gas cushion height, Hg, is given as a function of the gas production rate for dolomite with fixed host rock conductivity of 10^{-10} m/s and conductivity in the lineaments of $3 \cdot 10^{-9}$ m/s. The dependence is close to linear except for the lowest values of gas production rate. The reason for this non-linearity is the dependence of the relative permeability on the capillary pressure. The capillary pressure is, in turn, an almost linear function of the Hg.

A few calculations have also been made using a similar model developed for a granite rock with uniformly sized fissures at arbitrary distances. The results show that the gas transport capacity is sufficiently high for a host rock conductivity higher than $1 \cdot 10^{-9}$ m/s with 1-0.05 fissures per metre. The corresponding fissure widths are $8 \cdot 10^{-6}$ -$2 \cdot 10^{-5}$ m and the calculated height of the gas cushion is 1.0-5.3 m. A host rock conductivity of $1 \cdot 10^{-10}$ m/s was not sufficient to balance the rate of gas production without displacement of contaminated pore-water.

Table 39. The release time required to obtain steady-state conditions, i.e. balance between gas formation rate and the gas transport capacity, Case D_4

Conductivities (m/s)		Release time for different rock types (a)		
Lineaments	Host rock	Dolomite	Sandstone	Limestone
$1 \cdot 10^{-7}$	$1 \cdot 10^{-8}$	0.7	0.9	10.4
	$1 \cdot 10^{-10}$	1.6	1.6	22.8
	$3 \cdot 10^{-11}$	1.6	1.6	24.3
	$1 \cdot 10^{-12}$	1.8	1.6	24.3
$3 \cdot 10^{-9}$	$1 \cdot 10^{-8}$	0.0	0.9	10.4
	$1 \cdot 10^{-10}$	3.5	2.0	46.8
	$3 \cdot 10^{-11}$	7.2	2.8	10.4
	$1 \cdot 10^{-12}$	-	6.3	-
$2 \cdot 10^{-9}$	$1 \cdot 10^{-8}$	0.7	0.9	10.7
	$1 \cdot 10^{-10}$	3.8	2.3	40.5
	$3 \cdot 10^{-11}$	8.2	3.0	-
	$1 \cdot 10^{-12}$	-	-	-
$1 \cdot 10^{-9}$	$1 \cdot 10^{-8}$	0.7	0.9	11.1
	$1 \cdot 10^{-10}$	3.8	2.3	49.6
	$3 \cdot 10^{-11}$	9.8	3.5	-
	$1 \cdot 10^{-12}$	-	-	-

_: denotes that the calculated gas transport capacity was found insufficient to balance the gas production rate without displacement of contaminated pore-water in the repository.

Table 40. The saturation degree in the rock with steady-state conditions, i.e. balance between the gas formation rate and the gas transport capacity, Case D_4

Conductivities (m/s)		Saturation degree for different types (a)		
Lineaments	Host rock	Dolomite	Sandstone	Limestone
$1 \cdot 10^{-7}$	$1 \cdot 10^{-8}$	0.97	0.95	0.97
	$1 \cdot 10^{-10}$	0.86	0.85	0.92
	$3 \cdot 10^{-11}$	0.86	0.85	0.91
	$1 \cdot 10^{-12}$	0.82	0.85	0.91
$3 \cdot 10^{-9}$	$1 \cdot 10^{-8}$	0.94	0.95	0.97
	$1 \cdot 10^{-10}$	0.63	0.65	0.808
	$3 \cdot 10^{-11}$	0.44	0.42	0.67
	$1 \cdot 10^{-12}$	-	0.11	-
$2 \cdot 10^{-9}$	$1 \cdot 10^{-8}$	0.97	0.95	0.97
	$1 \cdot 10^{-10}$	0.61	0.57	0.79
	$3 \cdot 10^{-11}$	0.41	0.38	-
	$1 \cdot 10^{-12}$	-	-	-
$1 \cdot 10^{-9}$	$1 \cdot 10^{-8}$	0.97	0.95	0.97
	$1 \cdot 10^{-10}$	0.61	0.57	0.79
	$3 \cdot 10^{-11}$	0.36	0.32	-
	$1 \cdot 10^{-12}$	-	-	-

_: denotes that the calculated gas transport capacity was found insufficient to balance the gas production rate without displacement of contaminated pore-water in the repository.

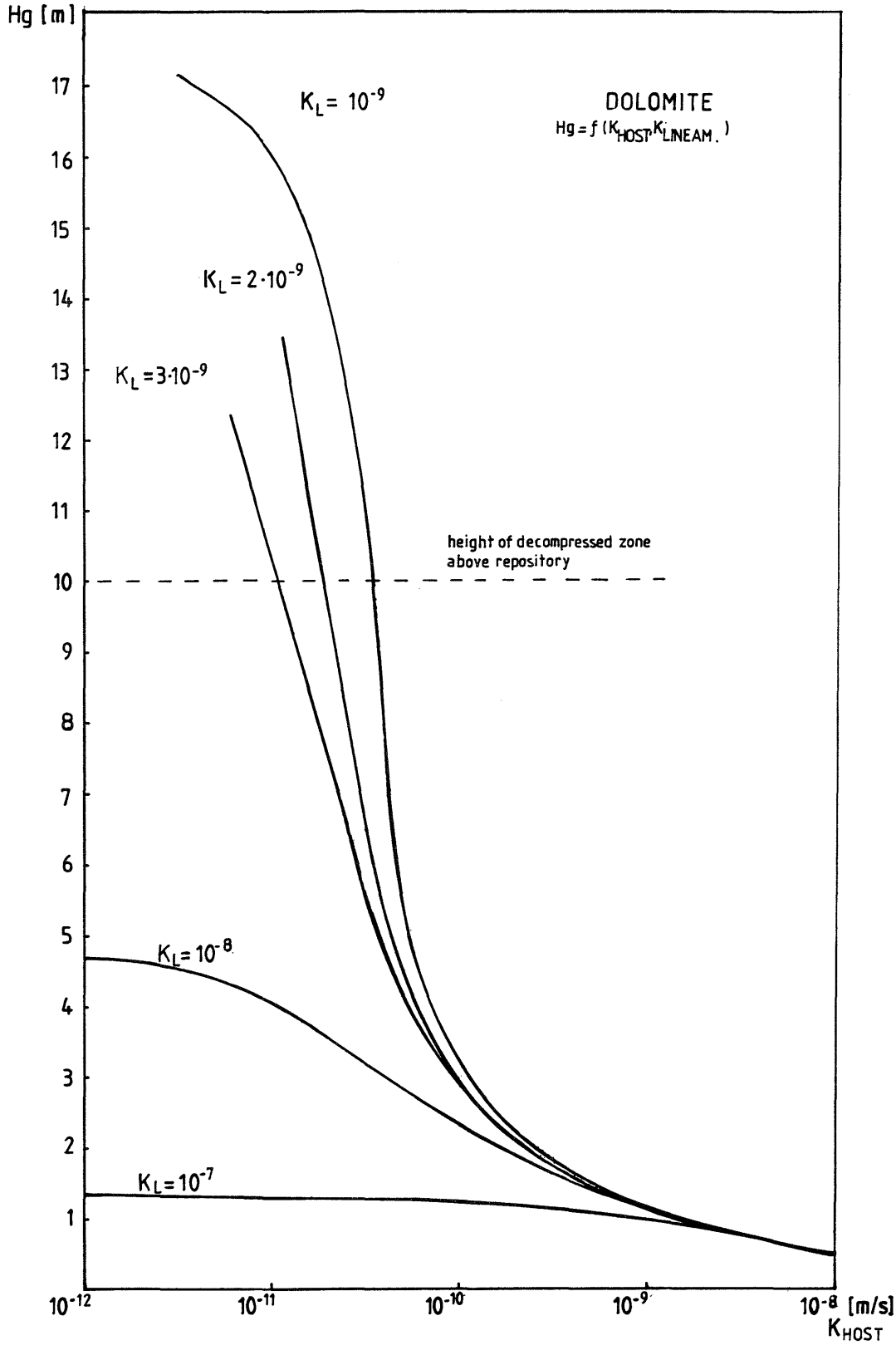

Figure 38. The calculated gas cushion height, Hg, as a function of the hydraulic conductivities in the host rock and in the lineaments with steady-state conditions i.e. when gas transport capacity equals gas production rate. Capillary data for Dolomite. Case D4

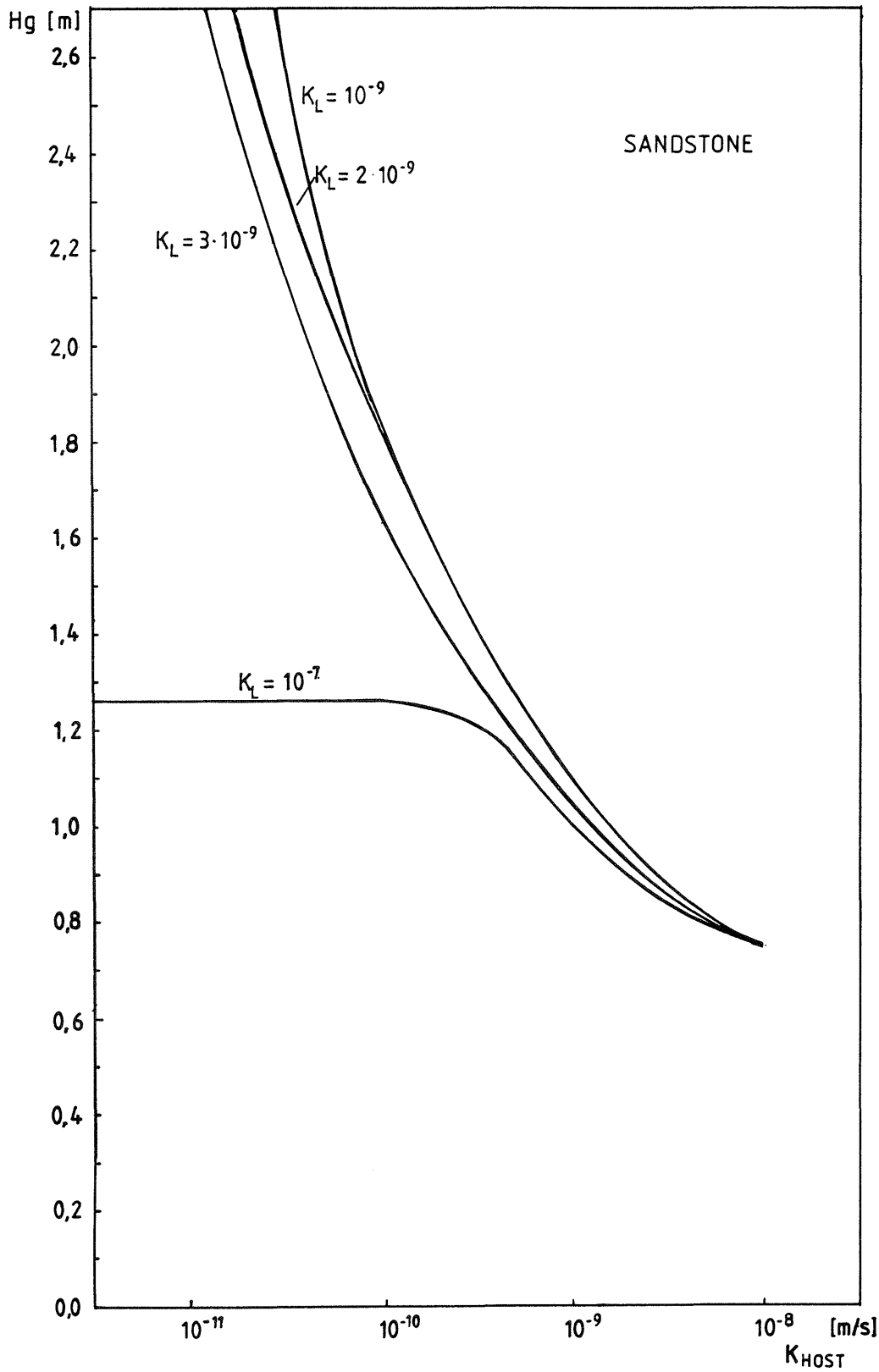

Figure 39. The calculated gas cushion height, Hg, as a function of the hydraulic conductivities in the host rock and in the lineaments with steady-state conditions i.e. when gas transport capacity equals gas production rate. Capillary data for Sandstone. Case D4

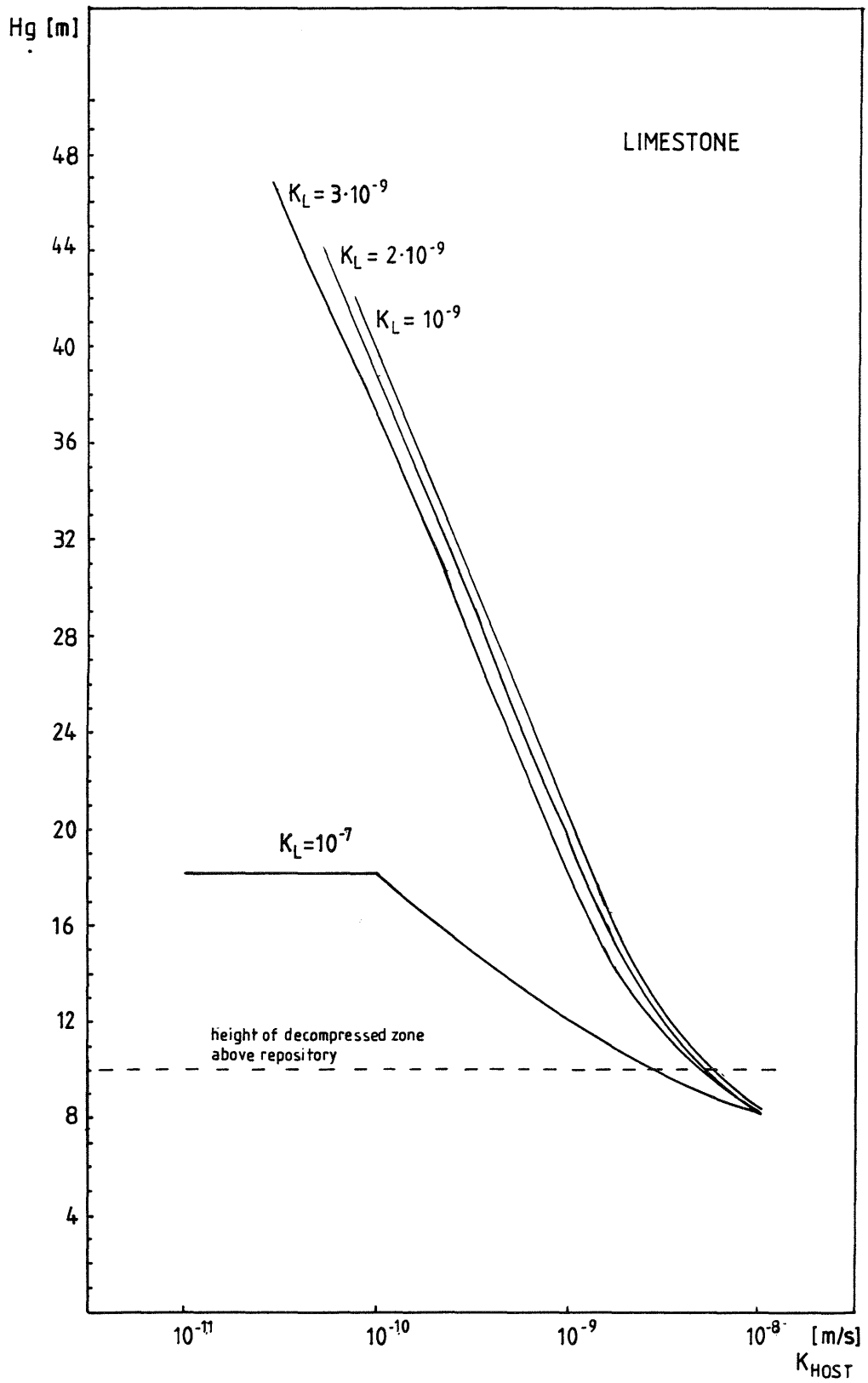

Figure 40. The calculated gas cushion height, Hg, as a function of the hydraulic conductivities in the host rock and in the lineaments with steady-state conditions i.e. when gas transport equals gas production rate. Capillary data for Limestone. Case D4

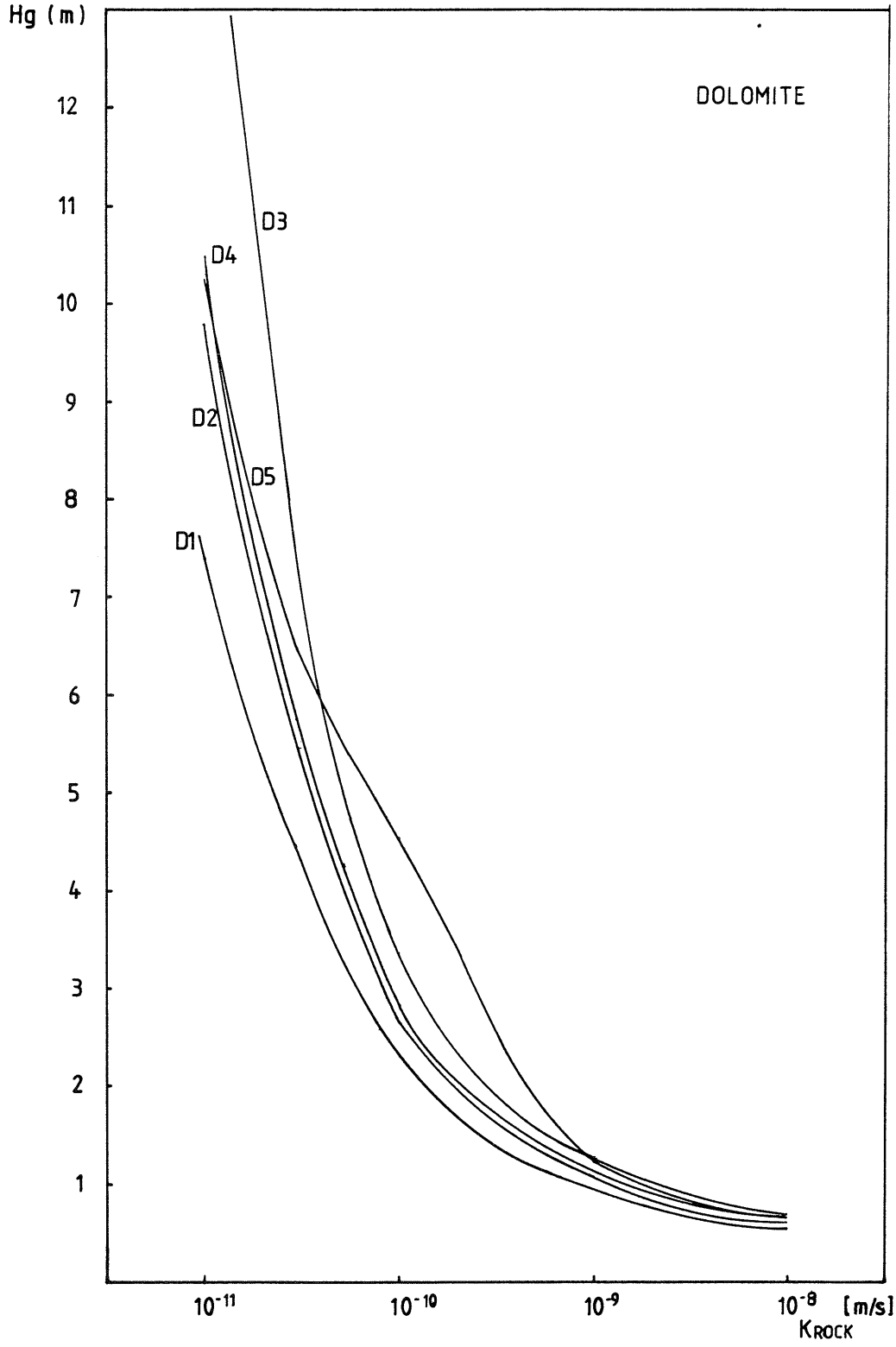

Figure 41. The calculated gas cushion height, Hg, at which gas production equals gas transport as a function of the host rock conductivity and the assumed geometry and volume of the decompressed zone with constant conductivity in the lineaments of $3 \cdot 10^{-9}$ m/s

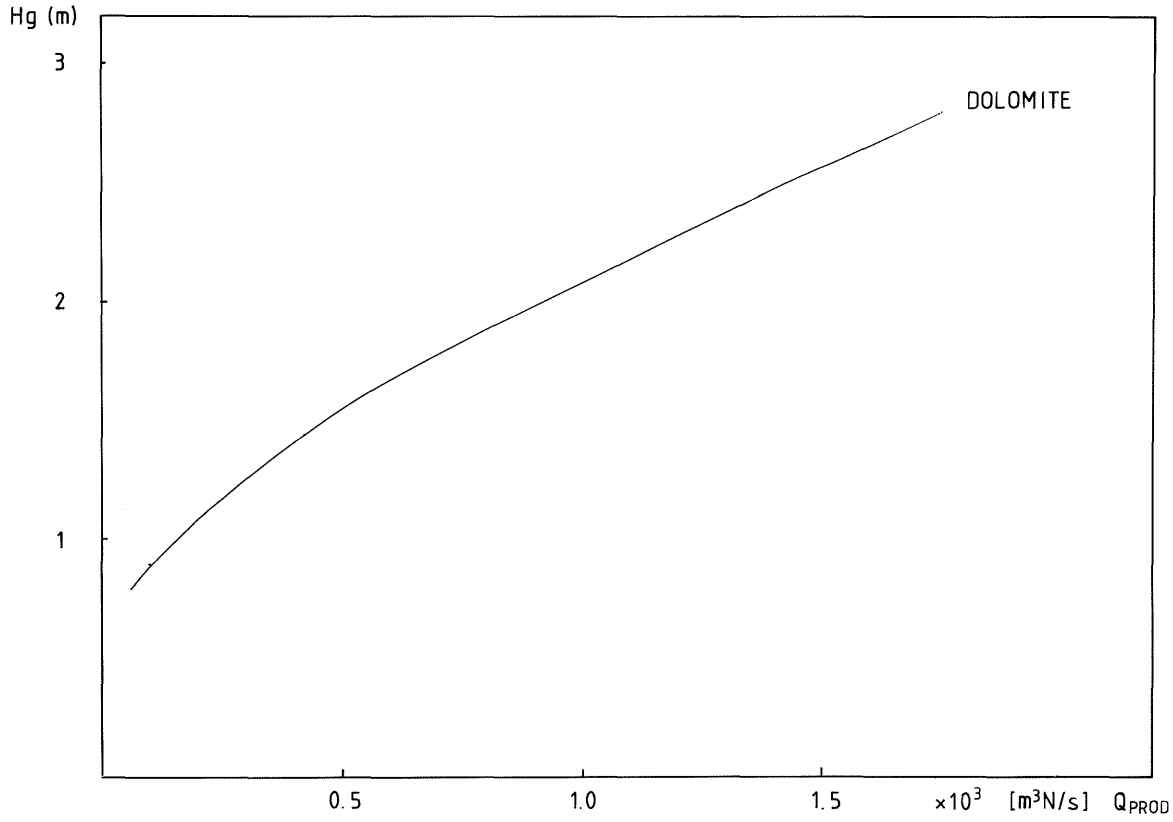

Figure 42. The calculated gas cushion height at which gas transport equals gas production as a function of the gas production rate. Dolomite rock is assumed. Host rock conductivity is 10^{-10} m/s and conductivity in lineaments is $3 \cdot 10^{-9}$ m/s. Case D4

7 CONCLUDING REMARKS

7.1 General

Significant volumes of gases are, without doubt, generated in the type B repository.

A useful measure of the rate of gas generation is a comparison with the total pore volume in the repository, which is 160,000 m^3. The same gas volume at prevailing pressure will be generated within 100 to 600 years with a base case estimate of 120 years.

The annual amount of gas leaving the repository at steady state and prevailing pressure, 1.5 MPa, is about 0.02 m^3 per m^2 of total repository cross-sectional area.

The gases as such have no detrimental effect on the safety of the repository. Indirectly they can, however, influence the transport of radionuclides from the repository in two ways and thereby affect safety:

- As a driving force for the transport of contaminated pore-water
- By decreasing the transport resistance by fracturing barriers.

The escape of gases from the repository through cracks in the technical barriers and collection as a gas cushion in the zone of decompressed rock above the repository has been judged to be the most probable scenario. Due to the accumulation of gases, groundwater with only a low content of radionuclides will be displaced from the decompressed zone. When the gas pressure becomes high enough, water will be displaced from the fissures by the gas. Eventually, gas-permeable channels will develop through the rock and gases are released.

7.2 Gas formation

Knowledge of the amounts of materials which cause gas formation in the repository is generally sufficient. The information about the content of zinc and aluminium, however, is less detailed and is an area where improvement is required. The information about the amount of cellulose and steel waste do not agree fully with NGB 85-07, since this report is based on a updated waste inventory, /NTB 84-47/.

The most important source of gas formation is corrosion of carbon and stainless steel, which are present in large quantities. The uncertainty with respect to corrosion rates is indicated by the difference of a factor of ten between the calculated maximum and minimum case.

As the corrosion of steel is the main source of the total amount of gases formed, more reliable data for the long-term corrosion rate of steel in concrete at prevailing pressure are required and should be examined experimentally.

During the first few decades, aluminium, which is present in limited amounts, may constitute one of the predominant sources of gas formation. The reason is the high corrosion rate (2 mm/a) which must be assumed for aluminium, given present knowledge. The corrosion rate of aluminium embedded in concrete is not sufficiently well known; consequently, experimental research is needed.

Microbial degradation of organic material is also a source of large amounts of gas. Cellulose is, together with aluminium, believed to be the predominant source of insoluble gases during the first 200 years.

Degradation rates of cellulose are known, at least under certain environmental conditions. However, the degradation rate might be different under repository conditions. The uncertainty is even larger regarding the rate of degradation of bitumen, plastic and ion exchange resins, which are also present in large quantities.

Gas formation rates given in this report are derived from experimental investigation. The experimental data are recalculated to be valid for degradation of 1 kg of organic material and have been used in a long-term aspect. To decrease the uncertainty in this area, experimental research under prevailing conditions is required.

The formation of carbon dioxide by microbial degradation is of such a magnitude that it will, at least locally, have a significant effect on the barrier properties, i.e. on the concrete degradation. Since carbon dioxide is a soluble gas in concrete porewater, the carbon dioxide formation does not contribute to the build-up of a gas cushion.

The gas formation caused by radiolytical decomposition is insignificant compared to the other processes. It is also of short duration, less than about 100 years. However, degradation products such as methylamines and other compounds acting as complexing agents may well prove to be important.

7.3 Gas transport

The transport of gases from a type B repository located at the Oberbauen Stock model site has been studied.

Four different zones essential for gas transport have been investigated; the host rock, the fracture zones, the decompressed zone around engineered caverns and the system of engineered barriers.

The predominant transport path outside the repository has been found to be the host rock and the fracture zones, whereas transport along the connecting tunnel has been found to be negligible.

The gases can be assumed to be released from the repository barriers without significant pressure build-up inside the repository. This has been verified by calculations of gas transport in existing fractures in the concrete barriers. The possibility that the gases will fracture the barriers has also been demonstrated by simple calculations.

For gases to escape from the repository, the hydrostatic and capillary pressure of the technical barriers and the host rock must be exceeded. In the case of all barriers and rock materials having the same capillary characteristics, the gases will migrate through the series of barriers and rock formations without the formation of a gas cushion. This is also true if the capillary pressure decreases along the path of gas migration.

On the other hand, if a layer of relatively impermeable material with higher capillary pressure occurs in the series, the formation of a gas cushion cannot be avoided below this particular material layer. Once a gas cushion is formed, water will be displaced from this location at a rate proportional to the growth of the cushion.

The importance of displacement of water depends on where the gas cushion is formed. If gases are accumulated inside the repository lining, the pore-water inside the repository will be displaced. Such water will contain a certain amount of radionuclides and therefore the potential for enhanced release of nuclides from the near-field of the repository has been studied.

In the repository studied, the situation is that there are two different locations where the formation of a gas cushion is possible;

- Inside the repository lining, since a high quality concrete in the lining might have a higher capillary pressure and lower permeability than the backfill material in the repository.

- At the top of the decompressed zone which may exist around the excavated area where the porosity, fracture sizes and overall permeability may be increased compared to the overlying undisturbed marl.

The conditions for accumulation of gases in the decompressed zone are:

- that such a decompressed zone is formed during the excavation of the repository,

- that the porosity of the decompressed zone is high enough to contain significant volumes of gases and,

- that the capillary pressure in the decompressed zone is lower than in the overlying rock.

The rock mechanical studies made in the area of the repository indicate that the formation of such a zone with an increased porosity might be possible.

For the gas transport calculations, gases are assumed to accumulate in the decompressed zone around the repository tunnel. In Figure 43, the formation of a gas cushion is illustrated.

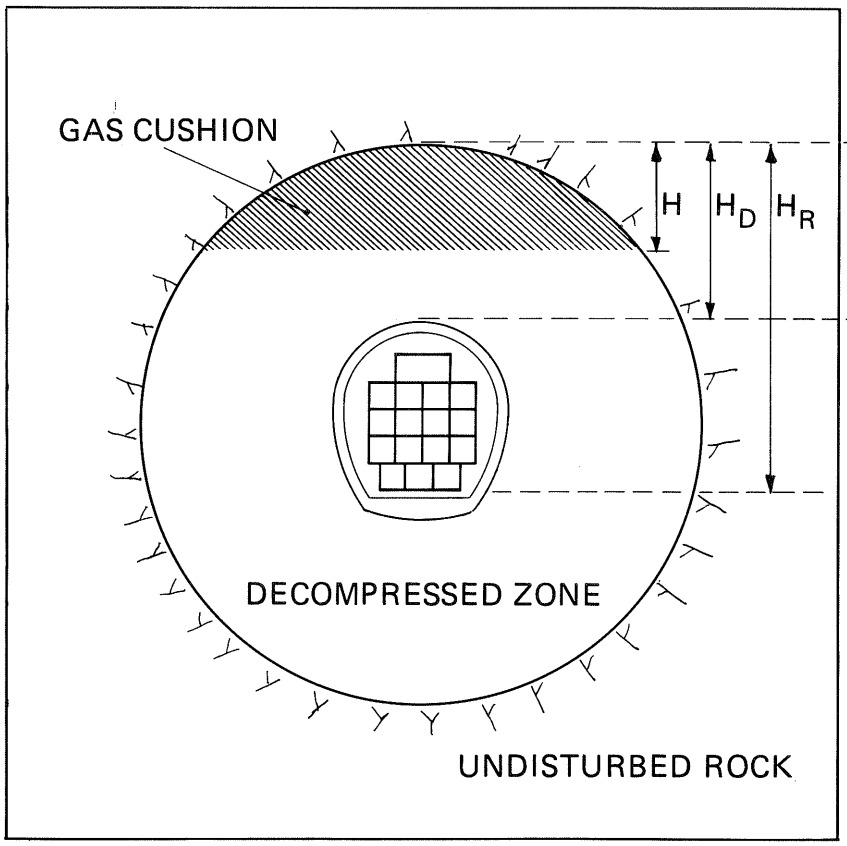

Figure 43 An illustration of the formation of a gas cushion in the decompressed zone. H denotes the calculated gas cushion height, H_D is the gas cushion height at which displacement of pore-water from the repository starts, while H_R is the gas cushion height for which all pore-water must be regarded to be displaced from the repository.

The size of the decompressed zone is estimated to be large enough to allow accumulation of significant volumes of gas in the pores. No data are available regarding the capillary pressure distribution, either for the undisturbed marl or for the decompressed zone. In the calculations, the decompressed zone has been assumed to have low capillary pressure and, therefore, the gas can easily penetrate this zone.

As a consequence of the gas accumulation, water is displaced from the decompressed zone. Simultaneously, the gas pressure increases. Once the gas pressure exceeds the sum of the hydrostatic pressure and the capillary pressure in the overlying rock, gas will penetrate the fissures in the rock.

Water in the fissures will be displaced when gas penetrates the fissures. The displacement is assumed to take place in a fissure with impermeable walls. Thus, the displacement is simplified to a one-dimensional analysis. The time for a complete displacement of water from the fissure has been calculated.

Primarily, the gas will penetrate the major fissures, but, with increasing gas pressure, smaller fissures will be penetrated. Finally, a steady-state situation will be reached when the gas transport capacity equals the rate of gas formation, taking into account the effect of decompression of gases during transport through the rock.

To characterize the rock material, two major parameters are used:

- hydraulic conductivities
- capillary pressure versus water saturation curves

The hydraulic conductivities are based on estimations made for Project "Gewähr" /NGB 85-07, NGB 85-08/. The estimated conductivities have been checked against observations of the water entering an existing tunnel in Valanginian marl. The amount of water that can be transported out with ventilation air was balanced against the water entering the tunnel from the rock. The results show that the estimated conductivities are of the correct order of magnitude.

As regards the capillary pressure curves, the host rock has been assumed to be a porous medium that resembles one of three different rock types:

- dolomite
- sandstone
- limestone

The capillary data have been calculated from data reported in the literature. The Valanginian marl is expected to have characteristics close to those of dolomite. These data are probably conservative since the measurements have been made with very small rock samples where larger discontinuities are not represented.

The importance of the size and shape of the decompressed zone as well as conductivities and capillary data for the undisturbed marl have been studied for a large number of assumed parameter values.

Except for very low conductivities, less than 10^{-10} m/s, or for rock materials with very high capillary pressures, e.g. Limestone, the calculations show that the gases can escape through the undisturbed marl without creating a gas cushion of such a size that radionuclide-contaminated porewater from the repository will be displaced.

In the long-term perspective, the plasticity of the marl may affect the function of the decompressed zone as a gas reservoir in that the decompressed zone might be recompressed. Therefore, further investigations are required to obtain as reliable information as possible on the size of the decompressed zone and on the characteristic material properties such as:

- hydraulic conductivities
- porosities
- capillary data

The influence of gas production on solute transport is not yet fully understood and quantified. Three scenarios might be possible.

- Displacement of contaminated water by the formation of a growing gas cushion within the repository.

- A pumping effect caused by pressure variations in a gas cushion in the repository.

- A mixed flow of contaminated water and gas.

Of these three alternatives, only the first was treated in this report.

An improved understanding of the fundamental transport mechanisms of gases in both the rock and in the barrier materials is necessary for future studies.

The hydraulic conductivities and the presence of fissures in both the rock and the barrier materials should be determined with greater accuracy than is available at present.

If the hydraulic conductivities are found to be low, capillary data for the rock and barrier materials are also required.

LITERATURE

/1/ Schneider, T. R. (1984): Geologische, hydrogeologische und Biosphären-Situation am Beispiel-Standort Oberbauen Stock für ein Endlager für schwach-und mittelradioaktive Abfälle, NAGRA Technical Report 84-20 .

/2/ Wranglen G., (1967), Metal corrosion and surface protection, Almqvist & Wiksell, Stockholm, (in Swedish, available in English).

/3/ Höglund, L. O., Wiborgh, M., Dahl, L. (1983): Gas-formation in SFR, SKBF/SKB AR 83-03, (in Swedish).

/4/ Escalante, E. and Ito, S. (1981): Measuring the rate of corrosion of steel in concrete, Corrosion/81 Conference, Apr. 1981, Nat. Assoc. of Corrosion Engineers, Toronto, Canada.

/5/ Hübner, W. (1979): Hydrogen generation in waste repository, SKBF/KBS AR 80-19 (in Swedish)

/6/ Ullmans Enzyklopädie der Technischen Chemie, Bd. 1

/7/ Pourbaix, M. (1966): Atlas of Electrochemical Equilibria in Aqueous Solutions, Pergamon Press, Oxford

/8/ Silverman, D. (1982): Corrosion-NACE, 38, 453

/9/ Stepina, T. G. and Iofa, Z. A. (1979): Elektrokhimiya 15, 151

/10/ Linnenbom, V. J. (1958): Jorn. Electrochem. Soc., 105, 322

/11/ Stepina, T. G. and Iofa, Z. A. (1980): Elektrokhimiya 16, 888

/12/ Vetter, K. J. (1961): Elektrochemische Kinetik, Springer

/13/ Preece, C. M. (1982): Corrosion of Steel in Concrete, KBS TR 82-19

/14/ Uhlig, H. H. (1948): The Corrosion Handbook, John Wiley & Sons Inc., New York

/15/ McKinley, I. G. and West, J. M. (1983): Radionuclide sorption/desorption processes occurring during groundwater transport, Progress report July 1981-June 1982 Fluid Processes Unit, FLPU 83-2, Inst. of Geol. Sc., Harwell, January 1983

/16/ Drever, J. I. (1982): The Geochemistry of natural waters, Prentice-Hall, Inc., Englewood Cliffs, N I 07632

/17/ Brandberg, S. and Wiborgh, M. (1982): Long-term changes, SKBF/KBS Working Report SFR 81-10 (in Swedish) Rennerfelt, J., in Appendix

/18/ Wetzel, R. G. (1975): Limnology, Saunders, Philadelphia, 743 pp.

/19/ Ghosh, S. and Klass, D. L. (1976): Solid Waste Resource Recovery: The "biogas concept", Public Works 2 71-75

/20/ Pfeffer, J. T. (1974): Temperature effects on anaerobic fermentation of domestic refuse, Biotechnology and bioengineering Vol. XVI, 771-787

/21/ Khan, A. W. (1977): Anaerobic degradation of cellulose by mixed culture, Div. of Biol. Sci., Natl. Res. Counc. Canada, Ottawa Can. J Microbiol., 23: 1700-1705

/22/ Winter, I. U. and Cooney, C. L. (1980): Fermentation of cellulose and fatty acids with enrichments from sewage sludge, Eur. I. Appl. Microbiol. Biotechnol. 11, 60-66

/23/ Stafford, D. A. (1974): Methane production from waste, Effluent Water Treat J v 14 2: 2 Feb 1974, 73-79 Coden: EWTJA

/24/ Molecke, M. (1979): Gas generation from transuranic waste degradation, data summary and interpretation. sand 79-1245

/25/ Molecke, M. (1980): Degradation of transuranic-contaminated wastes under geologic isolation conditions, IAEA-SM-246/37

/26/ Schwartz, A. (1963): Mikrobielle Korrosion von Kunststoffen und ihren Bestandteilen, Abhandlung der Deutschen Akademie der Wissenschaften zu Berlin

/27/ Roffey, R. (1982): Microbial decomposition of bitumen and asphalt, SKBF/KBS Working Report AR 82-49, (in Swedish)

/28/ Mohorcic, G. and Kramer, V. (1968): Gases evolved by CO-60 radiation degradation of strongly acidic ion Exchange Resins, J. Polymer Science, Part C, 16, 4185-4195

/29/ Draganic, I. G. and Dragonic, Z. D. (1971): The radiation chemistry of water, Academic Press, New York

/30/ Swyler, K. J., Dodge, C. J., Dayal R. (1983): Irradiation effects on the storage and disposal of radwaste containing organic ion-exchange media. Nureg/ CR-3383

/31/ Hall, G. R. and Streat, M. (1963): Radiation-induced decomposition of ion-exchange resins. Part I. Anion-exchange resins, Dep. of Chem. Eng. and Chem. Techn. Imp. College of Sci and Techn., London

/32/ Kosiewicz, S. T. (1980): Gas generation from the alpha-radiolysis of Bitumen, Nuclear and chemical waste management, Vol 1, 139-141

/33/ Christensen, H. (1981): SKBF/KBS Working Report AR 82-04, (in Swedish)

/34/ Kazanjian, A. R. and Horrell, D. R. (1974): Radiation effects on ion-exchange resins - I gamma irradiation of Dowex 50 XW, USAEC Report RFP-2140, Rocky Flats Division, Golden, Colorado

/35/ Gangwer, T. E., Goldstein, M., Pillay, K. K. S. (1978): Radiation effects on ion exchange materials, Brookhaven Nat. Lab. Rep. BNL-50781

/36/ Mohorcic, G., Kramer, V., Pregelj, M. (1974): Interaction of a sulfonic acid ion exchange resin with tritiated water on - irradiation, Int. J. Appl. Rad. and Isotopes, 25, 177-182

/37/ Semashim, A. M., Shistyakow, D. A., Kuzin, I. A. (1979): Investigation of the influence of oxygen on the radiolysis of the sulfonic acid cation exchanger, Kn-2X8, Zh Prikl. Khimii 52, 294-299 (in English)

/38/ Ahmed M. T., Clay, P. G., Hall G. R. (1966): Radiation induced decomposition of ion-exchange resins, Part II. The mechanism of the deamination of anion-exchange resins, J Chem. Soc. B, 1155-1157

/39/ Hall, G. R., Streat, M., Creed, G. R. B. (1968): Ion exchange in nuclear chemical processes - I. The effect of heat and ionising radiation on resin performance, Trans. Instn. Chem. Engrs, Vol.46

/40/ Carleson, G. (1983): Studsvik Technical Report NW 83/490, (in Swedish)

/41/ Porat, J. et al. (1981): Calculation of radiation dose and resulting radiolytic gas generation and temperature rise in bitumenized waste products, SKBF/KBS Working Report SFR AR 81-03

/42/ El-Khatib, N. A. F. (1980): The relative permeabilities of an idealized model of two-phase flow in porous media, Appl. Math. Modelling, 4, 463-466

/43/ Dullien, F. A. L. (1979): Porous Media Fluid transport and pore structure, Academic Press

/44/ Wolfseher, U. and Gertis, K. (1976): Isothermer Gastransport in porösen Stoffen aus gaskinetischer Sicht., Deutscher Ausschuss für Stahlbeton, Heft 258, Wilhelm Ernst und Sohn, Berlin-München

/45/ Nyame, B. K. and Illston, J. M. (1980): Capillary Pore Structure and Permeability of Hardened Cement Paste, 7th International Congress on the Chemistry of Cement, VI-181, Paris

/46/ Bird, R. B., Stewart, W. E., Lightfoot, E. N. (1960): Transport phenomena, Wiley and Sons, New York

/47/ Möller G., Petersons N., Samuelsson P., editors (1982) Betong-handboken Material, AB Svensk Byggtjänst, 2nd Edition (in Swedish).

/48/ Braester, C. and Thunvik, R. (1982): An analysis of the conditions of gas migration from a low-level radioactive waste repository, SKBF/KBS, Technical Report 83-21

/49/ Wardlaw, N. C. and McKellar, M. (1981): Mercury porosimetry and the interpretation of pore geometry in sedimentary rocks and artificial models, Powder Technology, 29, 127-143

/50/ Chatzis, I. and Dullien, F. A. L. (1981): Mercury porosimetry curves of sandstones. Mechanisms of mercury penetration and withdrawal, Powder Technology 29, 117-125

/51/ De Wiest R.J.M editor, Flow Through Porous Media (1969), Academic Press, New York.

NAGRA PROJECT "GEWÄHR"

NGB 85-02 Radioaktive Abfälle: Eigenschaften und Zuteilung auf die Endlager-Typen. Baden January 1985.

NGB 85-06 Endlager für schwach- und mittelaktive Abfälle: Bautechnik und Betriebsphase. Baden 1985.

NGB 85-07 Endlager für schwach- und mittelaktive Abfälle: Das System der Sicherheitsbarrieren. Baden January 1985.

NGB 85-08 Endlager für schwach- und mittelaktive Abfälle: Sicherheitsbericht. Baden January 1985.

NAGRA TECHNICAL REPORTS

NTB 82-03 The Long-Term Stability of Cement and Concrete for Nuclear Waste Disposal under Normal Geologic Conditions; Woo Sewung Shin, Battelle, Geneva; März 1982.

NTB 83-16 Experimente zur korrosionsbedingten Wasserstoffbildung in Endlagern für mittelaktive Abfälle; R. Schenk, Gebrüder Sulzer AG, Winterthur; Dezember 1983.

NTB 83-18 Literaturstudie über den Abbau von Bitumen durch Mikroorganismen; A. Dubach, A. Tesch, Institut für Pflanzenbiologie und Mikrobiologie der Universität Zürich; Dezember 1984.

NTB 84-07 Mögliche Mikrobiologische Vorgänge in unterirdischen Kavernen im Hinblick auf die Endlagerung radioaktiver Abfälle (Literaturstudie); D. Lüscher, R. Bachofen, Universität Zürich; Dezember 1984.

NTB 84-20 Geowissenschaftliche Grundlagen des Sondierstandortes Oberbauenstock; T. Schneider, S. Kappeler; Dezember 1984.

NTB 84-47 Inventar und Charakterisierung der radioaktiven Abfälle in der Schweiz; Dezember 1984.

NTB 85-19 Organic Complexing Agents in Low and Medium Level Radioactive Waste; B. Allard, RCG Konsult, Schweden; in Vorbereitung.

NTB 85-30 Auflockerungszonen um Stollen und Kavernen im Valanginienmergel des Oberbauenstocks; M. Gysel, Motor Columbus Ingenieurunternehmung AG, Baden; Januar 1985.

Appendix A

Duration of the initial aerobic phase

At the end of the operational phase, the repository will be closed. The maximum amount of oxygen entrapped in the repository is determined by the porosity of the waste and the filler material.

For concrete, the porosity is about 10-20%. Assuming a total volume of the repository of 820,000 m^3 and a porosity of 20%, the volume of air is 164,000 m^3. Air contains 21% oxygen. Thus, the maximum amount of oxygen is 34,450 m^3(STP), corresponding to $1.54 \cdot 10^3$ kmoles.

The entrapped oxygen will be consumed by aerobic corrosion of steel and microbial degradation of organic materials.

The rate of oxygen consumption will be different in different parts of the repository, depending on the materials present. Aluminium, unalloyed steel and cellulose will be the most important oxygen-consuming materials.

The total metal surface area of steel drums and reinforcement bars can be estimated to be $5.1 \cdot 10^6$ m^2.

For the reaction

$$Fe(s) + H_2O + 1/2 O_2 \rightarrow Fe(OH)_2(S)$$

One mole of oxygen reacts with two moles of iron. To consume all the oxygen in the repository, $2 \times 1.54 \cdot 10^3 = 3.1 \cdot 10^3$ kmoles or 170 tonnes of steel is corroded. Using a density of 7,800 kg/m^3, this equals 22 m^3 solid steel. For a surface area of $5.1 \cdot 10^6$ m^2, this corresponds to a layer $4.3 \cdot 10^{-6}$ metres thick.

Assuming a corrosion rate in the range of $1 \cdot 10^{-3}$-$2 \cdot 10^{-2}$ mm/year, the duration of the aerobic phase is 1 to 5 years.

Aluminium reacts according to

$$4\ Al + 6H_2O + 3O_2 \rightarrow 4\ Al(OH)_3$$

One mole of oxygen reacts with 4/3 moles of Al. This corresponds to $2 \cdot 10^3$ kmoles or 55 tonnes of Al with a volume of 20 m^3. The surface area exposed to corrosion is estimated to be $6 \cdot 10^3$ m^2. If all the oxygen is used up by Al-corrosion, it will correspond to a layer of 3 mm.

The corrosion rate is reported to be of the order of magnitude of 1 mm/year, which gives a duration for the aerobic phase of 3 years if controlled only by aluminium.

Cellulose consumes 37 moles O_2 per kg at a rate of 0.2 mol/kg, year /3/. As the total quantity present is 5,300 tonnes (Chapter 3.3.4), the rate of consumption of O_2 is $1 \cdot 10^3$ kmol/year. To consume all the oxygen present will therefore take 1.5 years by aerobic degradation of cellulose.

Summary

All the oxygen present in the repository will be consumed by each of the following materials within the time indicated.

Steel (unalloyed)	1-5 years
Aluminium	3 "
Cellulose	1.5 "

A practical conclusion is that some parts of the repository will become anaerobic within less than a year and some after up to 10 years after the oxygen supply is interrupted. This may well be before the closure of the repository.

The rate-controlling process will probably be the transport of oxygen and not corrosion or microbial degradation.